A DUAL REACTION-MASS DYNAMIC VIBRATION ABSORBER FOR ACTIVE VIBRATION CONTROL

by

John Heilmann

Thesis submitted to the Faculty of the

Virginia Polytechnic Institute and State University

in partial fulfillment of the requirements for the degree of

Master of Science

in

Mechanical Engineering

APPROVED:

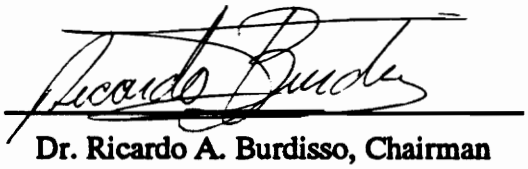

Dr. Ricardo A. Burdisso, Chairman

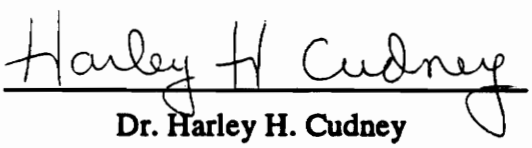

Dr. Harley H. Cudney

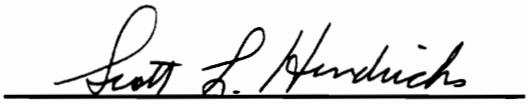

Dr. Scott L. Hendricks

August, 1996

Blacksburg, Virginia

Keywords: Active/Passive Control, Vibration Control, Dynamic Vibration Absorber

c.2

LD
5655
V855
1996
H455
c.2

A DUAL REACTION-MASS DYNAMIC VIBRATION ABSORBER FOR ACTIVE VIBRATION CONTROL

by

John Heilmann

Committee Chairman: Ricardo A. Burdisso

Mechanical Engineering

(ABSTRACT)

Traditional dynamic vibration absorbers (DVAs) consist of a mass-spring-damper system and are an effective means of attenuating structural vibration over a narrow frequency band. The effective bandwidth of the DVA can be increased by the addition of an externally controlled force, generally applied between the reaction-mass and the primary structure. Such devices are known as hybrid DVAs. This thesis presents a new hybrid DVA configuration which utilizes two reaction-masses in parallel. On this proposed hybrid dual-mass (DM) DVA, the control force is applied between the reaction-masses. It is shown that in broadband control applications, the proposed DM-DVA requires less control force to achieve the same primary attenuation as the traditional hybrid single-mass (SM) DVA. The hybrid DM-DVA was compared to the hybrid SM-DVA with two tests. A numerical simulation of the hybrid DVAs attenuating a single-degree-of-freedom structure was performed. To achieve an equal amount of primary attenuation, the hybrid SM-DVA required 65% higher root-mean-square (RMS) control effort than the hybrid DV-DVA. The numerical model also demonstrated that the hybrid DM-DVA was less sensitive to changes in the system as compared to the hybrid SM-DVA. Additionally, a prototype hybrid DVA was built which could be configured as either the hybrid SM or DM-DVA. The prototype hybrid DVA was used with the feedforward Filtered-X LMS

algorithm to control the vibration of a fixed-free beam. The hybrid SM and DM-DVAs attenuated the primary response by a factor of 11.5 and 12.3, while requiring control efforts of 4.9 and 2.7 V/N RMS, respectively. Thus, the hybrid DM-DVA required 45% less control effort while yielding a higher attenuation ratio in this experiment. These results demonstrate the superior performance of the proposed DM-DVA for broadband control applications as compared to the traditional SM-DVA.

Acknowledgments

First, I would like to thank my advisor, Dr. Ricardo Burdisso, for introducing me to the field of vibrations, for guiding my graduate study, and for offering me the chance to work on a practical and interesting project.

I would also like to acknowledge the other members of my committee, Dr. Harley Cudney and Dr. Scott Hendricks. Both gave me insight into the nature of my project and excellent classroom instruction.

A majority of my knowledge of experimental equipment and procedures must be credited directly to Jerome Smith. I am thankful for his patience, experience, and willingness to help me.

Many other individuals lended advice and assistance on various aspects of this project: Steve Booth, Dr. Jamie Carneal, Florence Deneufve, Dr. Al Wicks, and Dawn Williams.

In addition, I would like to thank my family and my beloved wife, Erica. Their encouragement, love, and support have made this accomplishment possible.

Table of Contents

Chapter 1

Introduction 1

1.1 Previous Work 1

1.2 Proposed Work 6

1.3 Thesis Organization 8

Chapter 2

Dynamic Vibration Absorber Theory 10

2.1 Passive Single-Mass Dynamic Vibration Absorber 10

2.2 Hybrid Single-Mass Dynamic Vibration Absorber 18

2.3 Passive Dual-Mass Dynamic Vibration Absorber 24

2.4 Hybrid Dual-Mass Dynamic Vibration Absorber 29

Chapter 3

Numerical Simulation 37

3.1 Parametric Study 37

3.1.1 Passive DM-DVA 38

3.1.2 Hybrid DM-DVA 47

3.2 Hybrid SM and DM-DVA Comparison 61

3.2.1 Primary Response Attenuation 63

3.2.2 Sensitivity Analysis 66

Chapter 4

Experimental Validation 73

4.1 Experimental Setup 73

4.1.1 Primary System 73

4.1.2 Prototype Hybrid DVA 74

4.1.3 Control Experimental Setup 83

4.2 Experimental Results 85

4.3 Modeling of Experiment 95

4.3.1 Experimental Model 98

4.3.2 Equal Mass Comparison 106

4.3.3 Optimal DM-DVA Tuning 109

Chapter 5

Conclusions and Recommendations 112

5.1 Conclusions 112

5.2 Recommendations 114

Bibliography 116

Appendix A

Frequency-domain feedforward control approximation for the SDOF primary/hybrid DM-DVA system. 120

Appendix B

Frequency-domain model of the experimental system 125

Vita 130

List of Figures

Figure 1.1 Schematic of proposed and traditional hybrid DVAs. 7
Figure 2.1 SDOF Primary System. 11
Figure 2.2 Mobility function of a SDOF primary system. 13
Figure 2.3 Primary/passive SM-DVA system. 15
Figure 2.4 Mobility functions of the primary and primary/passive SM-DVA systems. . . 17
Figure 2.5 Primary/hybrid SM-DVA system. 19
Figure 2.6 Force transmissibility function of the hybrid SM-DVA. 22
Figure 2.7 Applied-force transfer function for the hybrid SM-DVA. 25
Figure 2.8 Primary/passive DM-DVA system. 27
Figure 2.9 Mobility functions of the primary and primary/passive DM-DVA systems. . 28
Figure 2.10 Primary/hybrid DM-DVA system. 30
Figure 2.11 Effect of coupling impedance on the force transmissibility function of the hybrid DM-DVA. 32
Figure 2.12 Force transmissibility of the hybrid DM-DVA. 34
Figure 2.13 Applied-force transfer function for the hybrid SM and DM-DVA. 35
Figure 3.1 Contour of the performance index of the passive DM-DVA with $\mu = 3\%$. . 39
Figure 3.2 Inertance of the primary/passive DM-DVA system with tuning ratios from Fig. 3.2. 41
Figure 3.3 Inertances of the first and second reaction-masses of the passive DM-DVA. 43
Figure 3.4 Contour of the performance index of the passive DM-DVA with $\mu = 7\%$. . 44
Figure 3.5 Optimal tuning ratios for the passive DM-DVA. 46
Figure 3.6 Contour of the performance index for the passive DM-DVA. 48

Figure 3.7 Inertance of the primary, primary/passive, and primary/hybrid DM-DVA systems. 50
Figure 3.8 Contour of the performance index of the hybrid DM-DVA with μ = 3%. . . 51
Figure 3.9 Inertance of the primary/passive DM-DVA system with tuning ratios from Fig. 3.8. 53
Figure 3.10 Inertances of the first and second reaction-masses from the hybrid DM-DVA. 54
Figure 3.11 Contour of the RMS control force of the hybrid DM-DVA with μ = 3%. . 55
Figure 3.12 Contour of the performance index of the hybrid DM-DVA with μ = 5%. . .57
Figure 3.13 Optimal tuning ratios for the hybrid DM-DVA. 58
Figure 3.14 Surface plot of the hybrid performance index 60
Figure 3.15 Comparison of first and second reaction-mass inertance before and after control. 62
Figure 3.16 Inertance of the original primary, primary/passive SM-DVA, and primary/DM-DVA systems. 64
Figure 3.17 Inertance of the original primary, primary/hybrid SM-DVA, and primary/hybrid DM-DVA systems. 65
Figure 3.18 Normalized control force for the hybrid SM and DM-DVAs. 67
Figure 3.19 Hybrid SM and DM-DVA performance indices as functions of the average tuning ratio. 69
Figure 3.20 Required SM and DM-DVA control force as a function of the average tuning ratio. 70
Figure 4.1 Inertance of the free end of the primary structure. 75
Figure 4.2 First and second mode shapes of the primary structure. 76
Figure 4.3 Prototype hybrid DVA. 78
Figure 4.4 Hybrid DVA prototype in SM configuration. 80
Figure 4.5 Hybrid DVA prototype tuning test setup. 81

Figure 4.6 Experimental force transmissibility of the hybrid DVA prototype. 82
Figure 4.7 Vibration control test setup. 84
Figure 4.8 Inertance of the free end of the primary structure with passive DVAs. 86
Figure 4.9 Inertance of the free end of the primary structure with hybrid DVAs. 87
Figure 4.10 Error to reference signal coherence. 89
Figure 4.11 Control signal for the hybrid SM and DM-DVAs. 90
Figure 4.12 Comparison of RMS error signal and control effort levels. 93
Figure 4.13 Time histories of the original primary and primary/passive DVA systems. . 94
Figure 4.14 Time histories of the error and control signals for the hybrid DVAs. 96
Figure 4.15 Comparison of the predicted and measured SM-DVA force transmissibility 99
Figure 4.16 Comparison of the predicted and measured DM-DVA force transmissibility 100
Figure 4.17 Comparison of the predicted and measured inertance of the free end of the primary structure. 101
Figure 4.18 Comparison of the predicted and measured inertance of the primary/passive DM-DVA system. 102
Figure 4.19 Comparison of the predicted and measured inertance of the primary/hybrid DM-DVA system. 103
Figure 4.20 Comparison of the predicted and measured normalized control force of the hybrid DM-DVA. 104
Figure 4.21 Predicted inertance of the passive system for the equal mass comparison. 107
Figure 4.22 Predicted inertance of the hybrid system for the equal mass comparison. 108
Figure 4.23 Predicted control force for the equal mass comparison. 110

List of Tables

Table 3.1 Passive DM-DVA tuning study results. 45
Table 3.2 Hybrid DM-DVA tuning study results. 59
Table 3.3 Comparison of DM-DVA mass motion for varying reaction-mass sizes. 71
Table 4.1 RMS control experiment results. 92
Table 4.2 RMS time domain experiment results. 97
Table 4.3 Comparison of results from the exeriment and the numerical simulation. 105
Table 4.4 Numerical comparison results. 111

Chapter 1

Introduction

1.1 Previous Work

Since its invention in the early 1900's the dynamic vibration absorber (DVA) has been used to attenuate the vibration of many structures. The absorber usually consists of a spring-mass-damper system. When the absorber is mounted on a larger primary structure which is excited by some form of disturbance load, the motion of the structure at the natural frequency of the absorber is significantly reduced. The natural frequency of the absorber is thus selected to match the frequency of the disturbance for narrow-band excitations (i.e. pure tones), or to match a resonance of the primary structure for broad-band inputs. An excellent review of DVA technology can be found in Sun et al. (1995).

Dynamic vibration absorbers can also exist in configurations other than the spring-mass-damper type. The original vibration absorber patent was for a device used to attenuate ship sway (Frahm, 1911). It used two tanks partially filled with liquid. The tanks were linked by two pipes: the lower pipe allowed the liquid to flow back and forth

between the two tanks, while the upper pipe connected the two air cavities. The effect of gravity on the liquid was a restorative force analogous to a spring. Therefore, the mass of the liquid and the gravitational force gave the liquid an oscillatory frequency as it flowed back and forth between the tanks. This oscillation applied a force to the ship which counteracted the effects of the waves on the hull.

In addition to controlling ship sway, DVAs have been applied to many other vibration control problems. DVAs are good candidates for reducing the tonal cabin noise in jet aircraft. For example, on the McDonnell Douglas MD-80 three tonal disturbances related to the shaft speed of the jet engines were being transmitted through the pylons and caused noise to be radiated into the cabin. DVAs were tuned to attenuate the disturbances at each of these frequencies: one during idle, and two occurring at cruise speeds (Lang et al., 1992). These absorbers were mounted in the cabin as well as on the engines, and provided a 6 dB reduction in the sound pressure level measured at three seats in the passenger compartment as compared to the untreated case.

Vibration absorbers have also been used to attenuate the motion of tall buildings due to wind and seismic excitation. In 1977, both the Citicorp Center in New York and Hancock Tower in Boston had large DVAs installed near the top floors to attenuate wind sway (Engineering News-Record, 1977). Although four and six hundred tons, respectively, these DVAs weighed less than 1% of the building's total weight. The Hancock DVA was actually two 300 ton DVAs positioned to eliminate a torsional mode in the building. During heavy wind excitation, oil was pumped under the reaction-mass to elevate it onto a low friction surface. Compressed nitrogen cylinders functioned as the springs for the DVAs.

One of the drawbacks of traditional DVAs is that they may be tuned to only one frequency. In instances where the resonant frequencies of the primary structure and/or frequencies of the disturbance may change, an absorber which can alter its own parameters

would perform better. Several such absorbers, known as adaptive-passive vibration absorbers, have been invented. One such device consists of a mass at the end of a coil spring (Ryan et al., 1993). A servo-motor moves the spring back and forth through a plate effectively changing the number of spring coils between the plate and the mass and thereby changing the tuned frequency of the absorber. A feedback control algorithm uses the acceleration of the primary structure, which is excited by a pure tone, to determine the optimal tuning frequency. Another example of a self-tuning vibration absorber uses two masses mounted on leaf springs which may be tightened or loosened by a servo motor to change its tuning frequency (Wang et al., 1992). Masses which can move along fixed beams to tune the DVA have also been investigated (DiDomenico, 1994). All of these adaptive-passive absorbers rely entirely on the excursion of the absorber's mass to provide the interfering force to the primary structure.

A different approach for adaptive absorbers is the addition of an active force to the absorber. This force is usually applied between the absorber mass and the primary structure. These active/passive or hybrid DVAs provide effective vibration control over a broader frequency range as compared to passive or adaptive-passive DVAs (Sun et al., 1995). Also, in some applications the addition of an active control force reduces the stroke of the absorber, thereby allowing the absorber to be more compact and increasing the fatigue life of the elastic element (Chang et al., 1979).

Several control algorithms have been used with hybrid DVAs. The literature has many examples of hybrid DVAs being used with state feedback algorithms. The effective use of full state feedback to control tonal disturbances has been demonstrated by Chang et al. (1979), Abdel-Rohman (1984) and Lindner et al. (1991). Instead of feeding back all the states, Nishimura et al. (1993) used only the velocity of the primary structure and the position of the absorber mass. Nishimura et al. (1992) also investigated feeding back only the acceleration of the primary structure. This method was deemed effective, but at the

cost of increasing the motion of the absorber mass which may shorten its fatigue life. Nonami et al. (1994) investigated the use of state feedback in conjunction with a disturbance estimator and disturbance rejection controller. Adaptive feedforward algorithms have also been used to increase the effectiveness of DVAs. Burdisso (1995) investigated the use of the filtered-X LMS algorithm to improve the performance of DVAs with seismic disturbances in buildings. A numerical simulation using measured earthquake accelerograms demonstrated that feedforward control made the DVAs more effective.

The applications for hybrid DVAs are numerous and the following examples are intended to illustrate possible hybrid DVA uses. Nagase et al. (1993) suggested the addition of a hybrid DVA to Landmark Tower, in Yokohama, Japan to attenuate wind and seismic disturbances. An active device was chosen because an effective passive device would have been prohibitively large due to the size of the building. The control method employed was state feedback, and the control force was applied to the absorber mass by an AC servo motor. Experimental results obtained using a scale model of the building were promising.

Another application of hybrid DVAs is the reduction of elevator vibration. Most elevators use AC drive motors which produce constant vibration at the standard utility frequency (50 or 60 Hz). Because of the constant disturbance frequency, a passive DVA is well suited to attenuate this vibration. Newly developed high-speed elevators employ variable-speed AC motors. A hybrid DVA has been incorporated to attenuate the vibration of these new elevators (Okada et al., 1990). The control system used by Okada incorporated state feedback to add damping to the system and feedforward to reject certain disturbance frequencies.

During milling operations, an extension is often needed so that the cutter may reach the surface of the workpiece. These extensions add flexibility between the cutter

and the machine and are prone to vibration. The amplitude of this vibration is directly related to the surface finish of the workpiece, so it should be attenuated as much as possible. Hybrid DVAs are good candidates for this application because they can adapt to the various disturbances which will be encountered based on the parameters of the machining operation, e.g. mill size, feed rate, tool speed, and so forth (Liu et al., 1993).

The applications of hybrid DVAs are limited by some of their characteristics. To operate, a hybrid DVA needs a source of power to generate the control force. For this reason hybrid DVAs would be difficult to use in remote applications such as on pipelines. Additionally hybrid DVAs which will be used to attenuate building motion during storms and earthquakes must have auxiliary power units available because of the possibility of a blackout. It has also been claimed that hybrid DVAs exhibit poor reliability under extended operation. Another problem with DVAs is that while they require little control force when used at or near their natural frequency, the amount of control force needed when used above and particularly below their natural frequency increases dramatically (Okada et al., 1990).

Recently, a hybrid DVA was developed which requires less control force for initial activation as compared to a traditional hybrid DVA (Nishimura et al., 1993). It consisted of a passive DVA which had attached to it a smaller hybrid DVA. The hybrid DVA was activated by feeding back the velocity of the primary structure and the position of the passive absorber mass. The new device had several advantages over the traditional single-mass (SM) hybrid DVA. First, the size of the active part of the hybrid DVA was significantly reduced. Second, the control force required to activate this device was less than for a single-mass hybrid DVA alone. Third, the passive DVA, which was located between the primary structure an the hybrid DVA, acted as a low pass filter to remove high frequency noise vibration which occurred in the hybrid device alone. This device was primarily intended for controlling transient vibrations in large civil engineering structures.

1.2 Proposed Work

The most active area of DVA research is in hybrid systems. Hybrid absorbers are favored over purely active systems for two reasons. Purely active systems require significant control effort and are often not reliable, especially for continuous operation. The passive component of the hybrid DVA is reliable and will provide some attenuation, even if the active component fails. Due in part to the passive component, hybrid DVAs in general require less control effort as compared to the purely active system. The main goal in the development of hybrid DVAs is to improve their performance. This can be achieved by the correct integration of passive and active components.

In this thesis, a new hybrid DVA configuration is proposed and investigated. A schematic of this new hybrid DVA is shown in Fig. 1.1 (a). The new DVA consists of two masses, each independently coupled to the primary structure to be controlled. Additionally, the masses may be coupled to each other. In this hybrid dual-mass DVA (DM-DVA) the active force is applied between the two masses. This configuration should be contrasted to the traditional hybrid DVA configuration shown in Fig. 1.1 (b). The traditional DVA consists of only one mass coupled to the primary structure. The main difference between the traditional and proposed hybrid DVA is in the implementation of the control force. In the traditional DVA the control force is applied between the mass and the primary structure while in the new proposed DVA the control force is acting between the masses.

There are two main objectives in developing the hybrid DM-DVA. The first objective is to show that the hybrid DM-DVA can achieve the same structural vibration

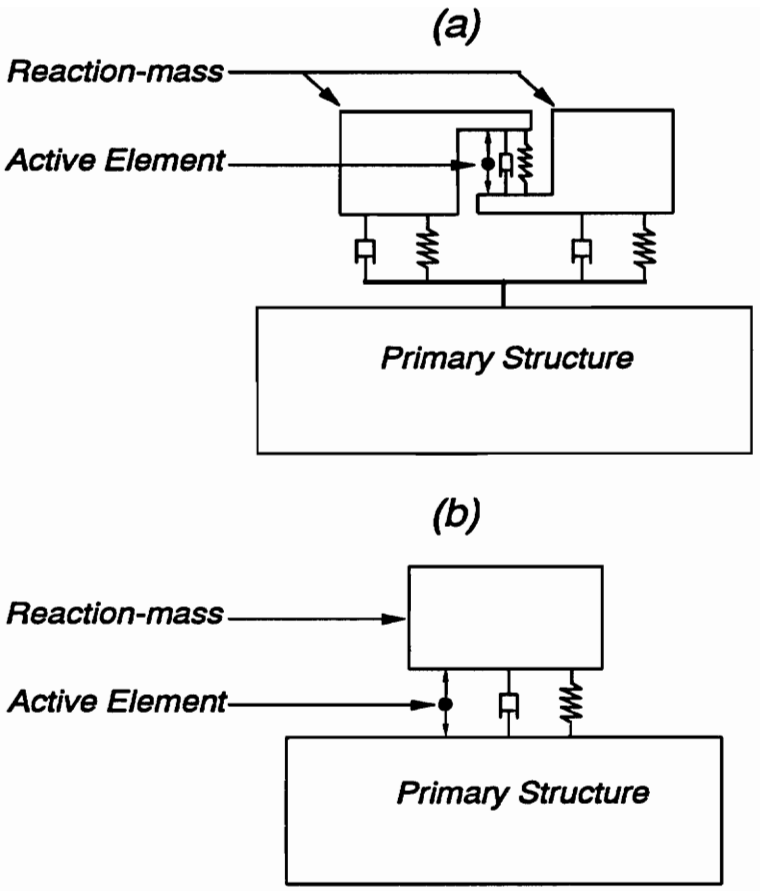

Figure 1.1 Schematic of (a) proposed and (b) traditional hybrid DVAs.

attenuation as an optimally configured SM-DVA while requiring a lower control force. The second objective is to show that the performance of the DM-DVA is less sensitive to changes in the system than the SM-DVA.

The approach taken to achieve these objectives had three distinct stages. First, to gain insight into the physics of both the SM and DM-DVAs, a theoretical analysis of the DVAs was conducted. Both SM and DM configurations were analyzed in both passive and hybrid operation. Second, a computer model of the passive and hybrid DM-DVAs coupled with a single-degree-of-freedom (SDOF) primary structure was used to conduct a parametric study. The goal of this study was to establish guidelines to help in the design of DM-DVAs (i.e. selecting natural frequencies, damping ratios, and so forth) to attenuate the vibration of a simple system. Using the computer model, the sensitivity of the DM-DVA to changes in its configuration was also investigated and compared to the sensitivity of the SM-DVA. Third, an experimental comparison of the hybrid SM and DM-DVA was carried out. A prototype hybrid DVA, which could be configured to function as either a SM or DM-DVA was built and used to control the vibration of a fixed-free beam. The control approach used in the experiments was the adaptive feedforward filtered-X LMS algorithm (Widrow et al., 1985).

1.3 Thesis Organization

This thesis documents the approach taken to investigate the hybrid DM-DVA. In Chapter 2, the vibration absorber theory is presented. As a review, the theory for the passive SM-DVA and the hybrid SM-DVA are presented. Next, the dynamics of the passive DM-DVA are presented. Last, the equations describing the proposed hybrid DM-DVA are detailed.

Chapter 3 presents the frequency domain numerical simulation. This simulation was used primarily to conduct several parametric studies of the passive and hybrid DM-

DVA. The primary system used in these studies was a SDOF, lumped-parameter system. In addition to the parametric studies, the numerical simulation was used to compare the performance of the hybrid SM and DM-DVAs. The control force required by each hybrid DVA and the sensitivity of each hybrid DVA to changes in their natural frequencies were compared.

Chapter 4 explains the setup, procedures, and results from an experimental comparison of the performance of the hybrid SM and DM-DVAs. A prototype hybrid DVA was built which could be configured as either a SM or DM-DVA. In the experiments, the vibration of a fixed-free beam was controlled.

Chapter 5 contains the conclusions and recommendations of the thesis. The theoretical operation of the proposed hybrid DM-DVA is reviewed. The analytical and experimental comparison with the hybrid SM-DVA is also reviewed. The main conclusions of this work are described and recommendations are made on suggested future research opportunities involving the DM-DVA.

Chapter 2

Dynamic Vibration Absorber Theory

In this chapter, the operation of the DVAs is explained. The chapter begins with a review of the passive SM-DVA and then proceeds to a description of the currently-used hybrid SM-DVA. The passive DM-DVA is then presented followed by the hybrid DM-DVA. The motion of the structural systems is described in terms of impedances. Impedance notation was chosen for its compactness and generality. Examples are presented to illustrate various DVA principles, and for simplicity, these examples use simple lumped-parameter models with linear springs and viscous damping.

2.1 Passive Single-Mass Dynamic Vibration Absorber

Throughout this chapter the primary structure to be controlled will be assumed to be a SDOF, lumped parameter system as shown in Fig. 2.1. This simple primary structure was selected to illustrate the behavior of the various DVAs. The generality of the equations to be derived will not be affected by this choice of primary structure.

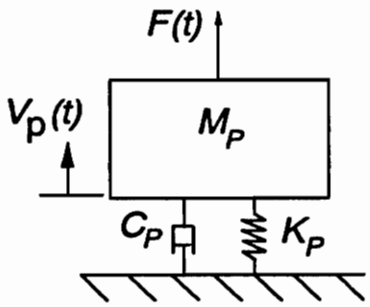

Figure 2. 1 SDOF Primary System.

The primary structure can be characterized by its input or driving-point impedance Z_p. The input impedance is the ratio of the applied force F to the velocity response V_p at the point of application of the force. The motion of the primary structure can then be represented using its input impedance as

$$V_p = \frac{F}{Z_p} = \frac{F}{Z_i} \qquad 2.1$$

where Z_i is the input impedance of the system. For the primary structure in Fig. 2.1 the input impedance is given as

$$Z_i = Z_p = C_p + i\left(\omega M_p - \frac{K_p}{\omega}\right) \qquad 2.2$$

where M_p, K_p, and C_p are the mass, stiffness, and viscous damping constant of the system, respectively; ω is the frequency of the disturbance force; and i is the imaginary number, i.e. $i = \sqrt{-1}$. The dynamic characteristics of a system defined by the input impedance in eq. 2.2 are commonly described by two parameters: the natural frequency ω_n, i.e. $\omega_n = (K_p M_p^{-1})^{1/2}$, and the damping ratio ζ, i.e. $\zeta = C_p/2M_p\omega_n$. The parameters of this structure were selected such that the damping ratio was 0.01 with a natural frequency 100 Hz (i.e. $\omega_n = 2\pi * 100$ Hz $= 200\pi$ rad/s).

Figure 2.2 shows the magnitude of the primary structure's mobility function plotted as a function of the disturbance frequency normalized by the natural frequency. The mobility of a system is the velocity normalized by the applied force and is thus equal to the inverse of the input impedance. When the normalized frequency approaches unity, the input impedance of the structure is small and thus the velocity response of the structure is large and bounded only by the damping in the system. The minimum input

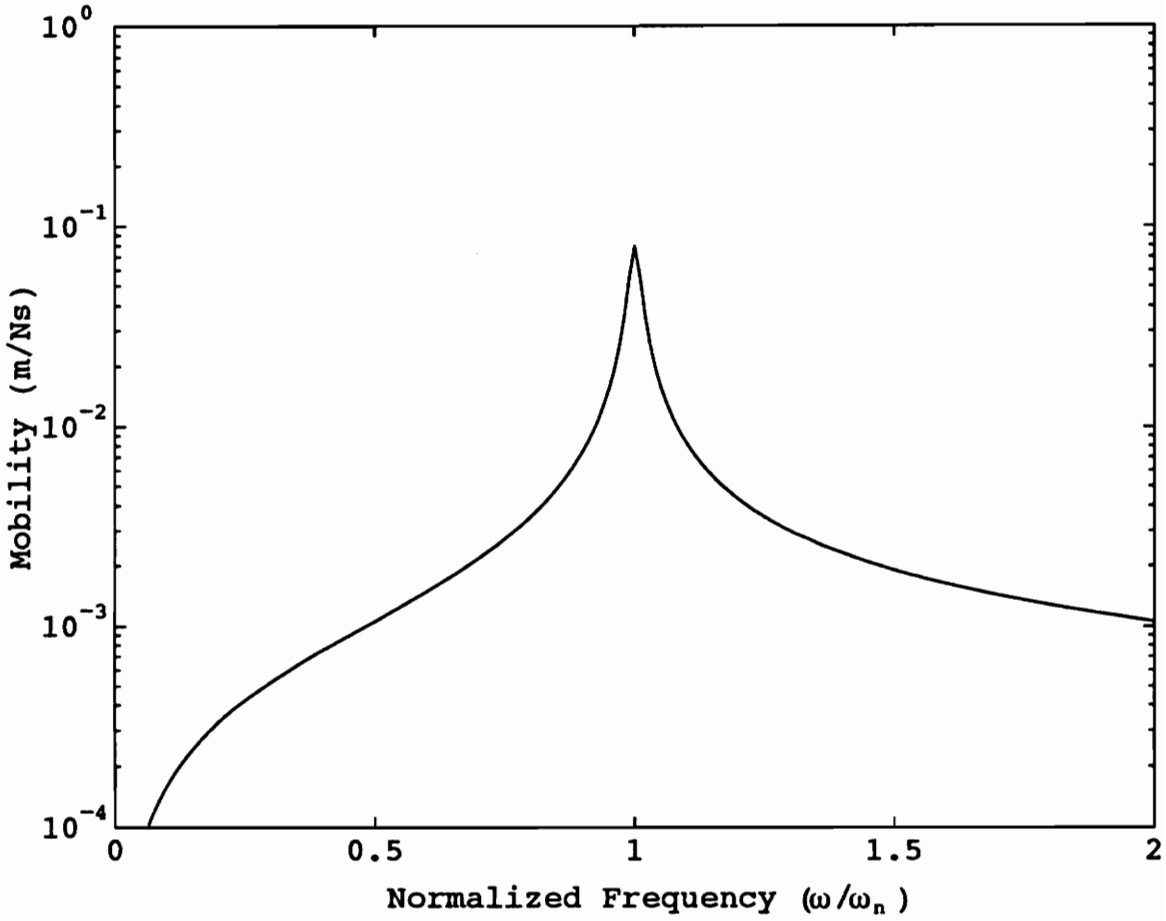

Figure 2. 2 Mobility function of a SDOF primary system.

impedance, and thus the maximum velocity response, occurs at an excitation frequency of $\omega = \omega_n$.

In general, a SM-DVA consists of a mass m_a coupled to the primary structure through a coupling impedance Z_c as shown in Fig. 2.3. The motion of the new primary structure/SM-DVA system is now described by

$$\begin{bmatrix} Z_p + Z_c & -Z_c \\ -Z_c & Z_a \end{bmatrix} \begin{Bmatrix} V_p \\ V_a \end{Bmatrix} = \begin{Bmatrix} F \\ 0 \end{Bmatrix} \qquad 2.3$$

where $Z_a = Z_c + i\omega m_a$ is the driving-point impedance of the absorber alone (i.e. mounted to a rigid base instead of the primary system) and V_a is the velocity of the absorber's mass. The resonance of the SM-DVA ω_a corresponds to the minimum value of its driving impedance Z_a. In this thesis, the natural frequency of the DVA will be referred to as the tuning frequency because the DVA is tuned by adjusting the natural frequency. For broadband frequency disturbances, the tuning frequency is adjusted to match a resonance of the primary structure. For tonal disturbances, the tuning frequency is designed to match the disturbance frequency.

The velocity of the primary structure is obtained from eq. 2.3 as

$$V_p = \frac{Z_a F}{Z_a Z_p + Z_c (Z_a - Z_c)} \qquad 2.4$$

which clearly shows that the velocity response of the primary structure is small at or near the resonance frequency of the SM-DVA when Z_a is small. By adjusting the SM-DVA's natural frequency (i.e. tuning the SM-DVA), the frequency range over which the response of the primary structure will be attenuated can be selected.

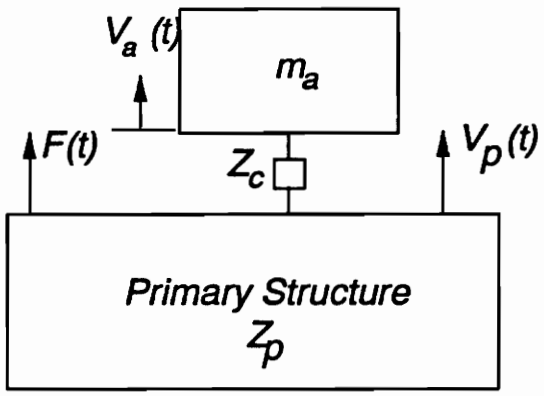

Figure 2. 3 Primary/passive SM-DVA system.

Figure 2.4 shows the magnitude of the primary structure/SM-DVA system's mobility function. For comparison purposes, the mobility function of the original primary system from Fig. 2.2 is also plotted. To generate the plot in Fig. 2.4, the coupling impedance was selected as $Z_c = c_c - ik_c/\omega$, where c_c and k_c are the viscous damping and linear spring constants of the absorber, respectively. Using this form for Z_c, the damping ratio of the SM-DVA ζ_a (i.e. $\zeta_a = c_c/2m_a\omega_a$) was set to 0.01 and the absorber's mass to primary structure's mass ratio $\mu = m_a/M_p$ was 0.05. For broadband vibration attenuation, the absorber is ideally tuned to the natural frequency of the primary structure times the tuning ratio $1/(1+\mu)$ (Snowden, 1968). The tuning ratio is defined as the ratio of the absorber (or tuning) to primary structure natural frequency, i.e. ω_a/ω_n. For the parameters used here, the optimum tuning ratio was 0.95 meaning that the SM-DVA was tuned to 95 Hz.

At or near the tuning frequency of the absorber, the velocity response of the primary structure is significantly attenuated. Even though the SM-DVA significantly attenuates the velocity response of the primary system at the tuning frequency of the SM-DVA, two new resonances are present in the combined system, one below and one above the tuning frequency of the DVA.

Two methods to treat the new resonances are available when using passive vibration absorbers. Firstly, the bandwidth of the trough between these new resonances may be increased by making the mass ratio larger which is not always practical. Secondly, the peaks of the two new resonances may be lowered by increasing the damping in the absorber, but the response of the primary structure at the tuning frequency of the absorber will then be increased (Snowden, 1974).

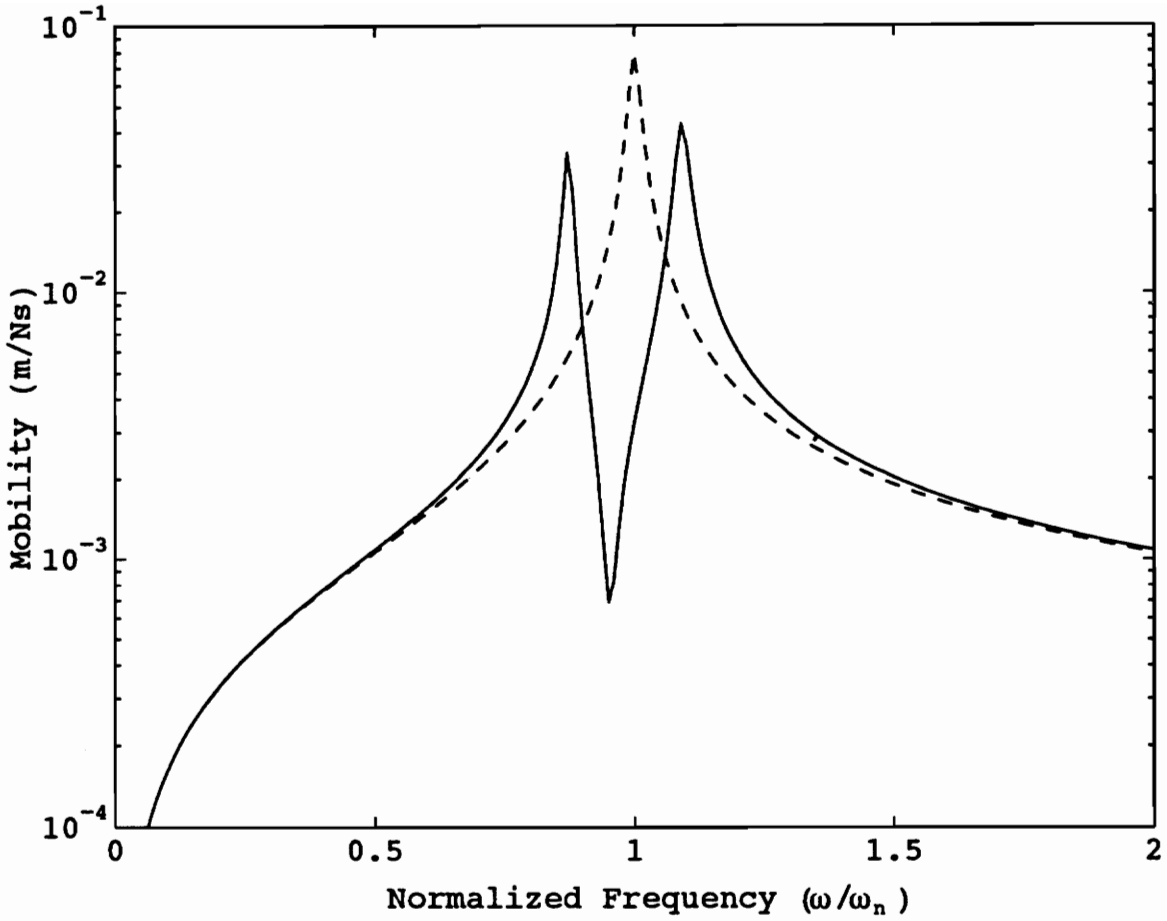

Figure 2. 4 Mobility functions of the (– –) primary and (——) primary/passive SM-DVA systems.

Another convenient way of explaining the effect of the SM-DVA on the primary response V_p is to solve for the new input impedance of the combined system. The input impedance seen by the force F is found from eq. 2.4 as

$$Z_i = Z_p + \frac{i\omega m_a Z_c}{Z_a} \qquad 2.5$$

which shows that the input impedance has two components. The first term is the input impedance of the original primary structure Z_p, while the second term is the contribution due to the SM-DVA. This equation shows that the input impedance of the system becomes large at or near the tuning frequency of the absorber, when Z_a becomes small. The large input impedance at this frequency is what yields the small response of the primary structure. In addition to raising the input impedance near the tuning frequency of the absorber, the SM-DVA causes the input impedance to become small at the two new frequencies which are the resonances that appeared in Fig. 2.4.

2.2 Hybrid Single-Mass Dynamic Vibration Absorber

It is clear that the passive SM-DVA is effective at or near its tuning frequency. Away from its tuning frequency, the effect of the SM-DVA on the primary system may be detrimental. In applications where the SM-DVA will be required to work effectively over a broad range of frequencies, one possible solution is the hybrid SM-DVA. A primary structure/hybrid SM-DVA system is shown in Fig. 2.5. In addition to the coupling impedance between the primary structure and the absorber's mass, the hybrid SM-DVA has a self-balanced active force pair F_c. This force pair will be referred to simply as the control force.

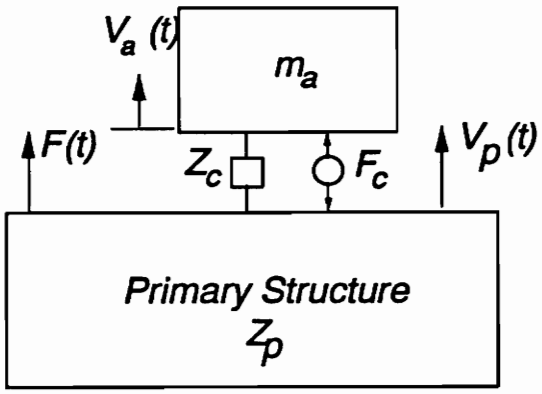

Figure 2. 5 Primary/hybrid SM-DVA system.

The motion of this hybrid system is represented as

$$\begin{bmatrix} Z_p + Z_c & -Z_c \\ -Z_c & Z_a \end{bmatrix} \begin{Bmatrix} V_p \\ V_a \end{Bmatrix} = \begin{Bmatrix} 1 \\ 0 \end{Bmatrix} F + \begin{Bmatrix} -1 \\ 1 \end{Bmatrix} F_c \qquad 2.6$$

In practice, the control force will be obtained by implementing one of the many algorithms available in the literature such as velocity feedback, adaptive feedforward, neural-networks and so forth. Each one of these control approaches offers some unique advantages and drawbacks. The performance of the hybrid DVA will clearly be influenced to some degree by the selected control algorithm. However, all control approaches have as a common goal the reduction of the primary response, i.e. increasing the input impedance Z_i. Thus, in this work the "ideal" control force is defined as the force required to drive the response of the primary structure to zero, thereby increasing the input impedance of the system to infinity. This definition of the control force allows the study to concentrate in the physics of the DVA without introducing particularities associated with the control approach.

Setting V_p = 0 in eq. 2.6, the "ideal" control to disturbance force ratio to yield infinite input impedance is given as

$$\frac{F_c}{F} = \frac{Z_a}{i\omega m_a} \qquad 2.7$$

which shows that this "ideal" control force is independent of the properties of the primary structure.

Further insight into the performance of the hybrid SM-DVA can also be gained by inspecting the hybrid SM-DVA's force transmissibility function. Here, the force transmissibility function T_s is defined as the ratio of the total force applied by the hybrid SM-DVA into an infinite impedance to the control force applied to the hybrid SM-DVA.

Thus, considering the system in Fig. 2.6 (a), the force transmissibility function is easily found as

$$T_s = \frac{F_T}{F_c} = \frac{-i\omega m_a}{Z_a} \qquad 2.8$$

where F_T is the total force applied by the SM-DVA to the infinite impedance. Figure 2.6 (b) shows the two forces which comprise F_T. One component, F_z, is the force transmitted through the coupling impedance while the other component, F_c, is the force generated by the active element.

Comparison of eqs. 2.7 and 2.8 shows that the force transmissibility function is the negative inverse of the "ideal" control force required to drive the primary structure/hybrid SM-DVA system's input impedance to infinity. For example, the larger the force transmissibility function T_s the smaller the required "ideal" control force. Moreover, it is reasonable to assume that the hybrid SM-DVA with the highest force transmissibility function T_s would require the least control effort to achieve a given primary response attenuation. Thus based on this assumption, the force transmissibility function is considered here to be an important first metric for evaluating the performance of hybrid SM-DVAs. The force transmissibility function has several characteristics which make it useful as a performance indicator: (1) the force transmissibility function does not depend on the characteristics of the primary structure, (2) the force transmissibility function is easily measured experimentally and (3) the force transmissibility function is not dependent on the actual control algorithm which will be implemented.

It is important to remark that while the force transmissibility function is a good metric for comparing hybrid SM-DVAs on the basis of the required control force, there are other factors to consider when selecting a hybrid SM-DVA for a specific application. For example, if a feedback control algorithm will be used with a hybrid SM-DVA, the

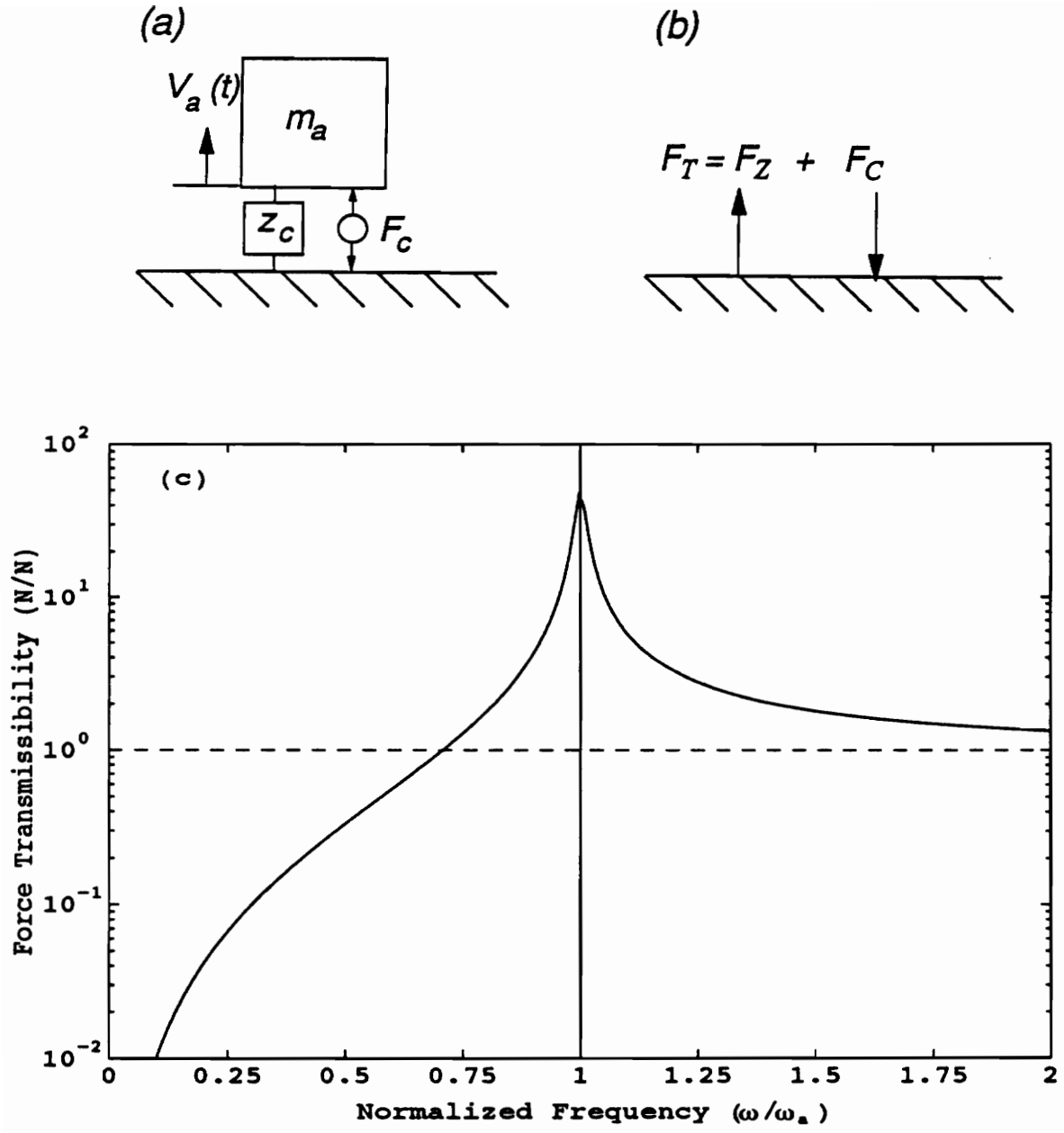

Figure 2. 6 (a) Hybrid SM-DVA on infinite input impedance, (b) the forces applied by the hybrid SM-DVA, (c) force transmissibility function of the hybrid SM-DVA, T_r.

stability of the control system is a critical issue to be taken into account. Also, causality of the control system is an important factor when using feedforward control approaches. These and other aspects in the actual implementation are not considered by using the "ideal" control force defined in eq. 2.7.

The SM-DVA shown in Fig. 2.6 (a) applies the two forces shown in Fig. 2.6 (b) to the infinite impedance. The two forces comprise the force transmissibility function, shown in Fig. 2.6 (c). The force transmissibility function is plotted as a function of the excitation frequency normalized by the tuning frequency of the SM-DVA. The characteristics of the force transmissibility function T_s can be categorized based on one of three frequency ranges of operation. At frequencies well below the tuning frequency of the SM-DVA, the force transmissibility function T_s is significantly less than unity, meaning that the SM-DVA applies less force to the structure than is being applied to it by the active element. Around the tuning frequency of the SM-DVA the force transmissibility function is high. In this frequency range, the total force on the input impedance is more than ten times greater than the control force applied to it. This is the region where the SM-DVA is most effective and has the most control authority. Above the tuning frequency of the SM-DVA the force transmissibility function T_s begins to decrease, and approaches a value of unity at high frequencies, i.e. the SM-DVA neither amplifies nor attenuates the control force.

To understand the behavior of the force transmissibility function T_s in these three distinct frequency regions, the transfer function between the force applied through the coupling impedance F_z and the force control force F_c is investigated. This transfer function is easily shown to be

$$\frac{F_z}{F_c} = -\frac{Z_c}{Z_a} \qquad 2.9$$

The negative sign arises because the control force causing the response of the reaction mass is in the opposite direction from the control force applied to the infinite impedance.

The magnitude and phase of the force transfer function in eq. 2.9 is shown in Fig. 2.7. At low frequencies the two forces applied by the SM-DVA are nearly equal in magnitude and opposite in phase and thus cancel each other. Near the tuning frequency of the SM-DVA, the transfer function becomes large (i.e. $F_z >> F_c$). This is because at the resonance of the SM-DVA, the motion of the absorber's mass imparts a large force F_z to the primary structure. Above the resonance of the SM-DVA, as the frequency increases the inertia of the mass causes its motion to decrease thereby reducing the force applied through the coupling impedance F_z. Therefore, at high frequencies the total applied force F_T approaches the applied control force F_c and the force transmissibility function T_s approaches unity.

2.3 Passive Dual-Mass Dynamic Vibration Absorber

The hybrid SM-DVA had one region of high force transmissibility near its resonance, as was shown in Figure 2.6 (c). In certain applications such as for a broadband disturbance, a DVA with high force transmissibility over a large frequency range may be required. This is the goal of the proposed hybrid DM-DVA.

Before analyzing the hybrid DM-DVA, the equations of motion for a passive DM-DVA will first be investigated. As with the passive and hybrid SM-DVAs, understanding the characteristics of the passive DM-DVA is beneficial when studying the hybrid DM-DVA.

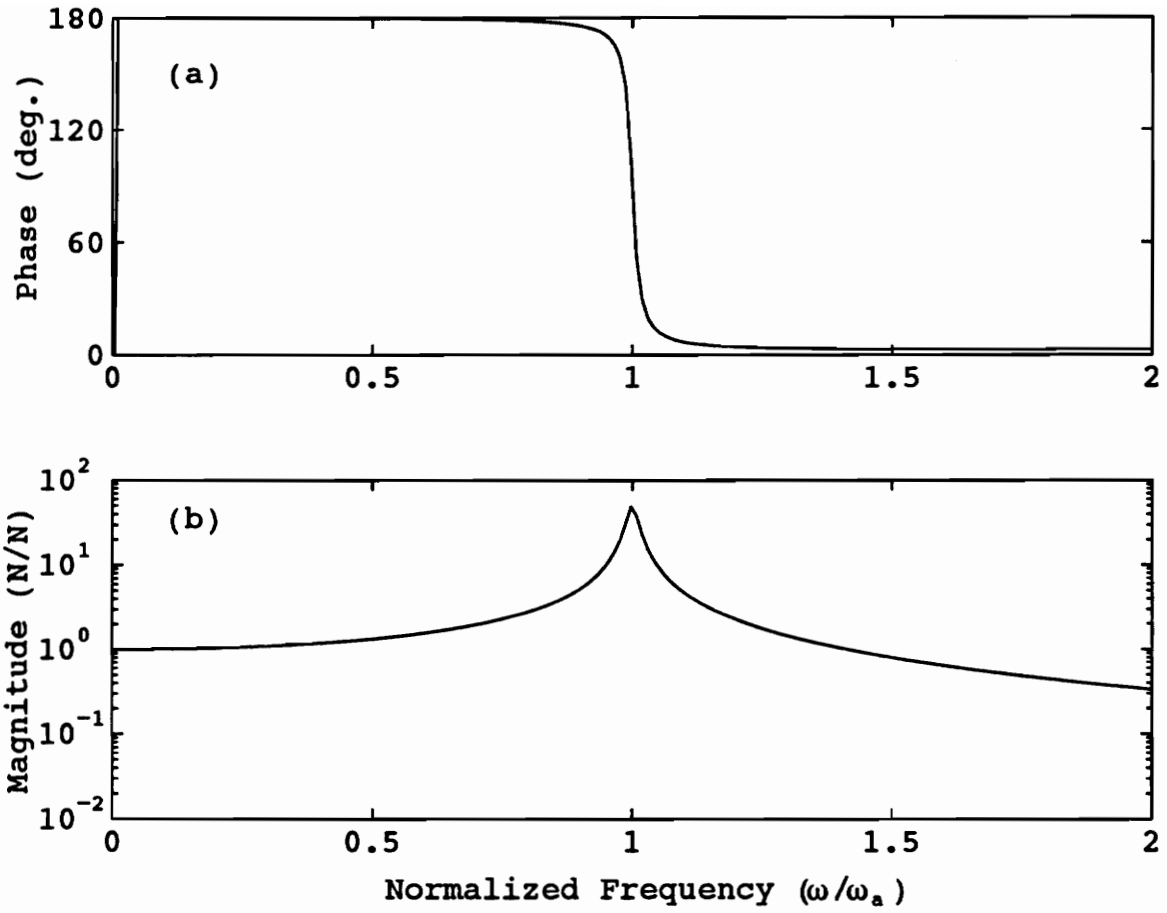

Figure 2. 7 (a) phase and (b) magnitude of the applied-force transfer function for the hybrid SM-DVA.

A passive DM-DVA attached to a primary structure is shown in Fig. 2.8. It consists of two reaction masses, each attached to the primary structure through coupling impedances, Z_{c1} and Z_{c2}, and to each other by Z_{cc}. The dynamics of this system are represented as

$$\begin{bmatrix} Z_p + Z_{c1} & -Z_{c1} & -Z_{c2} \\ -Z_{c1} & Z_{a1} + Z_{cc} & -Z_{cc} \\ -Z_{c2} & -Z_{cc} & Z_{a2} + Z_{cc} \end{bmatrix} \begin{Bmatrix} V_p \\ V_1 \\ V_2 \end{Bmatrix} = \begin{Bmatrix} F \\ 0 \\ 0 \end{Bmatrix} \qquad \textbf{2.10}$$

where V_1 and V_2 are the velocities of the reaction masses, respectively and Z_{a1} and Z_{a2} are the driving-point impedances of the first and second reaction-masses, respectively. The driving-point impedance Z_{a1} and Z_{a2} are of the form $Z_{ak} = Z_{ck} + i\omega m_{ak}$ for $k = 1,2$.

As it will be shown in Section 2.4, the coupling impedance between the absorber's masses Z_{cc} is detrimental to the performance of the hybrid DM-DVA. Thus it will be dropped from the analysis of the passive DM-DVA. Setting $Z_{cc} = 0$ in eq. 2.10 allows the absorbers to be decoupled and the input impedance of the primary system with the passive DM-DVA can be written as

$$Z_i = Z_p + \frac{i\omega m_{a1} Z_{c1}}{Z_{a1}} + \frac{i\omega m_{a2} Z_{c2}}{Z_{a2}} \qquad \textbf{2.11}$$

which shows that the passive contribution of the DM-DVA to the input impedance of the system is simply the combination of the contributions of the two passive SM-DVAs.

The magnitude of the primary/passive DM-DVA system's mobility function is shown in Fig. 2.9. Again for simplicity, the coupling impedances are selected to be linear springs and viscous dampers. Thus, the DM-DVA has two damping, mass, and tuning ratios each of which is defined as for the SM-DVA. The damping ratios are both set to 0.01. The mass ratios are assumed to be equal and combined into an overall mass ratio

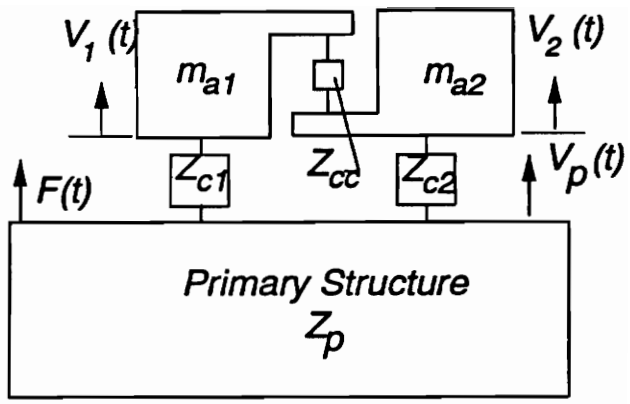

Figure 2. 8 Primary/passive DM-DVA system.

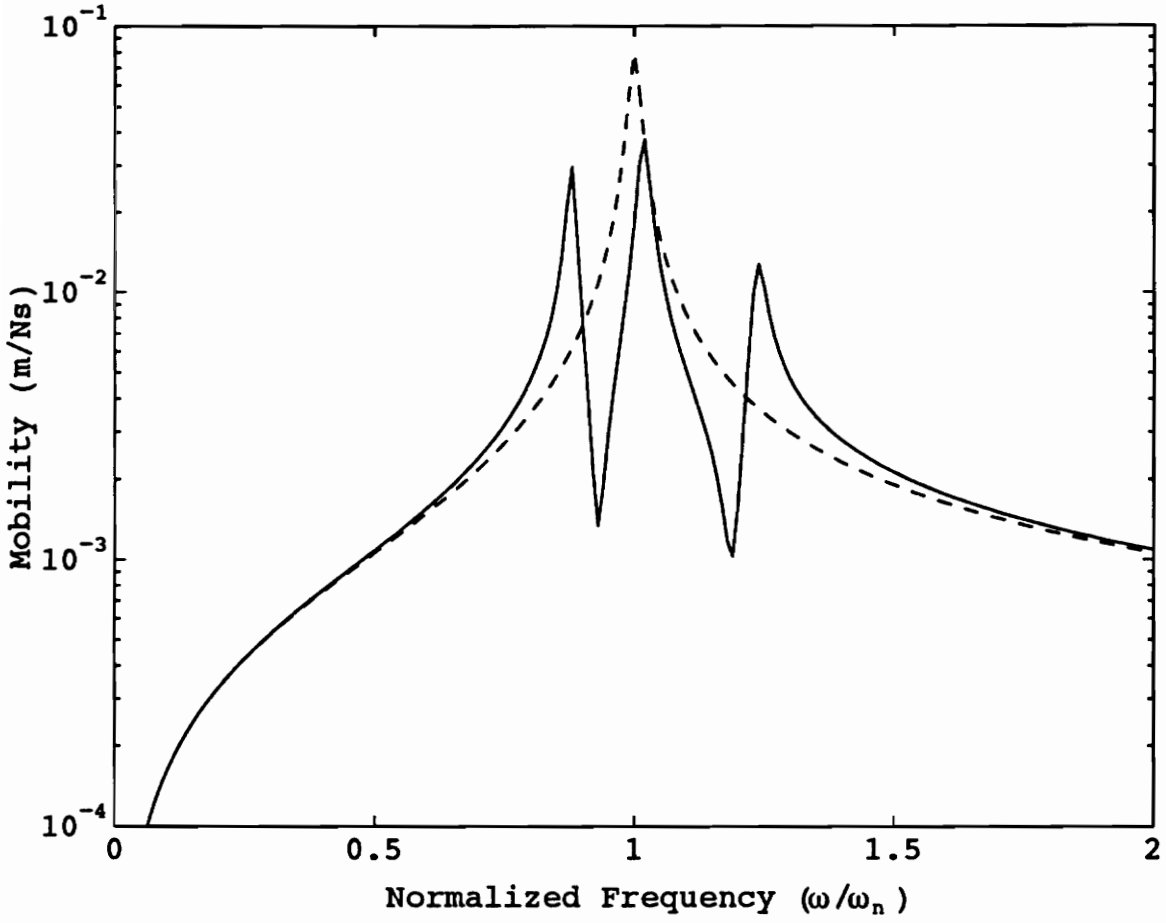

Figure 2. 9 Mobility function of the (– –) primary and (——) primary/passive DM-DVA systems.

$\mu = (m_{a1}+m_{a2})/M_p$. The total mass ratio was 0.05. The tuning ratios of the DM-DVA were also defined as the tuning frequencies of the DM-DVA divided by the natural frequency of the primary system. The tuning ratios were 0.93 and 1.16, which were selected based on the parametric study performed in Chapter 3.

Fig. 2.9 shows that the attenuation achieved by the passive DM-DVA was not significant near the natural frequency of the primary system. The passive DM-DVA caused two notches to appear in the response of the primary structure, but they do not correspond to the resonance frequency of the primary structure. As expected, the passive DM-DVA also caused two additional resonances.

2.4 Hybrid Dual-Mass Dynamic Vibration Absorber

The hybrid DM-DVA consists of the passive DM-DVA with an active control force pair F_c applied between the reaction masses as shown in Fig. 2.10. The active force acts in parallel with the coupling impedance Z_{cc} and couples the two SM-DVAs. The motion of the primary system coupled with the hybrid DM-DVA is described by

$$\begin{bmatrix} Z_p + Z_{c1} & -Z_{c1} & -Z_{c2} \\ -Z_{c1} & Z_{a1} + Z_{cc} & -Z_{cc} \\ -Z_{c2} & -Z_{cc} & Z_{a2} + Z_{cc} \end{bmatrix} \begin{Bmatrix} V_p \\ V_1 \\ V_2 \end{Bmatrix} = \begin{Bmatrix} 1 \\ 0 \\ 0 \end{Bmatrix} F + \begin{Bmatrix} 0 \\ 1 \\ -1 \end{Bmatrix} F_c \qquad 2.12$$

where $Z_{ak} = Z_{ck} + i\omega m_{ak}$ for $k = 1,2$ is the driving-point impedance of the k_{th} reaction-mass alone, Z_{ck} for $k = 1,2$ is the coupling impedance between each mass and the primary structure and V_1 and V_2 are the velocities of m_{a1} and m_{a2}, respectively. The DM-DVA coupling impedances Z_{c1}, Z_{c2}, and Z_{cc} will be assumed to have the same form as the SM-

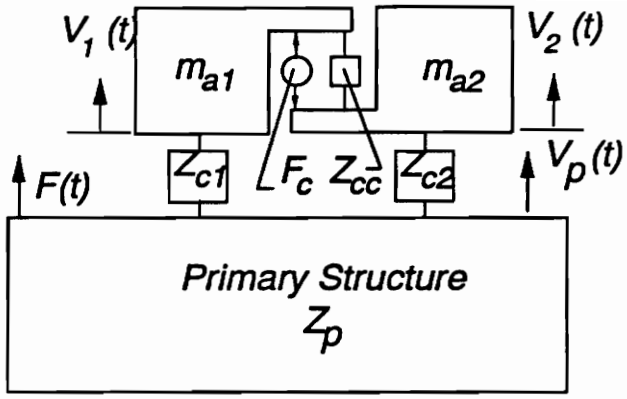

Figure 2. 10 Primary/hybrid DM-DVA system.

DVA coupling impedance Z_c (i.e. linear springs and viscous dampers) in all the example plots.

As with the hybrid SM DVA, the role of the control force is interpreted as actively increasing the input impedance of the primary structure. The "ideal" control force which yields infinite input impedance Z_i is again obtained by setting the velocity of the primary structure $V_p = 0$ in eq. 2.12. The force transmissibility function of the DM-DVA is also a good first metric for evaluating the hybrid DM-DVA's performance. As with the hybrid SM-DVA, the negative inverse of the "ideal" control to disturbance force ratio is equal to the force transmissibility function of the hybrid DM-DVA. The force transmissibility function T_d of the hybrid DM DVA is given by

$$T_d = \frac{Z_{c1}Z_{a2} - Z_{c2}Z_{a1}}{Z_{a1}Z_{a2} + Z_{cc}(Z_{a1} + Z_{a2})} \qquad 2.13$$

To explore the effect of the coupling impedance between the masses Z_{cc} on the DM-DVA force transmissibility function T_d, the force transmissibility functions of hybrid DM-DVAs with and without this coupling impedance were compared. On the uncoupled DM-DVA, the damping ratios were set to 0.01. These corresponding damper values were also used with the coupled DM-DVA. Both DM-DVAs had tuning ratios of 0.7 and 1.3.

Figure 2.11 (a) shows the force transmissibility function of the hybrid SM-DVA with and without a spring coupling the reaction-masses, i.e. $Z_{cc} = -ik_{cc}/\omega$ and $Z_{cc} = 0$. The magnitude of the force transmissibility function was lowered regardless of the value of the coupling impedance. For the example shown, the spring values in the coupled system were on the same order of magnitude, with the values of k_{c1}, k_{c2}, and k_{cc} being $1\text{x}10^5$, $3.6\text{x}10^5$, and $2\text{x}10^5$ N/m, respectively. Figure 2.11 (b) shows the force transmissibility function of the hybrid SM-DVA with and without a damper coupling the reaction-masses, i.e. $Z_{cc} = c_{cc}$ and $Z_{cc} = 0$. Again, the magnitude of the force transmissibility function was

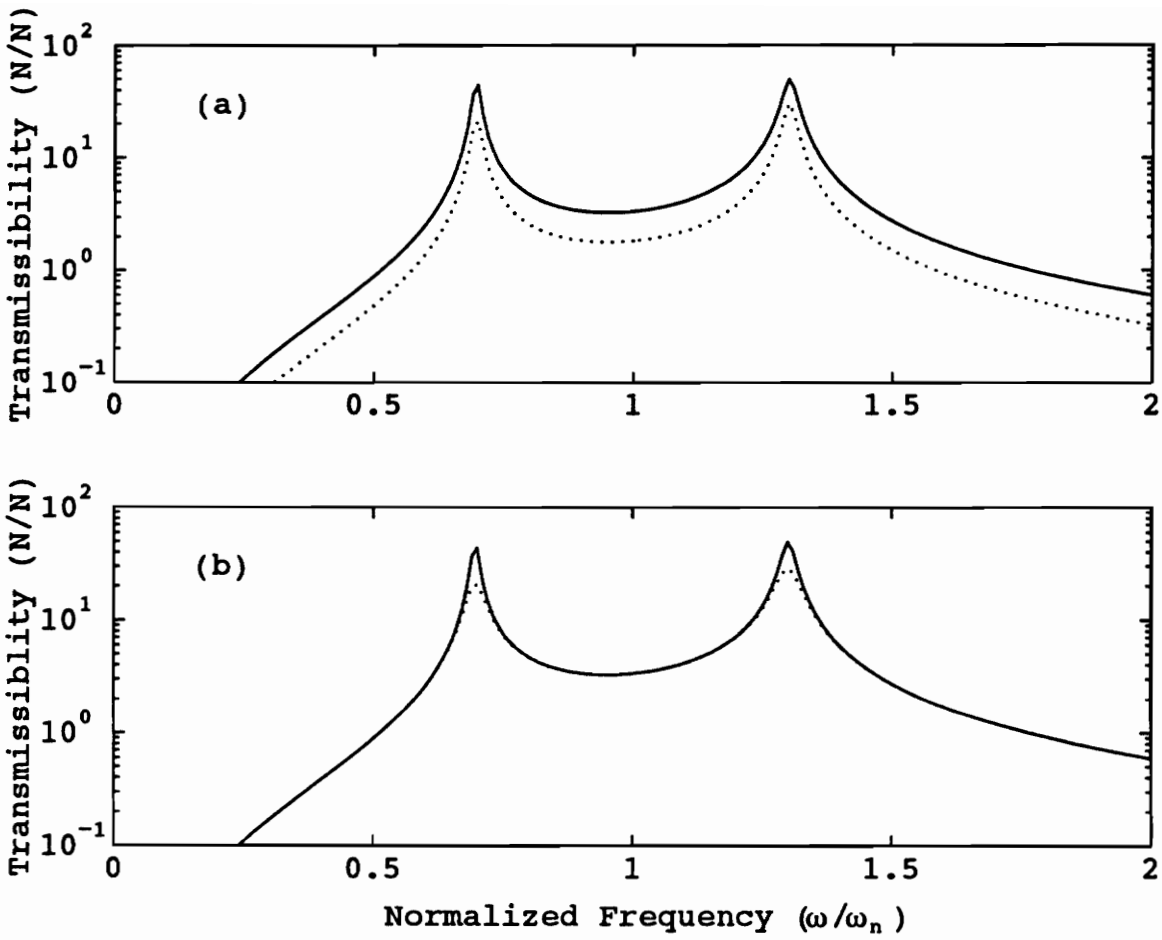

Figure 2. 11 (a) Force transmissibility function of the hybrid DM-DVA with (——) no and with (• • •) a spring coupling impedance, and with (——) no and with (• • •) a damper coupling impedance.

lowered regardless of the value of the coupling impedance. The damping values within the coupled system were again on the same order of magnitude, with the values of c_{c1}, c_{c2}, and c_{cc} being 8.7, 16.3, and 12 Ns/m.

The behavior of the force transmissibility function of the hybrid DM-DVA is now investigated and compared to the SM-DVA. To this end, the force transmissibility function T_d of the hybrid DM-DVA from eq. 2.13 (for $Z_{cc} = 0$) is shown in Fig. 2.12, along with the hybrid SM-DVA force transmissibility function T_s from Fig. 2.6. The hybrid DM-DVA has the same total reaction-mass as the hybrid SM-DVA ($m_{a1} + m_{a2} = m_a$). The tuning ratios of the DM-DVA for this primary structure which has a natural frequency of 100 Hz are again 0.7 and 1.3. In this figure, the frequency axis is normalized by the primary structure natural frequency. The force transmissibility function of the hybrid DM-DVA has two peaks, one at each tuning frequency of the DM-DVA. At low frequencies, T_d diminishes as does T_s but not as steeply. Above the second resonance of the DM-DVA, T_d drops to a value lower than T_s and eventually diminishes.

The behavior of the force transmissibility function of the hybrid DM-DVA can be explained by examining the transfer function between the two forces F_{z1} and F_{z2} applied by the DM-DVA to the infinite impedance (see Figures 2.13 (a) and (b)). It is easy to show that the force transfer function is

$$\frac{F_{z1}}{F_{z2}} = \frac{Z_{c1}Z_{a2}}{Z_{c2}Z_{a1}} \qquad \textbf{2.14}$$

This force transfer function from eq. 2.14 is shown in Fig. 2.13. The force transfer function F_z/F_c for the SM-DVA is also shown. The DM-DVA force transfer function has five distinct frequency ranges. At frequencies well below the first transfer function, the forces applied by the hybrid DM-DVA are of nearly equal magnitude and opposite phase. Thus, these forces cancel each other out, leading to the low force transmissibility function

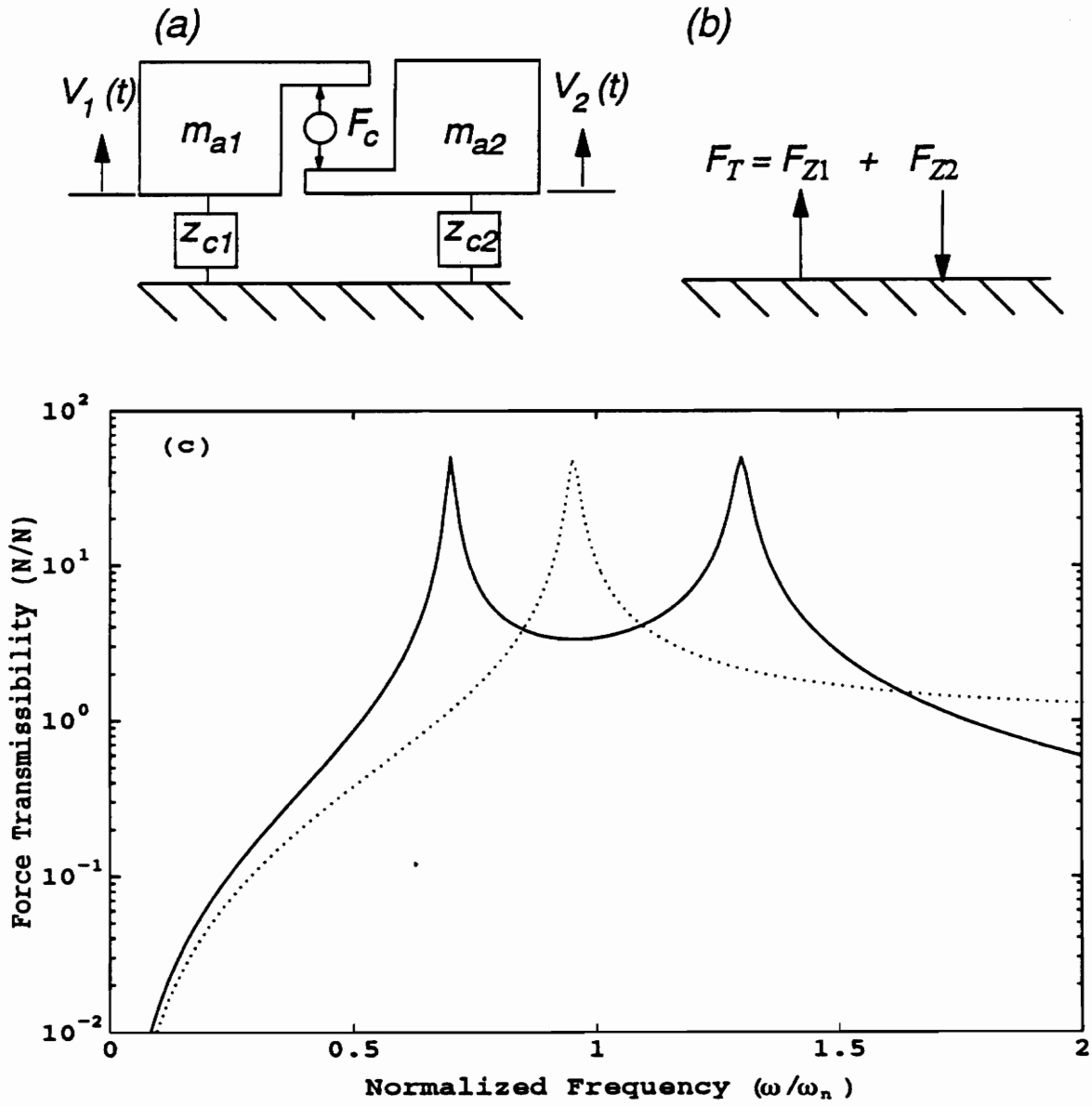

Figure 2. 12 (a) Hybrid DM-DVA on infinite input impedance, (b) the forces applied by the hybrid DM-DVA, (c) force transmissibility function of (• • •) the hybrid SM-DVA, T_s, and (——) the hybrid DM-DVA, T_d.

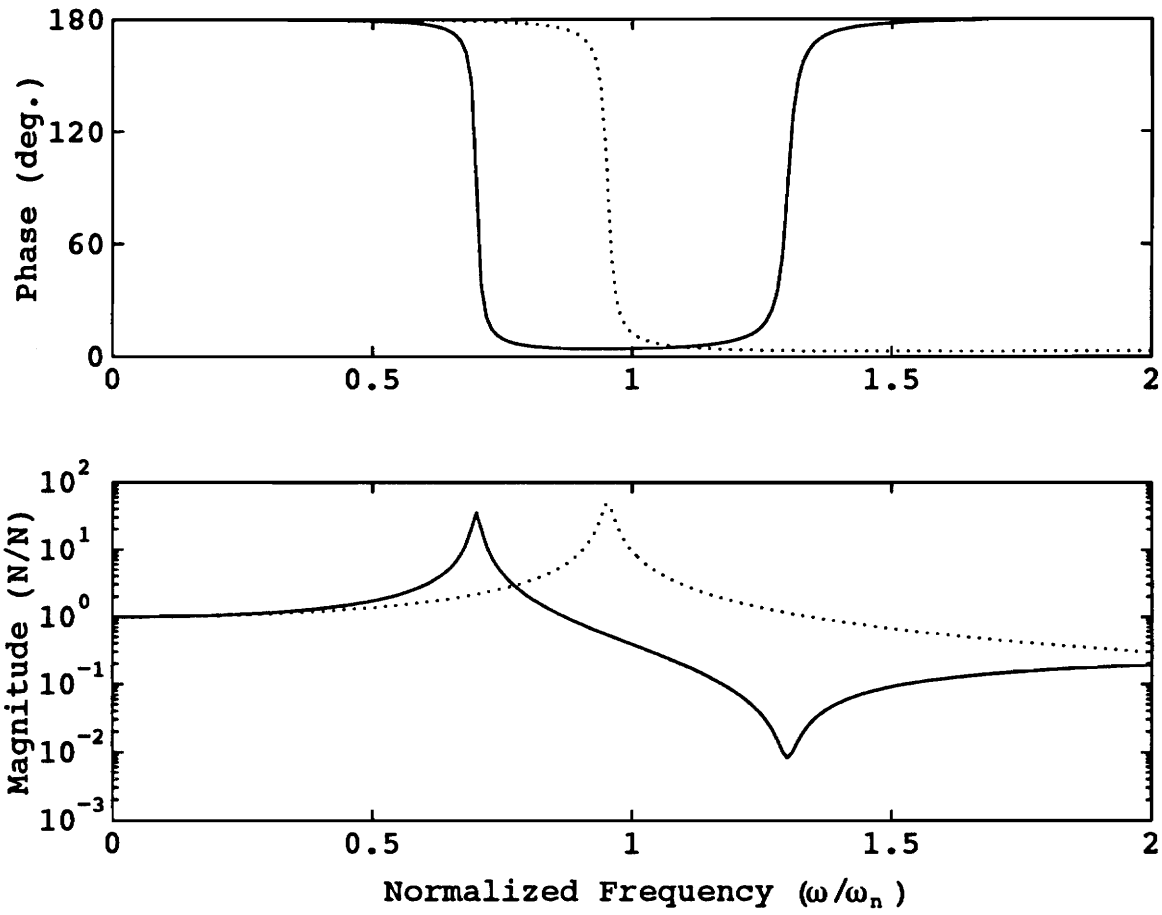

Figure 2. 13 (a) Phase and (b) magnitude of the applied-force transfer function for the (• • •) hybrid SM and (——) hybrid DM-DVAs.

at these frequencies. At or near the first tuning frequency of the DM-DVA, the magnitude of the force applied by the lower-tuning, or first, reaction-mass becomes much larger than the other applied force. This results in a large force transmissibility function magnitude. Between the first and second tuning frequencies, neither of the masses are at a resonance condition, but the forces they are applying are in phase, and thus do not cancel out. At or near the second tuning frequency, the force applied by the second reaction-mass is much larger than that from the first, which is apparent from a low force transfer function magnitude. However this force yields a high force transmissibility function magnitude. At frequencies well above the second tuning frequency of the DM-DVA, the applied forces are again of nearly equal magnitude and opposite phase. Thus, at high frequencies, the magnitude of the force transmissibility function of the hybrid DM-DVA approaches zero.

Chapter 3

Numerical Simulation

In this chapter, the effects of various DM-DVA parameters on its performance are investigated numerically. A parametric study of the effects of the damping and tuning ratios of both the passive and hybrid DM-DVA was conducted. Using the parametric study results, a comparison was made between the performance of the SM and DM-DVA.

3.1 Parametric Study

The properties of a SM-DVA are defined by the mass, damping and tuning ratios. The DM-DVA is characterized by the same parameters, except that there are two of each ratio. In this parametric study, the two mass and damping ratios of the DM-DVA are assumed to have the same values. Thus, there are a total of four parameters to be investigated: the mass ratio, the damping ratio, and the two tuning ratios.

The numerical model is of a SDOF primary/DM-DVA system. The SDOF primary structure was a spring-mass-damper system. This system was chosen because of its simplicity. Since the modes of a structure (in particular those with low modal densities) behave as SDOF systems, the guidelines established with the SDOF parametric study can be directly applied to more complex structures.

In the parametric studies the primary structure had a natural frequency of 100 Hz, a damping ratio of 0.01, and a mass of 1 kg. The acceleration of the primary system was selected as the response to be controlled in the [0 - 200 Hz] frequency range. To quantify the performance of the DVA over this frequency range, the root-mean-squared (RMS) value of the acceleration was computed for the passive and hybrid DM-DVA configurations. Moreover, a figure of merit or performance index Π was defined as the ratio of the RMS of the acceleration with the DVA (passive or hybrid) to the RMS value of the original primary system acceleration. The objective of the study was then to find an optimal DM-DVA configuration which minimized this performance index Π. For convenience, the DVA parameters which minimize the performance index will be referred to as the optimal values in this work. However, this does not imply that they are the results of an optimization study.

3.1.1 Passive DM-DVA

The effect of the tuning frequencies of the passive DM-DVA was investigated first. Two parameters were defined to describe the tuning frequencies of the DM-DVA: the bandwidth Γ, defined as the difference in tuning frequencies, and the average of the tuning frequencies Ω. The optimal tuning ratios can be easily determined from the optimal bandwidth Γ and average tuning frequency Ω. These optimal tuning ratios will be presented for mass ratios ranging from 0.01 to 0.10 and damping ratios of 0.05. Damping ratios of 0.01 and 0.025 were also investigated and were found to have little effect on the optimal tuning ratios.

Figure 3.1 shows a contour plot of the performance index Π as a function of both the bandwidth Γ and the average tuning frequency Ω of the DM-DVA for a mass ratio of 0.03. Both the bandwidth and average tuning frequency were normalized by the natural frequency of the primary structure. The contour plot has a minimum, indicated as point A,

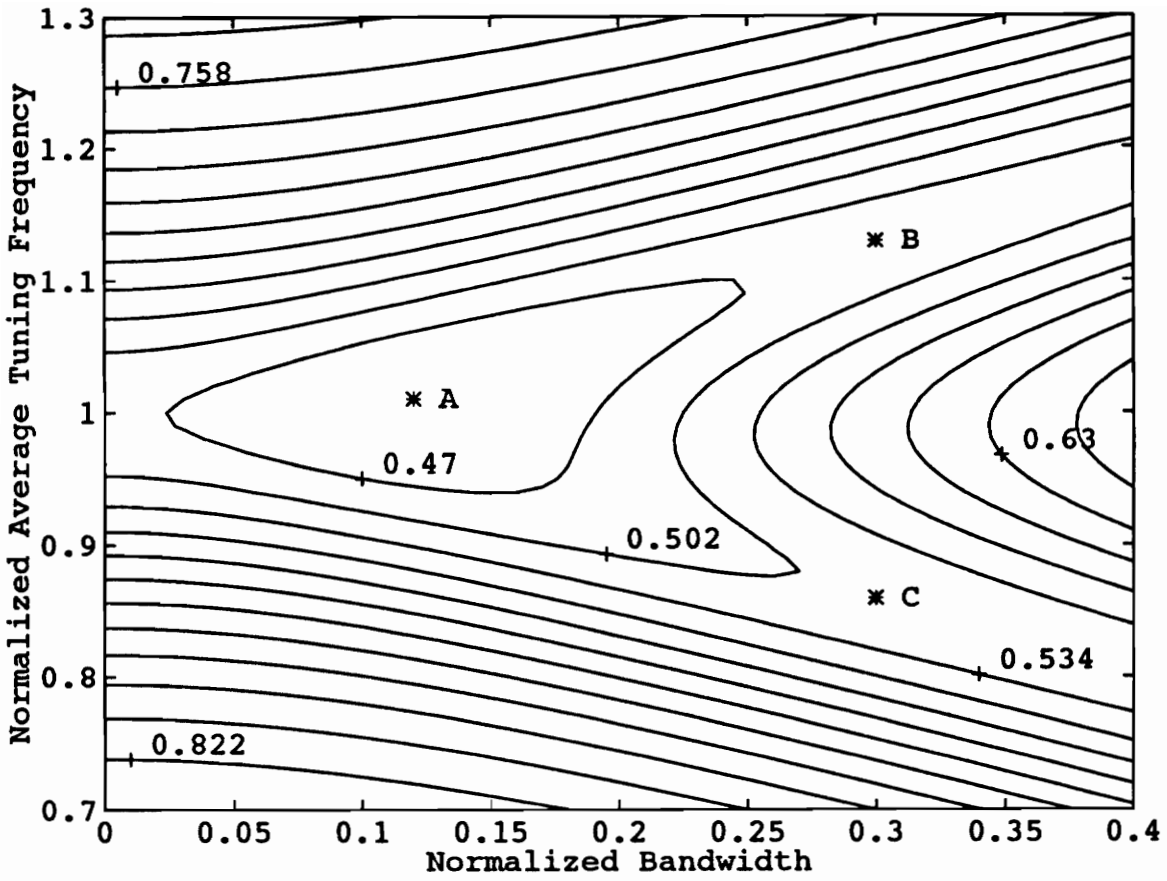

Figure 3. 1 Contour of the performance index for the passive DM-DVA with $\mu = 3\%$ as a function of the normalized bandwidth and average tuning frequency.

which corresponds to a normalized bandwidth of 0.12 and a normalized average tuning frequency of 1.01. Again, the minimum value of the performance index Π indicates the best DVA performance. These values mean that the natural frequency of the primary structure falls between the tuning frequencies of the DM-DVA. Moreover, the two tuning frequencies are close in value as compared to the natural frequency of the primary structure. The closeness of the contour lines in the vertical direction indicates that the performance index of the passive DM-DVA increases dramatically as the average tuning frequency of the DVA is changed while holding the bandwidth fixed. On the other hand, the performance index is more tolerant to changes in the bandwidth for a fixed average tuning frequency. In addition to the minimum at point A, the contour plot has two nearly symmetric valleys in which the performance index has values similar to that at the minimum, i.e. point A. These valleys are marked by points B and C.

Figure 3.2 shows the acceleration of the primary structure normalized by the input force, i.e. the inertance, with no DVAs and with DM-DVAs configured as shown at points A, B, and C in Fig. 3.1. This figure shows that the three DM-DVA configurations attenuate the primary structure resonance in two distinct ways. The configuration at point A has tuning frequencies which are both close to the resonance of the primary system, implying that both reaction-masses are contributing to the reduction of the primary response. This configuration has the best performance index, i.e. $\Pi = 0.44$. The configurations from points B and C each had one tuning frequency near the resonance frequency of the primary structure, with the other tuning frequency higher or lower than the primary structure resonance. The DM-DVA in either of these configurations is behaving as a SM-DVA because only one reaction-mass is responsible for the attenuation of the primary acceleration. These configurations did not work as well as the configuration from point A, with performance indices of 0.48 and 0.51 for the configurations from points B and C, respectively.

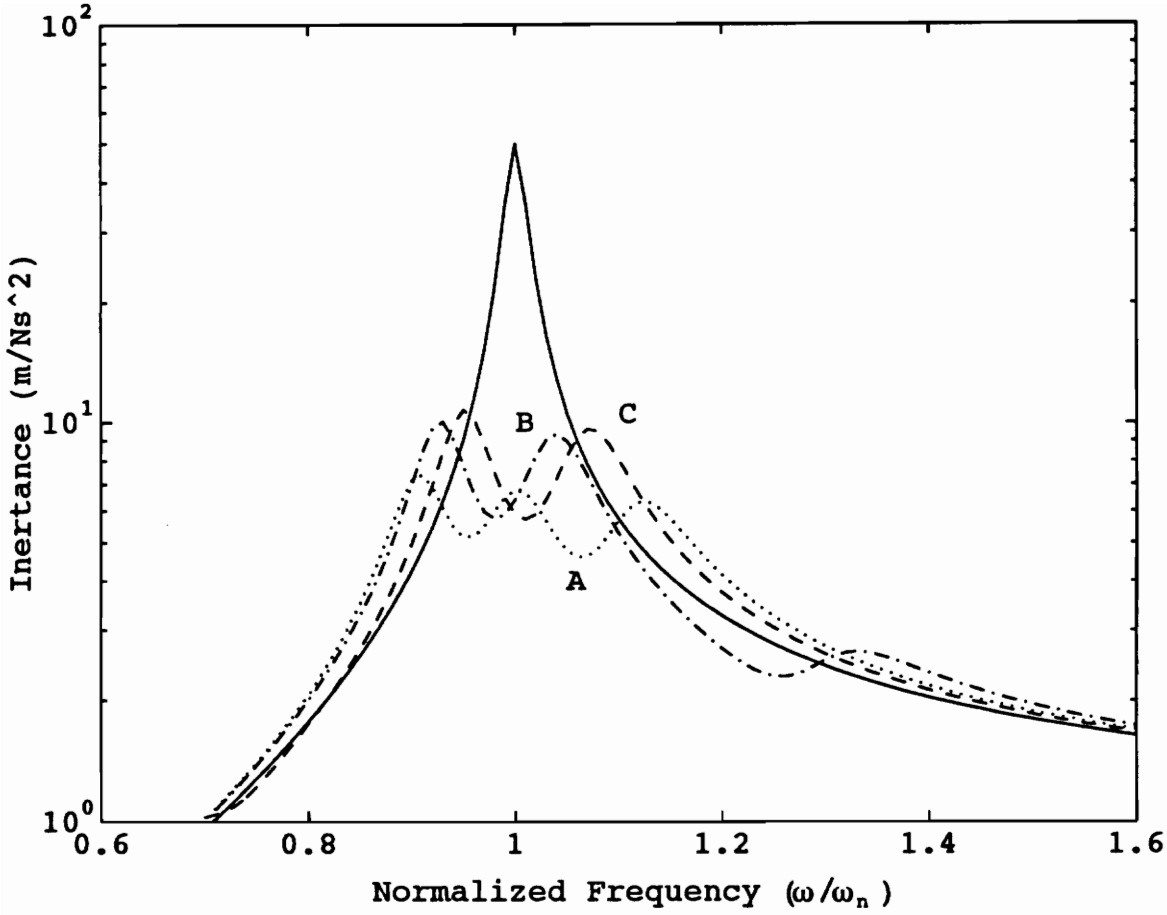

Figure 3. 2 Inertance of the (—) primary structure and of the primary/passive DM-DVA systems with tuning ratios from position (• • •) A, (—•—) B, and (– –) C from position 3.1.

Some insight into the contributions of the reaction-masses to the attenuation of the primary response may be found by looking at the motion of the reaction-masses. Figure 3.3 (a) shows the inertance of the reaction-masses for the DM-DVA in the configuration corresponding to point A from Fig. 3.2. The motion of the two masses is of similar magnitude. On the other hand, Fig. 3.3 (b) shows the reaction-mass motion for the DM-DVA in the configuration of point B. The motion of the lower-tuned mass, which was tuned near the resonance of the primary structure, has a high response again indicating that it is primarily working as an SM-DVA. Figure 3.3 (c) shows the results for the configuration from point C. The motion of the higher-tuned mass, which was tuned near the resonance of the primary structure, is higher indicating that it is behaving as a SM-DVA.

Figure 3.4 shows a contour plot of the performance index Π as a function of both the bandwidth Γ and the average tuning frequency Ω of the DM-DVA for a mass ratio of 0.07 and the same damping ratios of 0.05. The contour plot is similar to the contour in Fig. 3.1. There is still one minimum (i.e. point A) as well as two valleys (i.e. points B and C) as was seen for the case with the mass ratio of 0.03. The value of the performance index at the minimum is 0.38. This minimum performance index value is lower than the minimum with the 0.03 mass ratio, which shows that with increasing mass ratios the passive DM-DVA becomes more effective. The minimum occurs at a normalized bandwidth of 0.2 and an average tuning frequency of 1.02. Table 3.1 summarizes the results of this parametric study for mass ratios of 0.03 and 0.07.

The optimum (i.e. configuration A) tuning frequencies as a function of the mass ratio are shown in Fig. 3.5. This figure shows that the tuning frequencies of the passive DM-DVA are not symmetric about the resonance of the primary system. Also, as the mass ratio was increased, the optimal normalized bandwidth also increased. The average

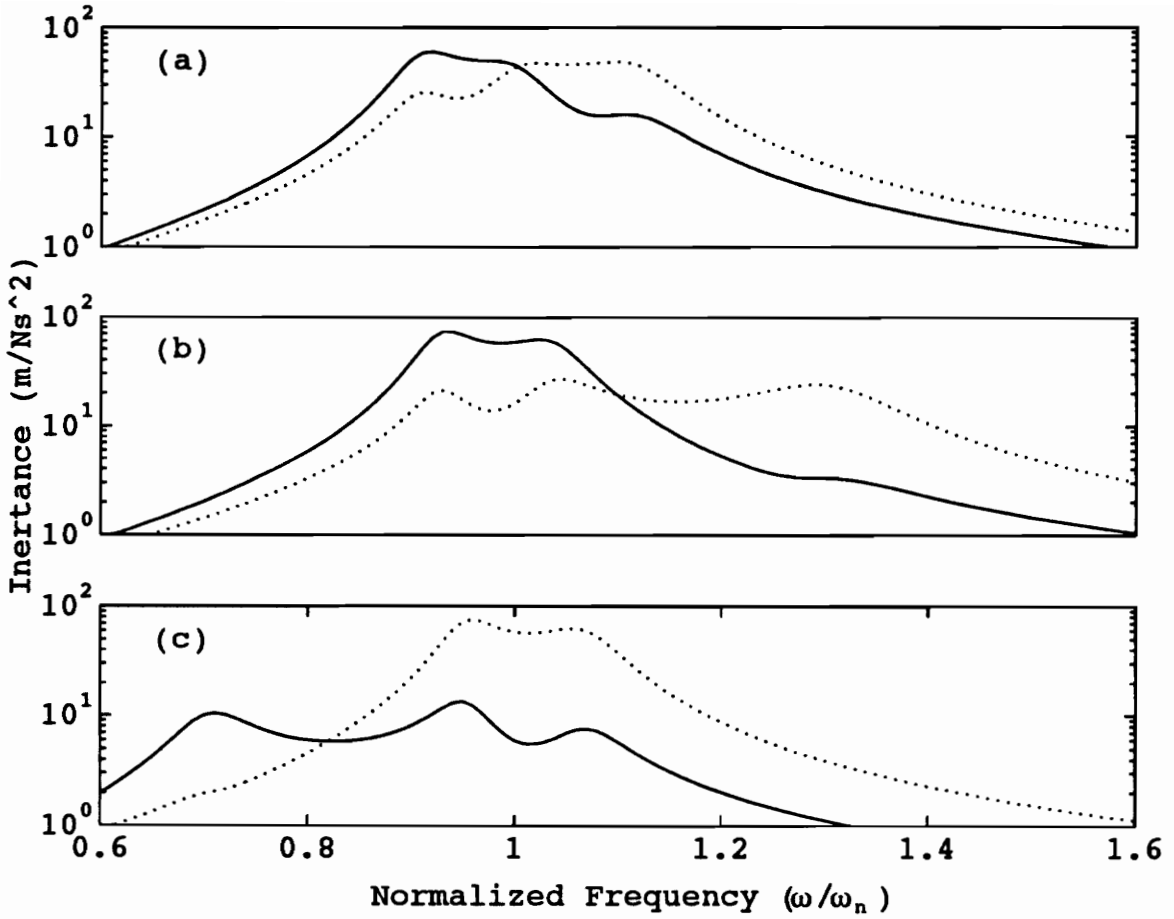

Figure 3. 3 Inertances of the (——) first and (• • •) second reaction-masses for the DM-DVA with tuning ratios from (a) position A, (b) position B, and (c) position C from Fig. 3.1.

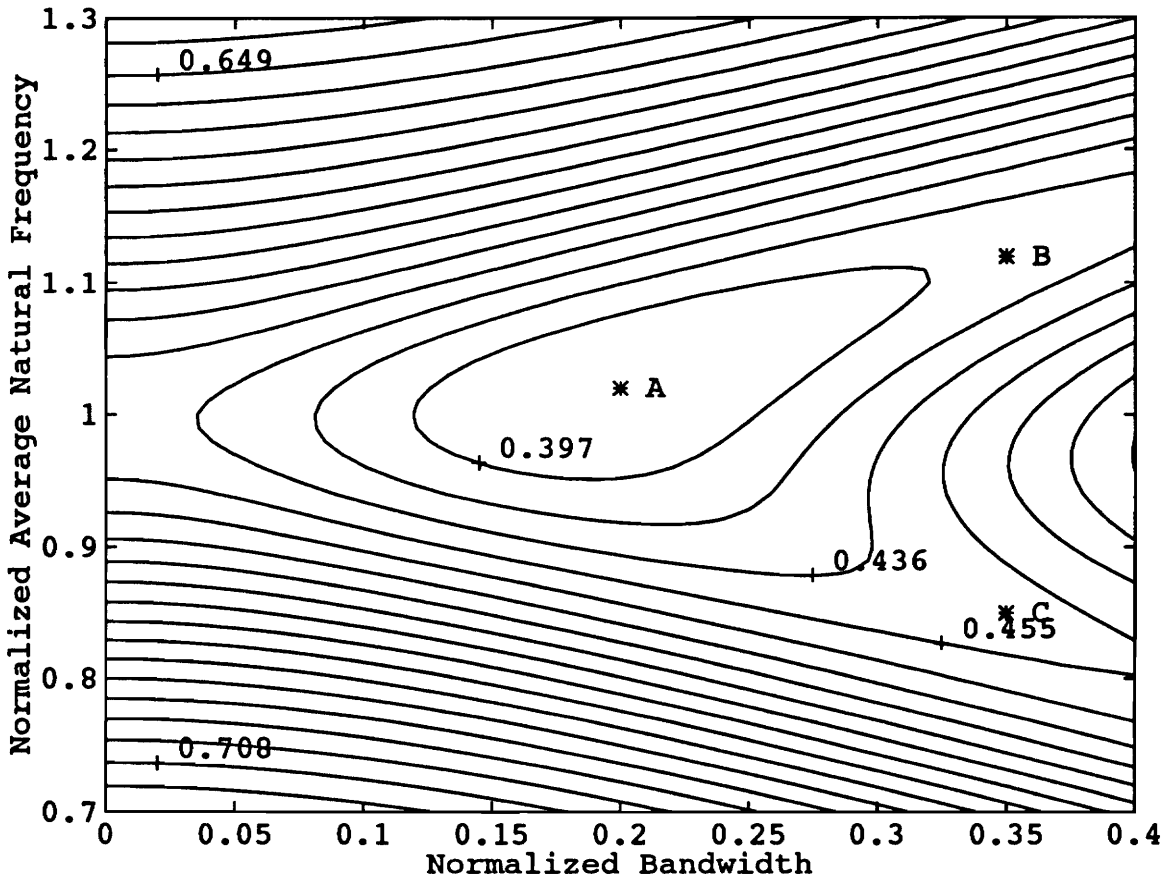

Figure 3. 4 Contour of the performance index for the passive DM-DVA with μ = 7% as a function of the normalized bandwidth and average tuning frequency.

Table 3. 1 Passive DM-DVA tuning study results.

DM-DVA Mass Ratio	Config.	Normalized Bandwidth	Normalized Avg. Tuning Frequency	Performance Index	RMS of $\ddot{X}_{a1}$ (m/Ns^2)	RMS of $\ddot{X}_{a2}$ (m/Ns^2)
3%	A	0.12	1.01	0.44	206.7	209.1
3%	B	0.3	1.13	0.48	257.7	142.6
3%	C	0.13	0.86	0.51	55.8	270.4
7%	A	0.20	1.02	0.38	137.5	142.7
7%	B	0.35	1.12	0.40	161.4	119.1
7%	C	0.35	0.85	0.45	42.9	181.7

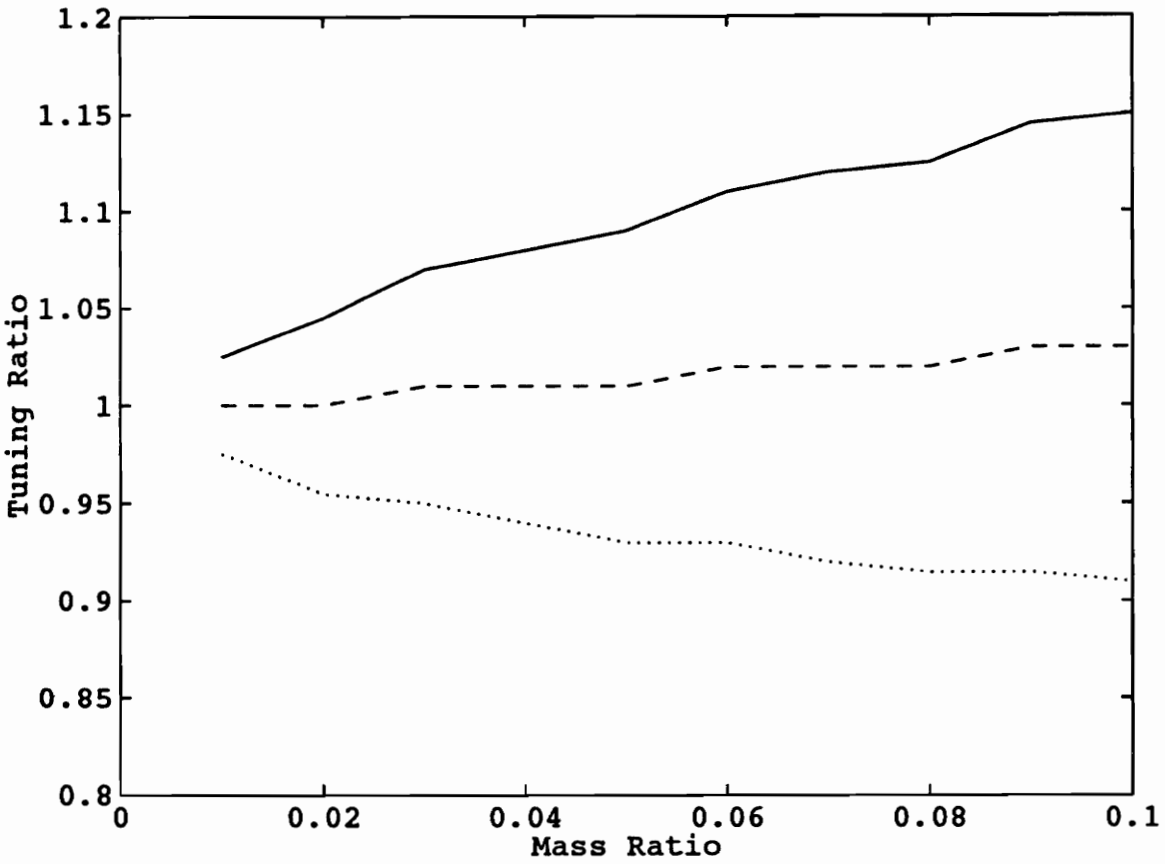

Figure 3. 5 Optimal (• • •) lower, (——) upper, and (– –) average tuning ratios for the passive DM-DVA as a function of the mass ratio.

tuning frequency is also presented in this plot. It can be seen that the normalized average tuning frequency did not change significantly with the change of mass ratios.

The effect of the damping ratio on the passive performance of the DM-DVA was also investigated. For simplicity, the two damping ratios of the DM-DVA were again assumed equal. The mass ratio of the DM-DVA was varied from 0.01 to 0.1 while the damping ratio was varied from 0.005 to 0.03. For each mass ratio, the DM-DVA was tuned to the optimal tuning frequencies shown in Fig. 3.5.

Figure 3.6 shows a contour plot of the performance index as a function of the mass and damping ratio of the DM-DVA. The dashed line indicates the optimum damping that yields the minimum performance index as a function of the mass ratio. This figure shows that the optimal damping ratio is nearly a linear function of the mass ratio, i.e. optimum damping increases with the mass ratio.

3.1.2 Hybrid DM-DVA

In Chapter 1, some of the control algorithms used with hybrid DVAs were discussed, i.e. full-state feedback, acceleration feedback, feedforward and so forth. The control method chosen to implement with the prototype hybrid DVA in the experimental tests (Chapter 4) was the filtered-X LMS feedforward algorithm (Widrow et al., 1985). Thus, a frequency domain approximation of this controller was developed. This control approximation obtains the control force so as to minimize a cost function which includes the motion of the primary system (as does the Filtered-X LMS algorithm) as well as the magnitude of the control force. By including the control effort in the cost function, the numerical results in this chapter can be compared to the experimental results in Chapter 4. Moreover, a penalty on the control effort was included as an efficient approach to consider practical limitations in the control authority of real systems. The derivation of the feedforward frequency-domain controller model is presented in Appendix A.

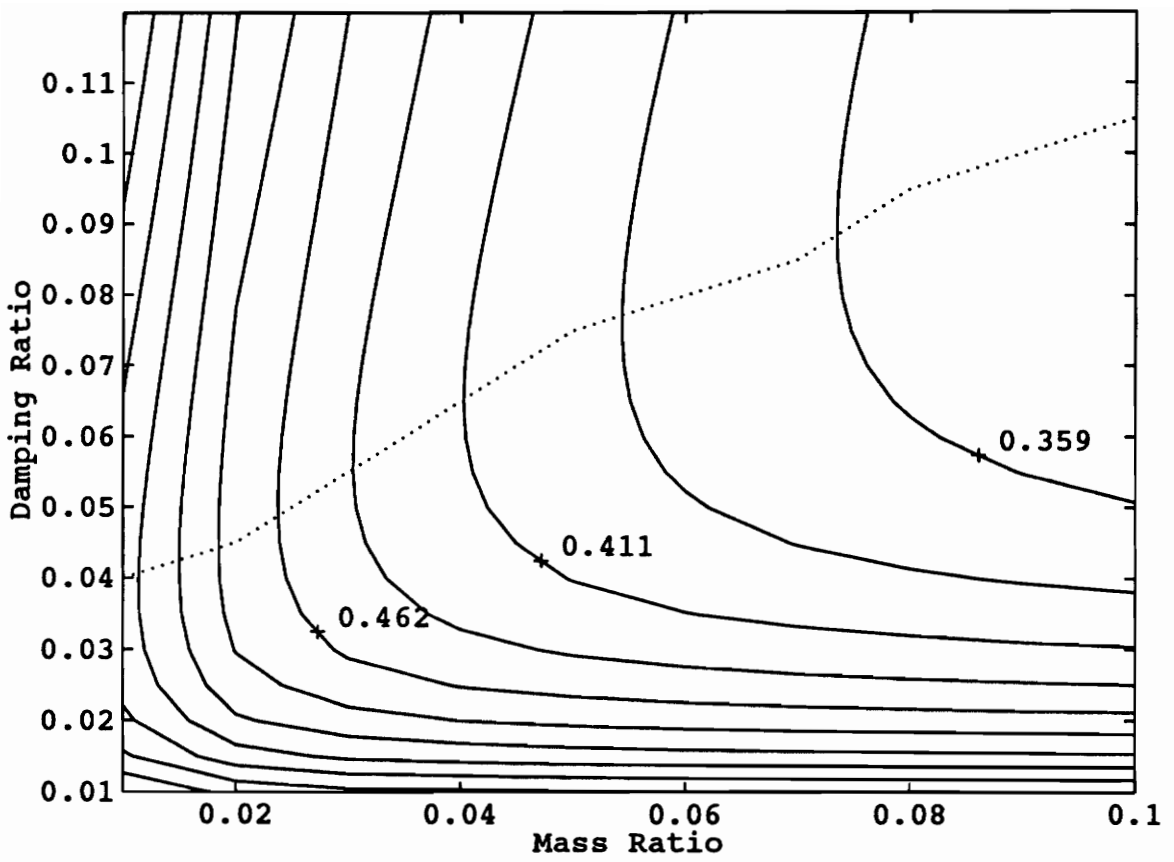

Figure 3. 6 Contour of the performance index for the passive DM-DVA as a function of the mass and damping ratios.

To illustrate the general behavior of the frequency domain control simulation, Figure 3.7 shows the response of the primary, the primary/passive DM-DVA, and of the primary/hybrid DM-DVA systems. The parameters used to obtain this plot are mass and damping ratios of 0.05 and tuning ratios of 0.93 and 1.09. These tuning ratios are optimal for the passive DM-DVA and were chosen to show the further attenuation yielded by the hybrid system. In the region between the tuning frequencies, the passive DM-DVA attenuates the motion of the primary system and significant additional attenuation is achieved by the hybrid DM-DVA. At frequencies outside the tuning frequencies of the DM-DVA, it was shown in Chapter 2 that the force transmissibility function of the DM-DVA is small. Thus, at these frequencies the DM-DVA can not affect the motion of the system without an extremely high control force that in practice the DVA will not provide. This behavior is similar to that of the actual filtered-X LMS controller.

The effect of the tuning frequencies on the performance of the hybrid DM-DVA were investigated first. The tuning of the DM-DVA was again described by the bandwidth and the average tuning frequency. These parameters were once again normalized by the natural frequency of the primary structure. The studies were carried out for mass ratios of 0.01 to 0.10 and damping ratios of 0.01, 0.025 and 0.05. The results for 0.01 and 0.025 damping ratios did not have significantly changed optimal tuning ratios, so only the results obtained with the 0.05 damping ratios will be presented.

Figure 3.8 shows a contour plot of the performance index as a function of the normalized bandwidth and normalized average tuning frequency of the hybrid DM-DVA. The mass ratio of the DM-DVA was 0.03. As with the performance index contour obtained with the passive tuning of the DM-DVA, this figure shows again one minimum labeled as point A. The normalized bandwidth and normalized average tuning ratio of the DM-DVA configured for position A are 0.52 and 1.05, respectively. Thus, while the ideal average tuning ratio has only increased slightly between the passive and hybrid cases, the

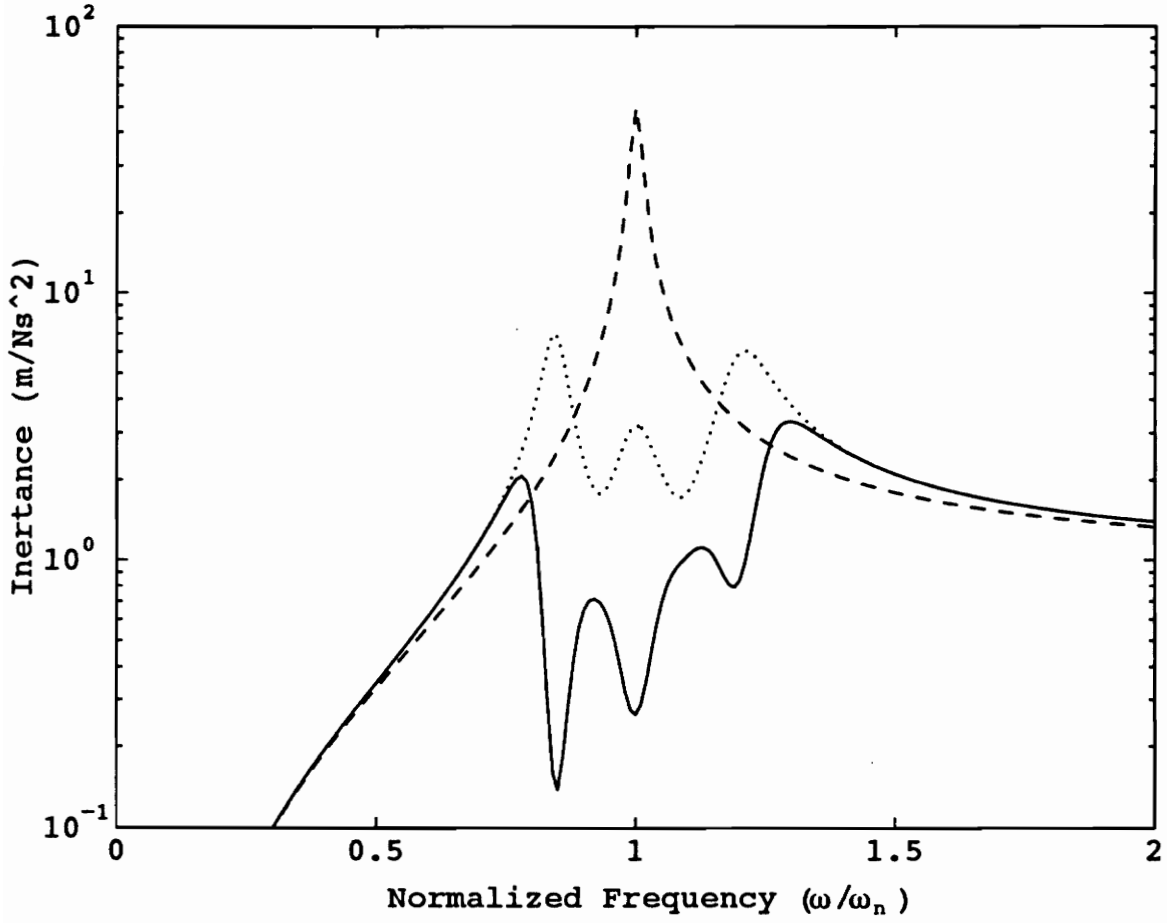

Figure 3. 7 Inertance of the (– –) primary, (• • •) primary/passive DM-DVA, and (——) primary/hybrid DM-DVA systems.

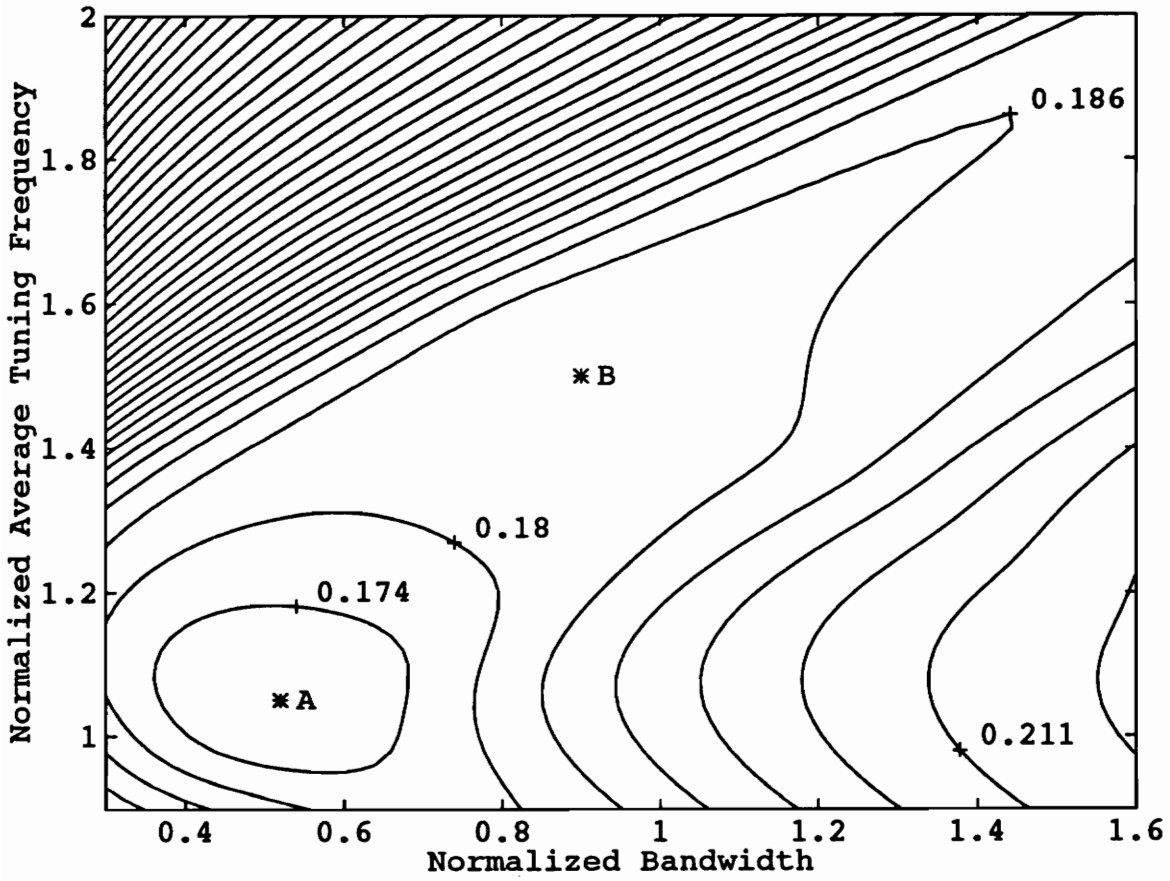

Figure 3. 8 Contour of the performance index for the hybrid DM-DVA with $\mu = 3\%$ as a function of the normalized bandwidth and average tuning frequency.

bandwidth has increased significantly. The value of the performance index associated with this point is 0.168. The contour plot also has a valley in which the performance index increases gradually as compared to the other regions on the contour. Position B lies in this valley. The normalized bandwidth and normalized tuning ratios associated with this point are 0.9 and 1.5, respectively. These parameters yield a lower tuning ratio for the DM-DVA which is near the resonance of the beam and an upper tuning ratio which is significantly higher.

To gain further insight, Fig. 3.9 shows the inertance of the primary structure and with the DM-DVAs configured as shown at points A and B. The hybrid DM-DVA achieved high primary attenuation over a larger bandwidth as compared to the hybrid DM-DVA configured as at position B.

The DM-DVA configuration, i.e. from point A or B, determines how the motion of the reaction-masses will contribute to the attenuation. Figure 3.10 (a) shows the amplitude of the reaction-mass inertances when configured as shown in position A. The peak amplitudes for each reaction-masses are nearly the same. It can be seen that they work together near the resonance of the primary structure and that above and below this resonance, one mass or the other contributes primarily to the attenuation. This plot should be contrasted with the reaction-mass inertances shown in Fig. 3.10 (b) which correspond to the tuning of position B. The inertance of the lower-tuned mass, which was near the resonance of the primary structure, is an order of magnitude higher than the motion of the upper tuned mass. Thus, the motion of the upper-tuned mass does not significantly contribute to the attenuation of the system.

Figure 3.11 shows the contour plot of the control force required by the hybrid DM-DVA corresponding to Fig. 3.8. This plot shows that the least amount of control effort also follows the valley which was present in Fig. 3.8. The steepest increase in required control force occurs when the average tuning frequency is moved away from the

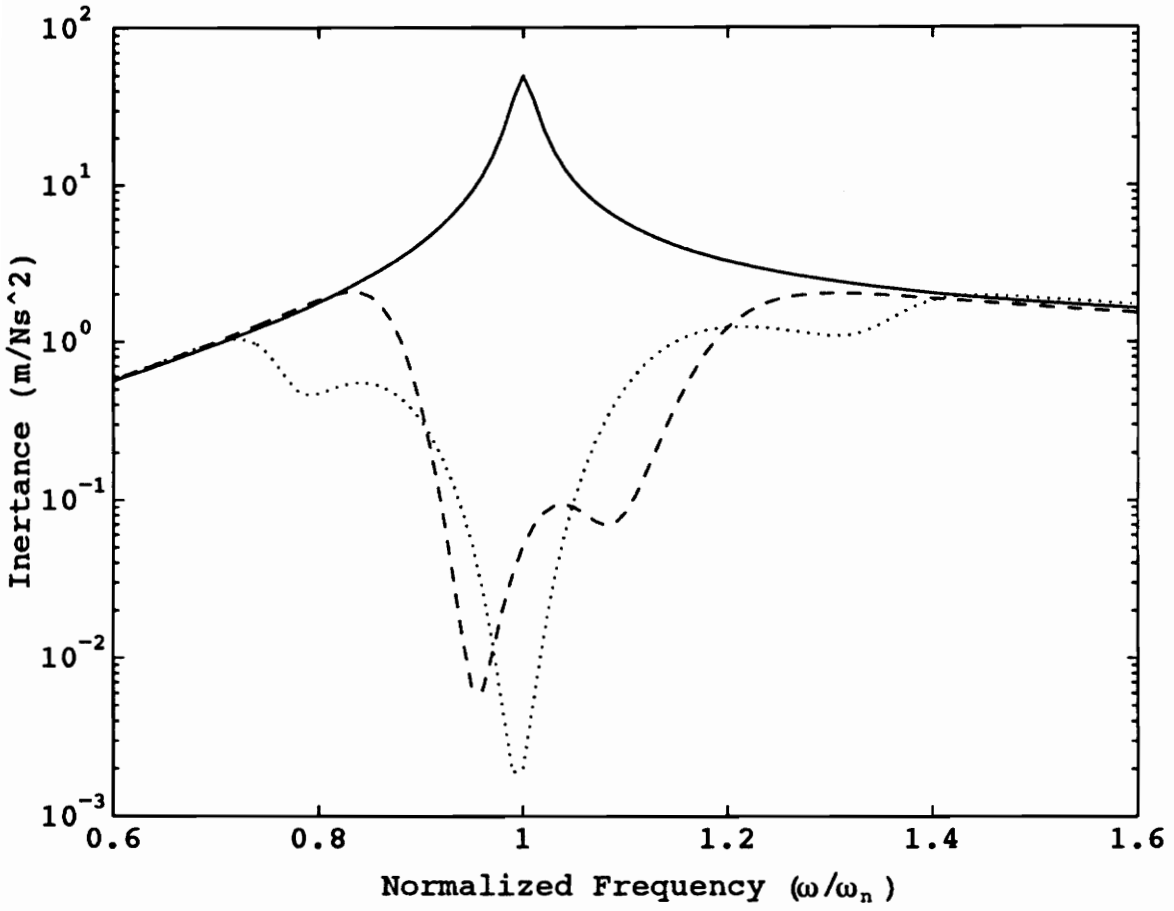

Figure 3. 9 Inertance of the (—) primary structure and of the primary/hybrid DM-DVA systems with tuning ratios from position (• • •) A and (– –) B from Fig. 3.8.

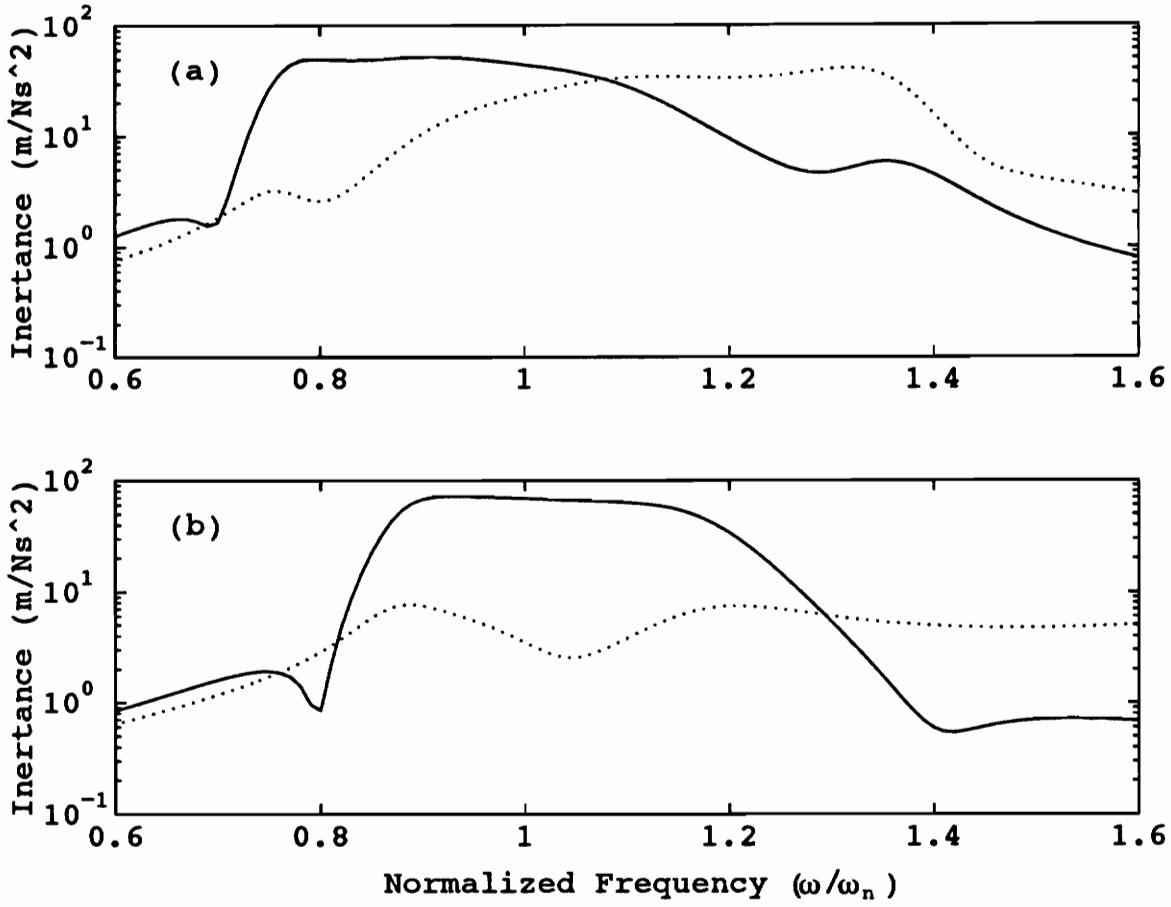

Figure 3. 10 Inertances of the (——) first and (• • •) second reaction-masses for the DM-DVA with tuning ratios from (a) position A and (b) position B from Fig. 3.8.

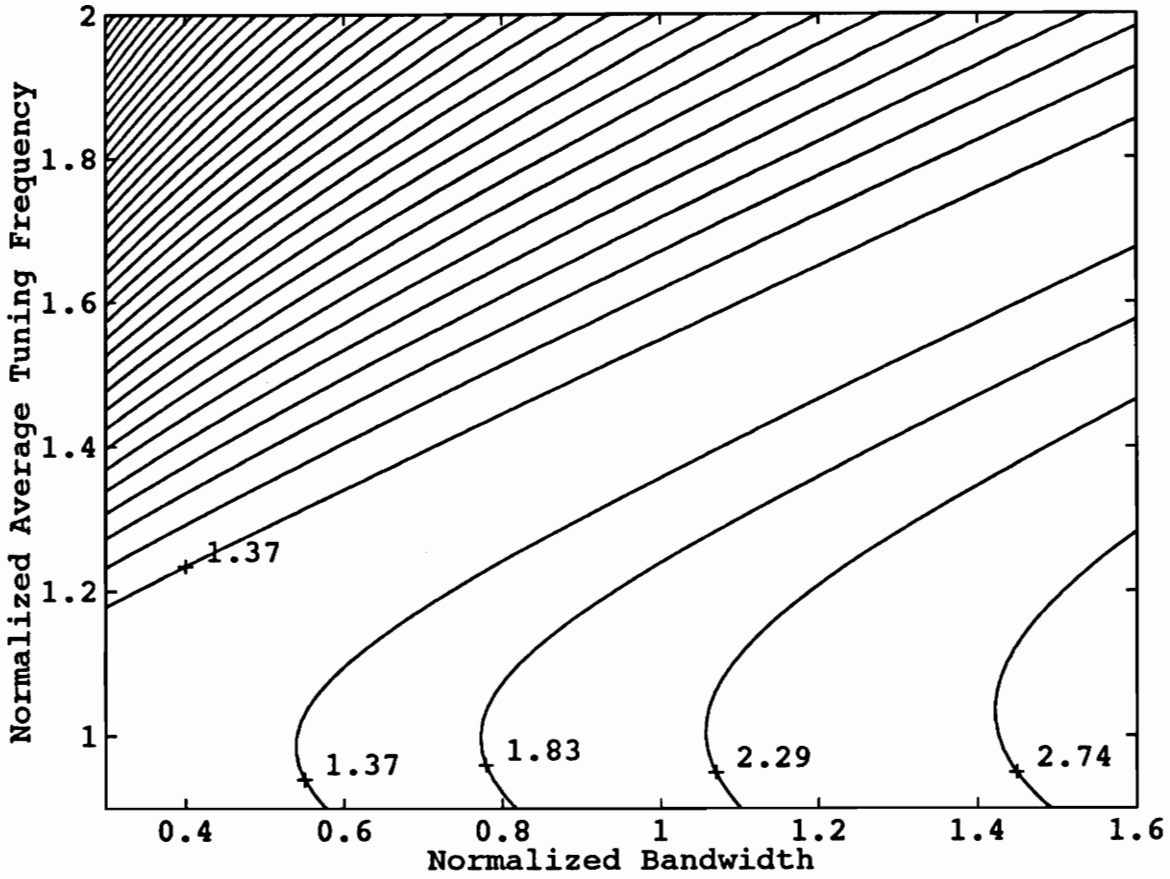

Figure 3. 11 Contour of the RMS control force for the hybrid DM-DVA with $\mu = 3\%$ as a function of the normalized bandwidth and average tuning frequency.

resonance frequency of the structure. On the other hand, the required control force is much less sensitive to changes in the bandwidth of the DM-DVA.

Figure 3.12 shows a contour plot of the performance index for the DM-DVA with a mass ratio of 0.05. Again the minimum performance index value $\Pi = 0.175$ corresponds to position A. The normalized bandwidth at position A is 0.52 and the normalized average tuning frequency is 1.06. These values are nearly the same as for the DM-DVA with a mass ratio of 0.03. The performance index at point B is 0.178 and corresponds to a normalized bandwidth of 0.92 and a normalized average tuning frequency of 1.5. Again, these values are nearly the same as for the DM-DVA with a mass ratio of 0.03. For higher mass ratios, i.e. above 0.05, a second minimum appears in the vicinity of point B. Based on the reaction-mass motion shown in Fig. 3.10 (b) and the fact that mass ratios this high are often not practical, this minimum will not be considered to be a useable solution in this study.

Figure 3.13 shows the optimal tuning ratios of the DM-DVA as a function of the mass ratio. For comparison, the optimal passive tuning ratios from Fig. 3.5 are also shown. Below mass ratios of 0.06, the tuning ratios are nearly constant at 0.8 and 1.3. At higher mass ratios, the optimal tuning ratios begin to increase. This figure also shows that the design of a hybrid DM-DVA is a tradeoff between its passive and active performance. If tuned properly, the passive DM-DVA would be effective as a backup system if the active system fails. From Fig. 3.13, it is clear that the optimum DM-DVA tuning ratios are between the curves for the passive and hybrid systems which will provide acceptable passive and hybrid performance. Table 3.2 summarizes the results of the hybrid DM-DVA tuning study for mass ratios of 0.03 and 0.05.

The effect of the damping ratio on the performance of the hybrid DM-DVA was also investigated. Figure 3.14 shows a three-dimensional plot of the performance index as a function of the damping and mass ratios. The hybrid DM-DVA was again optimally

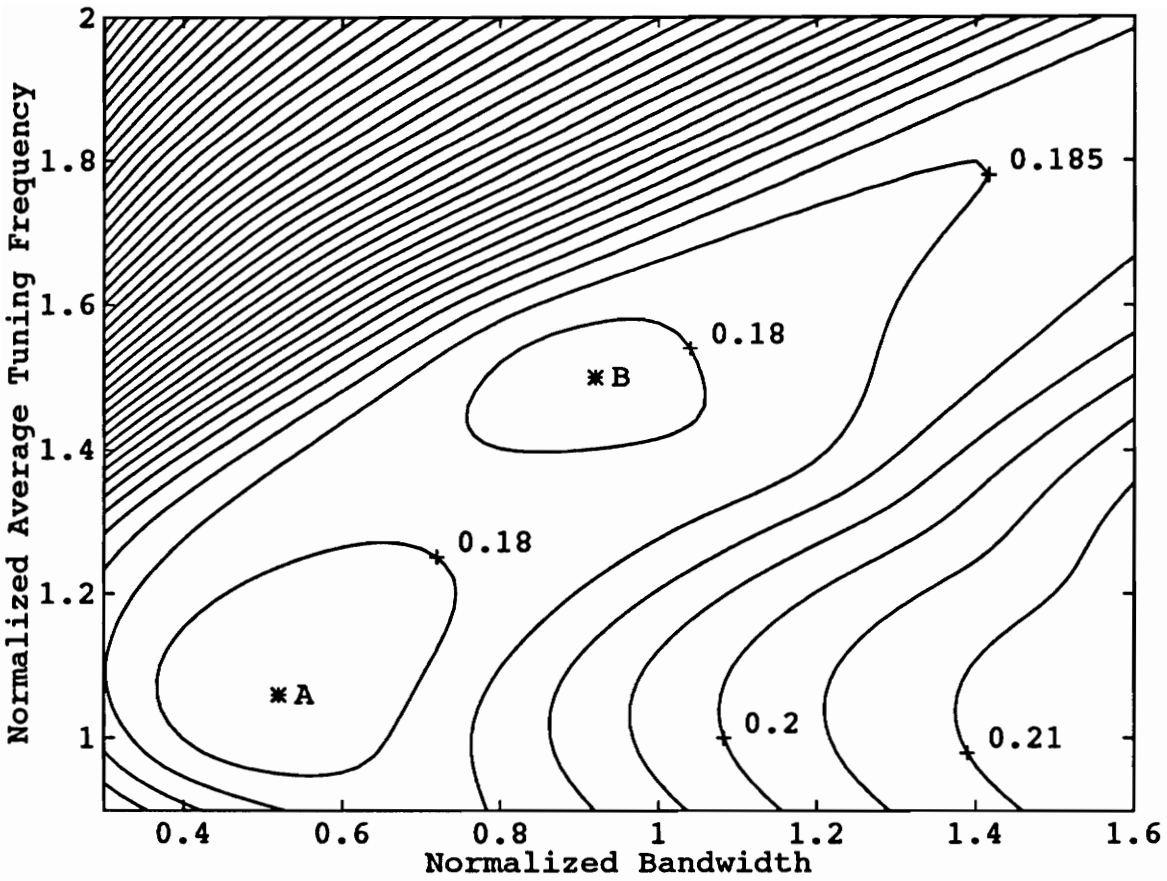

Figure 3. 12 Contour of the performance index for the hybrid DM-DVA with $\mu = 5\%$ as a function of the normalized bandwidth and average tuning frequency.

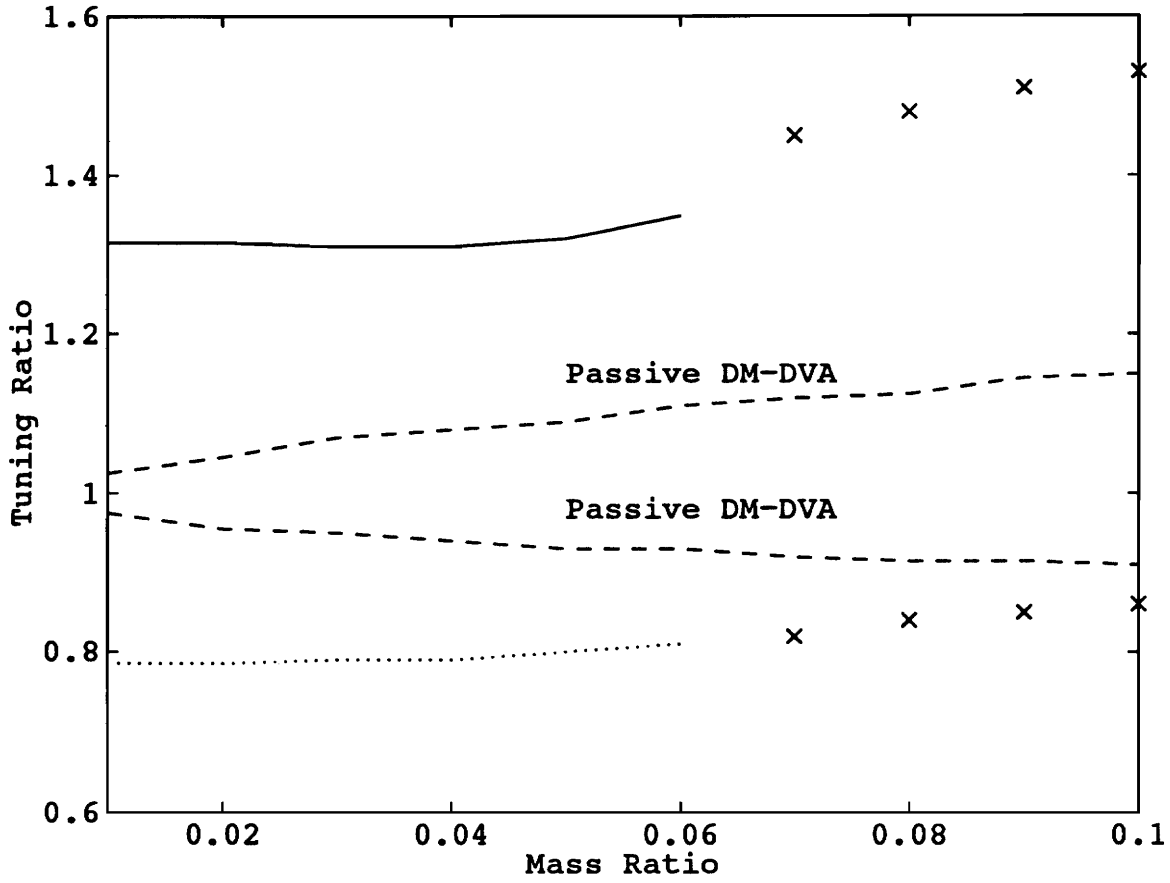

Figure 3. 13 Optimal tuning ratios for the hybrid DM-DVA as a function of the mass ratio.

Table 3. 2 Hybrid DM-DVA tuning study results.

DM-DVA Mass Ratio	Config.	Normalized Bandwidth	Average Tuning Ratio	Performance Index	RMS of $\ddot{X}_{a1}$ (m/Ns^2)	RMS of $\ddot{X}_{a2}$ (m/Ns^2)	Control Force
3%	A	0.52	1.05	0.17	280.2	222.0	1.28
3%	B	0.90	1.50	0.18	373.4	77.7	1.39
5%	A	0.52	1.06	0.18	172.1	138.2	1.24
5%	B	0.92	1.50	0.18	226.0	66.0	1.44

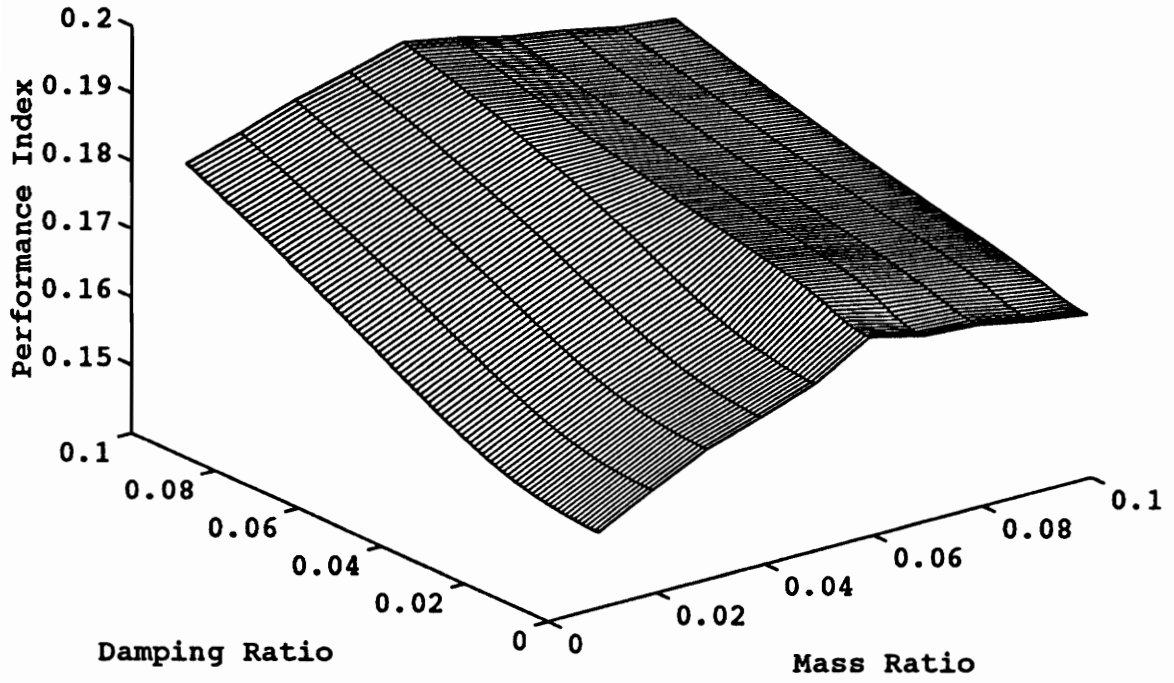

Figure 3. 14 Surface plot of the performance index as a function of the mass and damping ratios.

tuned for each mass ratio, i.e. optimum value from Fig. 3.13. For all mass ratios, the minimum value of the performance index was at the minimum damping ratio of 0.001. This implies that damping is harmful to the operation of hybrid DVAs because it dissipates energy. Damping is beneficial in passive systems because it limits the response at the resonances which are caused by the addition of the DVA. Once again, the damping ratio used in a given application will be based on a compromise between passive and hybrid performance. Damping was included in this study because it is always present in physical systems.

The effect of active control on the motion of the reaction-masses was also investigated. The mass ratio of the DM-DVA used in this test was 0.05 and it had optimal tuning ratios (i.e. 0.80 and 1.32). The damping ratios of the DM-DVA were 0.05. Figure 3.15 (a) shows the motion of the mass with the lower tuning ratio and Fig. 3.15 (b) shows the motion of the mass with the higher tuning ratio. The RMS value of the inertance of the mass shown in 3.15 (a) were 115.4 and 172.1 m/Ns^2 for passive and hybrid operation, respectively. For the mass in 3.15 (b), the RMS values were 156.5 and 138.2 m/Ns^2 for passive and hybrid operation, respectively. The addition of the active force component reduced the motion of one of the masses and increased the motion of the other. The cost function used by the controller in this study did not consider the motion of the reaction-masses. In an optimization of the DM-DVA, the motion of the reaction-masses should be taken into account.

3.2 Hybrid SM and DM-DVA Comparison

The previous parametric study yielded some insight into the behavior of the DM-DVA both as a passive and hybrid system. Moreover, it provided useful information for design guidelines. The purpose of this section is to compare the performance of a DM-DVA configured as per the guidelines established in Section 3.1 to an optimally-tuned

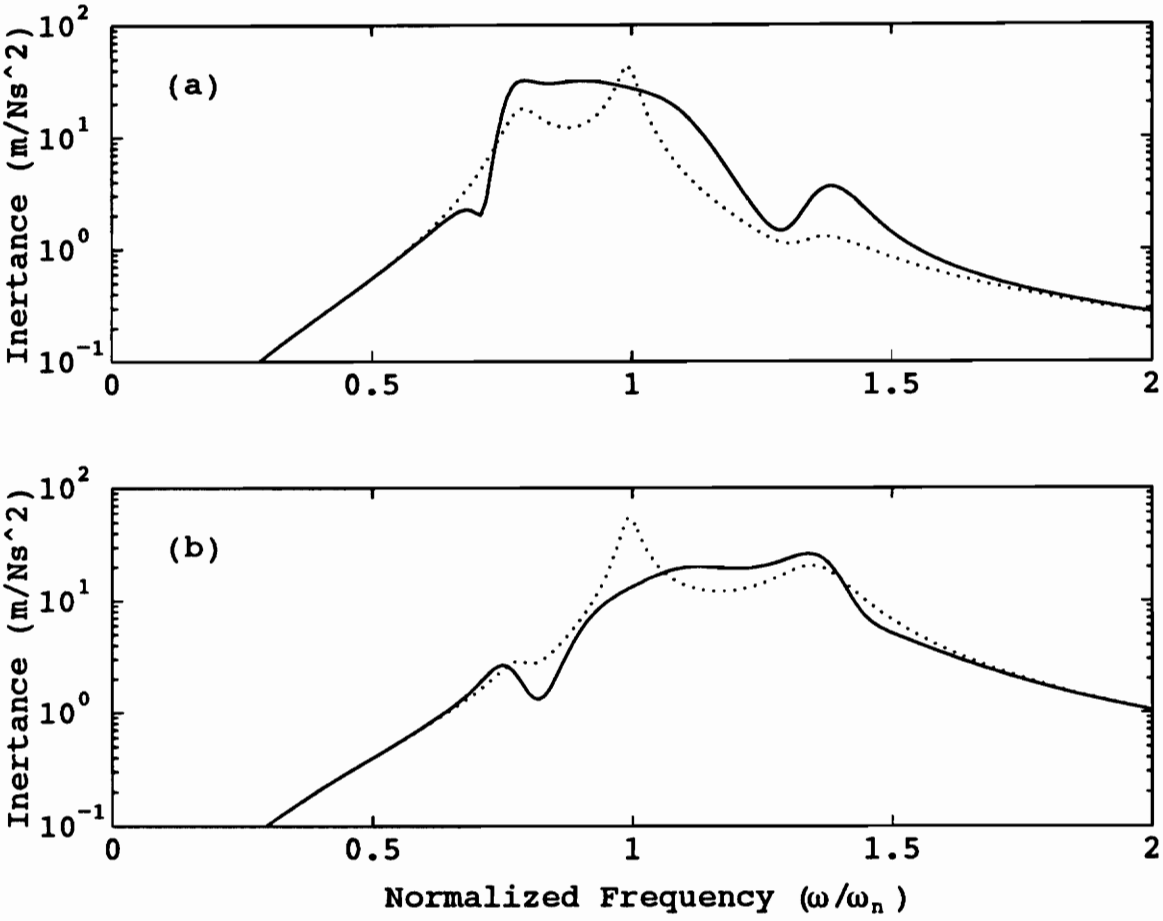

Figure 3. 15 Comparison of reaction-mass inertance for (a) the first and (b) the second masses (• • •) before and (——) after control.

SM-DVA. The hybrid SM-DVA is selected as a benchmark because these devices are widely used and they have been the subjects of many studies.

3.2.1 Primary Response Attenuation

The first comparison between the hybrid SM and DM-DVAs consisted of evaluating the control force required to achieve the same level of primary response attenuation. The mass ratios of both the hybrid SM and DM-DVA and the damping ratios were 0.05. The hybrid SM-DVA had a tuning ratio of 0.95, which is optimal for the passive device with a 0.05 mass ratio (Snowden, 1968). The hybrid DM-DVA had tuning ratios of 0.8 and 1.32, which were determined in the parametric study to be optimal for a 0.05 mass ratio.

Figure 3.16 shows the acceleration response for the primary system alone and for the primary/passive DVAs. The RMS inertance of the original primary structure was 89.1 m/Ns^2. The RMS inertance of the primary structure/passive SM-DVA was 41.9 m/Ns^2, while for the passive DM-DVA it was 57.5 m/Ns^2. Since the DM-DVA was configured for effective hybrid performance, it did not perform as well as the SM-DVA as a passive device. The passive DM-DVA did not have a tuning frequency near the natural frequency of the primary structure as did the SM-DVA, so it was unable to attenuate the motion in this frequency range very effectively.

Figure 3.17 shows the inertance of the primary structure for the hybrid DVA cases. For comparison the response of the original primary system alone is also included in the figure. To allow for a direct comparison, the penalty on the control effort in the cost function to be minimized (see Appendix A) for the hybrid SM-DVA was adjusted to achieve the same attenuation in the primary inertance as was obtained by the hybrid DM-DVA. Thus, the RMS of the primary/hybrid DVA (both SM and DM) inertance was 12.9

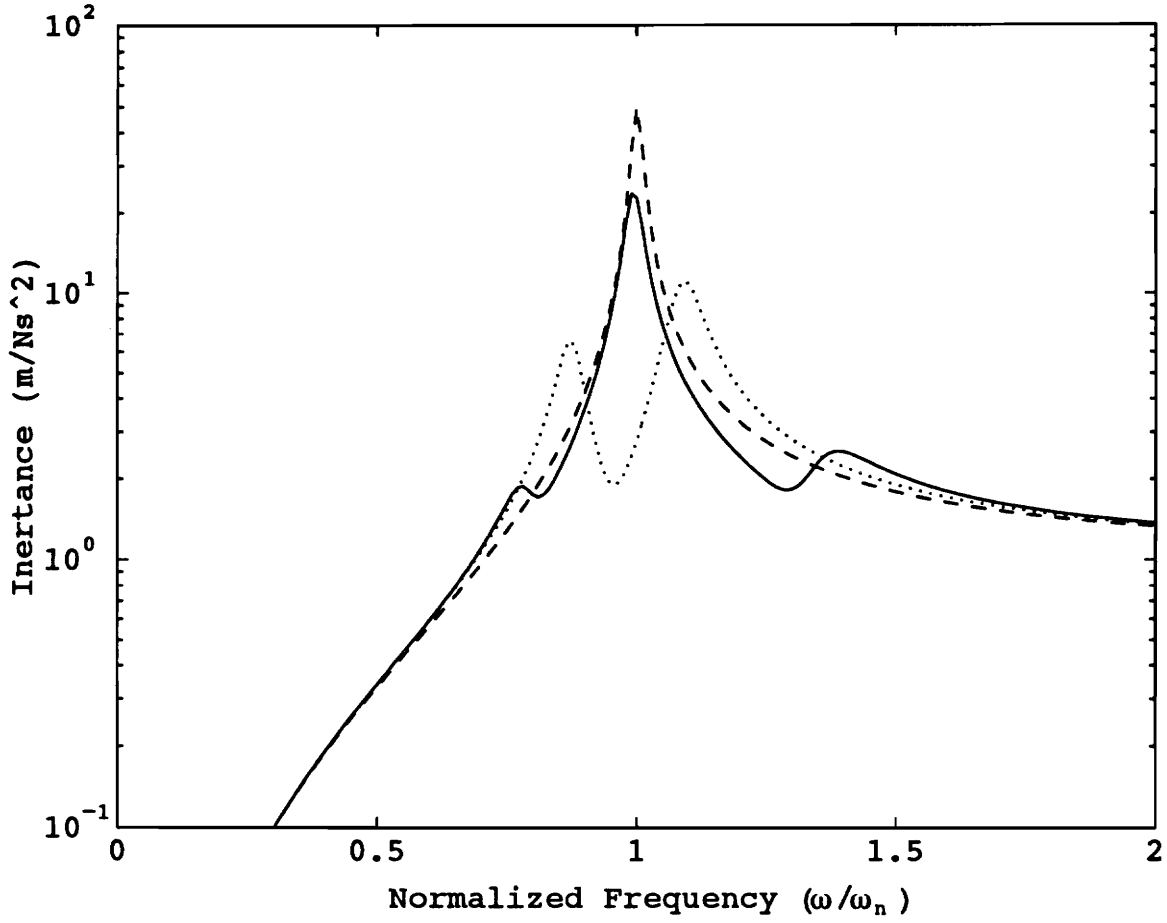

Figure 3. 16 Inertance of (– –) the original primary, (• • •) the primary/passive SM-DVA, and (——) the primary/passive DM-DVA systems.

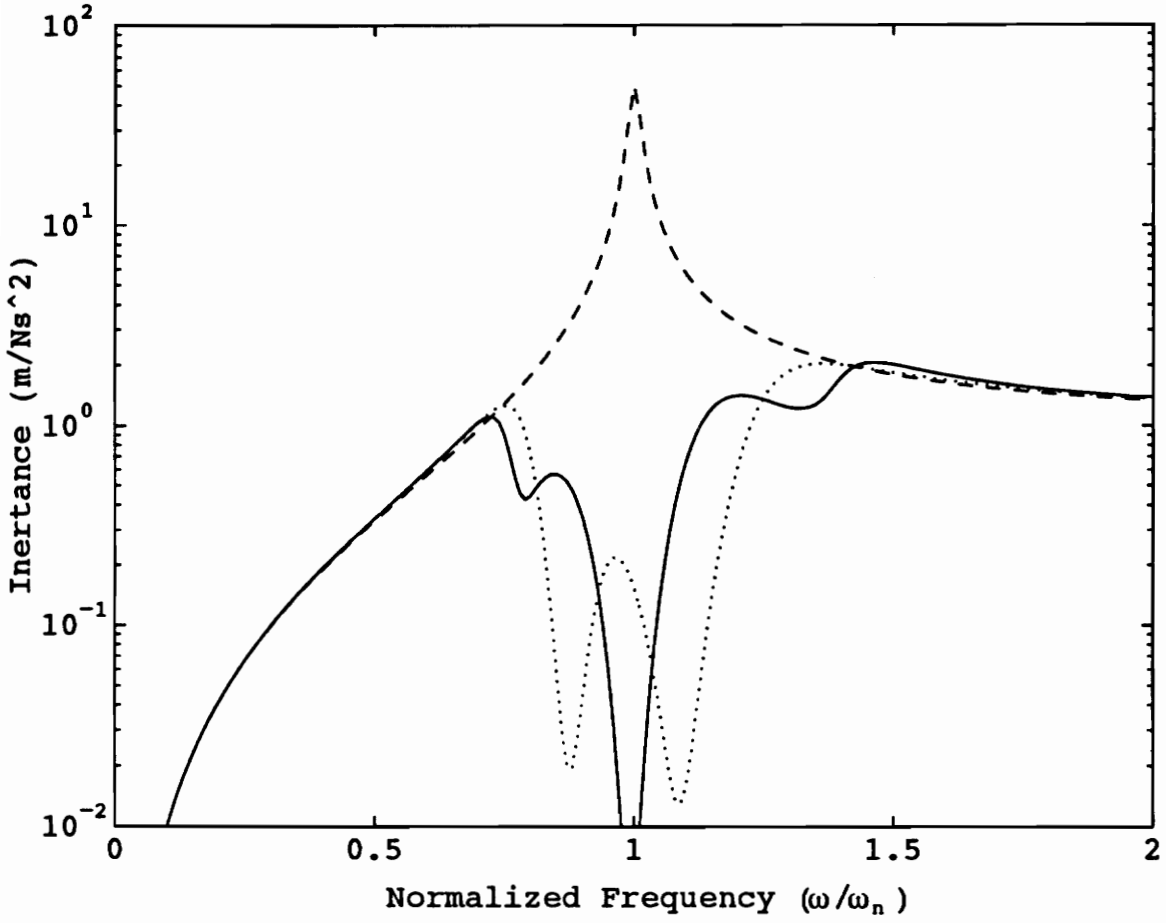

Figure 3. 17 Inertance of (– –) the original primary, (• • •) the primary/hybrid SM-DVA, and (——) the primary/hybrid DM-DVA systems.

m/Ns^2. Figure 3.17 shows that the band of effectiveness for the DM-DVA was slightly wider than for the SM-DVA.

Since the hybrid SM and DM-DVAs achieved the same attenuation, a direct comparison of their control forces is now possible. Figure 3.18 shows the control force normalized by the disturbance force F required by the hybrid SM and DM-DVAs to achieve this attenuation. In addition, the "ideal" control forces which would drive the primary response to zero are also shown. It is clear from this plot that the required control force for the DM-DVA is always lower than that required by the SM-DVA except at frequencies near the SM-DVA's tuning frequency. This is because near its resonance, the SM-DVA is a more efficient actuator due to its high force transmissibility (see Fig. 2.6). The RMS value of the control force for the SM-DVA was 2.42 while for the DM-DVA it was 1.47. This shows that for the SM-DVA to achieve the same attenuation in the vibration of the primary structure, it required a control force which was, in a frequency average sense, 65% higher than that required by the DM-DVA. The "ideal" control forces shown are an upper limit on the hybrid DVA control force. Further primary attenuation would cause the required control force curves to shift upward toward the "ideal" force curves.

3.2.2 Sensitivity Analysis

In any realistic system the properties of both the primary structure and the DVAs can change with time. Since these changes will affect their dynamics, hybrid DVAs need to have an acceptable performance even when they are not optimally configured for a particular application. To address this issue, a sensitivity study of the performance of the hybrid SM and DM DVA systems to changes in their parameters should be carried out. The single parameter for this study is the tuning frequency (average tuning frequency for the DM-DVA) since it is the most critical factor affecting the performance of these hybrid

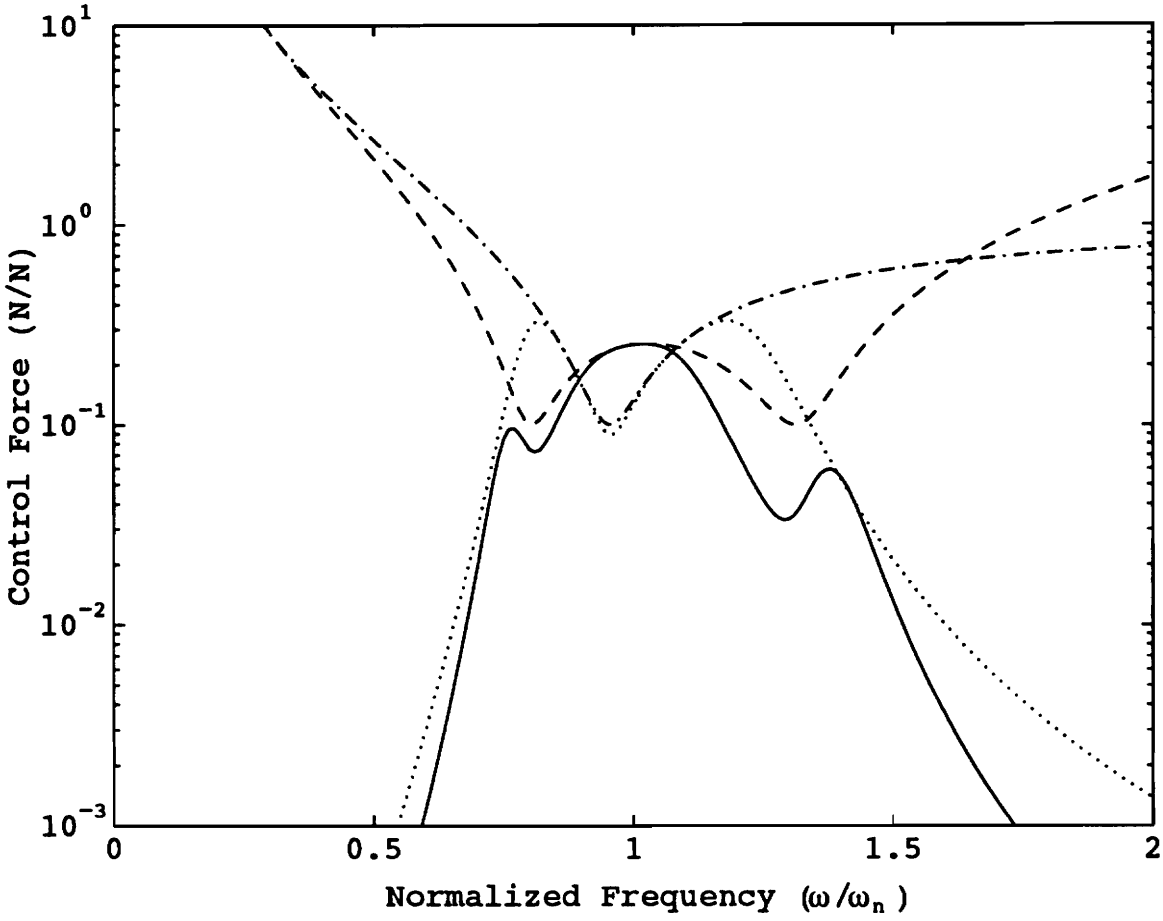

Figure 3. 18 Normalized control force for (• • •) the primary/hybrid SM-DVA, (——) the primary/hybrid DM-DVA systems. For comparison, the "ideal" (—•—)SM and (– –) DM-DVA control forces are shown.

DVAs. To test the sensitivity of the SM-DVA, the tuning frequency was changed while keeping the DVA's mass and damping ratios unchanged. To this end, both the stiffness and damper values had to be modified accordingly. For the case of the DM-DVA, the average tuning frequency was changed similarly while the bandwidth remained unmodified. The variation of the performance index and control force to changes in the bandwidth was previously shown to be much less sensitive to changes in the bandwidth than to changes in the average tuning frequency (Fig. 3.11).

Figure 3.19 shows the performance index of the two hybrid DVAs as functions of the tuning ratio (average tuning ratios for the DM-DVA). It is clear that the hybrid DM-DVA performs better than the SM-DVA for significant variation in the optimum tuning ratios. Moreover, the DM-DVA is clearly less sensitive to variations in the average tuning frequency over a large frequency range in the vicinity of the primary system resonance, i.e. average tuning ratios of 0.8 through 1.4. An extremely large shift in the tuning ratio would be required to enter the range of the plot where the SM-DVA is superior, i.e. tuning ratio of less than 0.6.

The control force required by the hybrid DVAs to achieve the performance index shown in Fig. 3.19 is presented in Fig. 3.20 This figure clearly demonstrates that the control effort of the DM-DVA is relatively insensitive to the average tuning frequency over the entire frequency range defined by the two tuning frequencies. On the other hand, the control effort of the SM-DVA increases rapidly as the tuning frequency is changed from its optimum value.

The sensitivity of the DM-DVA reaction-mass motion to the mass size was also explored. The results are tabulated in Table 3.3. The tuning ratios of the DM-DVA were optimal for its mass ratio, which was varied from 0.01 to 0.05. In each case, the DM-DVA was used to attenuate the primary response to approximately 15.5 m/Ns^2, as compared to 57.5 for the primary/passive DM-DVA system. Regardless of the mass ratio,

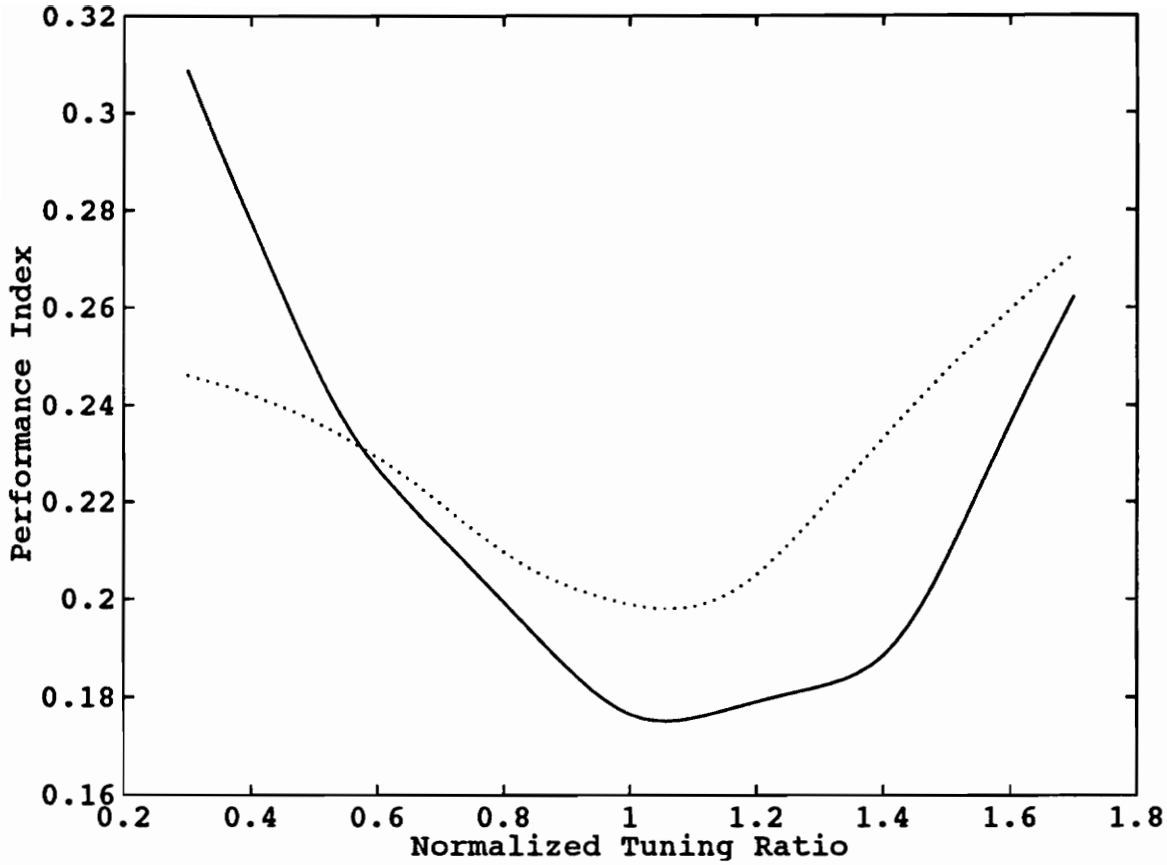

Figure 3.19 Hybrid (• • •) SM and (——) DM-DVA performance indices as functions of the average tuning ratio.

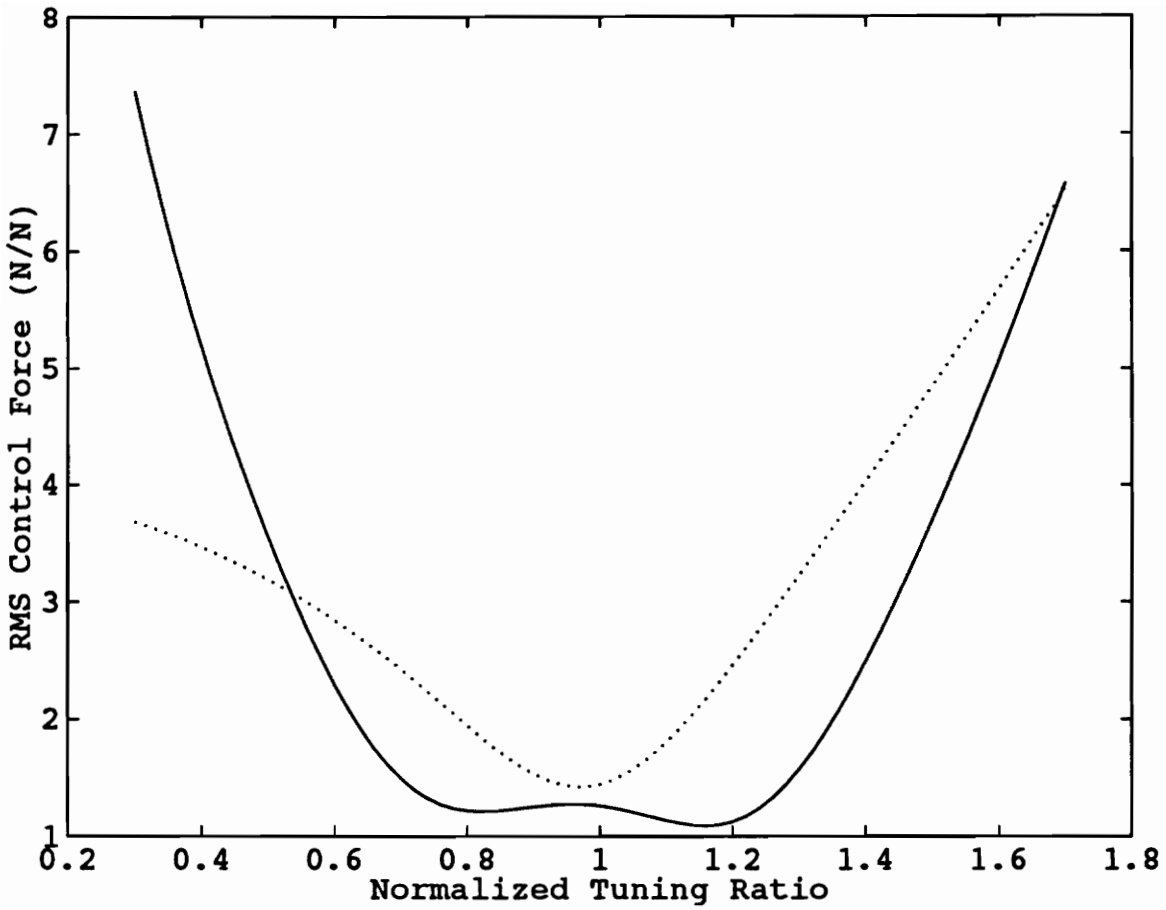

Figure 3. 20 Required control force for the hybrid (• • •) SM and (——) DM-DVA as a function of the average tuning ratio.

Table 3. 3 Comparison of DM-DVA mass motion for varying reaction-mass sizes.

DM-DVA Mass Ratio	RMS error (m/Ns^2)	RMS Control Force (N/N)	RMS of $\ddot{X}_{a1}$ (m/Ns^2)	RMS of $\ddot{X}_{a2}$ (m/Ns^2)
5%	15.6	1.25	168	141
4%	15.6	1.26	208	169
3%	15.4	1.26	272	212
2%	15.4	1.25	400	299
1%	15.4	1.25	783	565

the required RMS control force was approximately 1.25 N/N. Each successively smaller DVA was able to generate the same control force because the reaction-mass accelerations were increased. For comparison, a hybrid SM-DVA with a mass ratio of 0.05 which attenuates the primary response to 15.6 m/Ns^2 requires an RMS force of 1.8 N/N and has an RMS reaction-mass acceleration of 128 m/Ns^2.

Chapter 4

Experimental Validation

In this chapter, an experimental evaluation of the proposed DM-DVA is presented. To this end, a prototype hybrid DVA was built. The DVA could be configured to function as either a hybrid SM-DVA or a hybrid DM-DVA. This dual configuration allowed the SM and DM-DVA comparison from Chapter 3 to be performed experimentally. Both the hybrid SM and hybrid DM-DVA configurations were used to attenuate the vibration of a fixed-free beam.

The first part of this chapter includes a description of the primary system to be controlled, the prototype actuator, and the experimental setup and procedure. The second part presents and discusses the results from the experiments. The third part discusses additional results from a theoretical model of the experimental setup.

4.1 Experimental Setup

4.1.1 Primary System

The primary structure considered in the experiment was a steel beam, 1.15 meters in length with cross sectional dimensions of 38.1 x 25.4 mm. The beam had a total mass

of 8.75 kg. It was mounted vertically with the base fixed to a granite table and the top free.

A structure is characterized by its natural frequencies, damping ratios, and mode shapes. For simple structures, such as the beam used in this experiment, these parameters are easily obtained. Thus, a test was first conducted to determine the modal properties of the beam. The beam was excited by a shaker positioned at 0.64 m from the fixed end. The shaker was acting on the longer side of the cross section and driven with white noise in the [0 - 200 Hz] frequency range to include the second mode of the beam. The excitation force was measured by a force transducer. The response of the beam was measured along its length every 10 cm using an accelerometer.

The inertance at the free end of the beam is shown in Fig. 4.1 which indicates two resonances at 13 and 86 Hz, respectively. The damping ratios, found using the half-power rule, were estimated at 0.0196 and 0.0058 for the first and second modes, respectively (Rao, 1990). Because of the low damping, the resonances correspond closely to the true undamped natural frequencies of the system. Once the natural frequencies were estimated, the mode shapes were found. The mode shapes were obtained as the imaginary part of the inertance at the resonance frequency at each point along the beam. The first two mode shapes of the beam are shown in Fig. 4.2.

The modes of a fixed-free beam are well separated, so each mode behaves as a SDOF system. Thus, the second mode of the beam was targeted to be controlled using the hybrid DVAs.

4.1.2 Prototype Hybrid DVA

The most important component of a hybrid DVA is the actuation method, i.e. control force implementation. The actuation method determines the hybrid DVA's

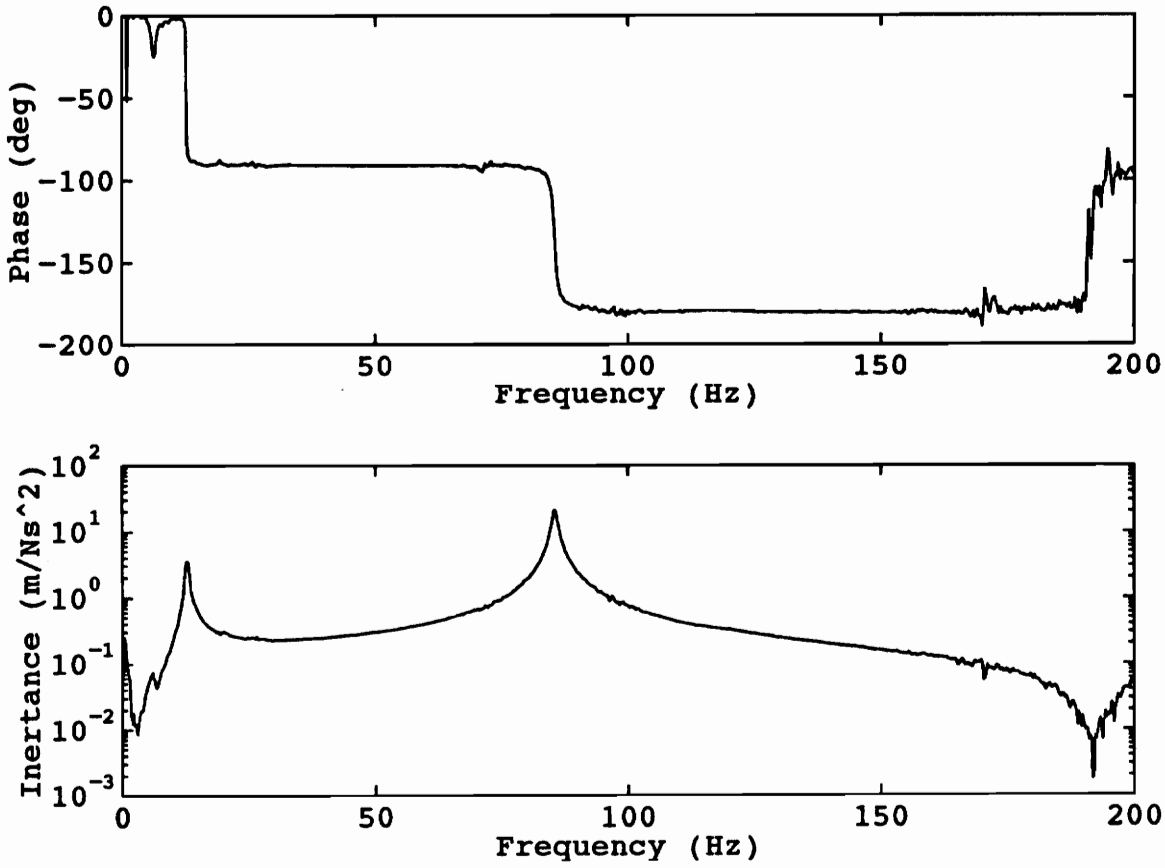

Figure 4. 1 Inertance of the free end of the primary structure.

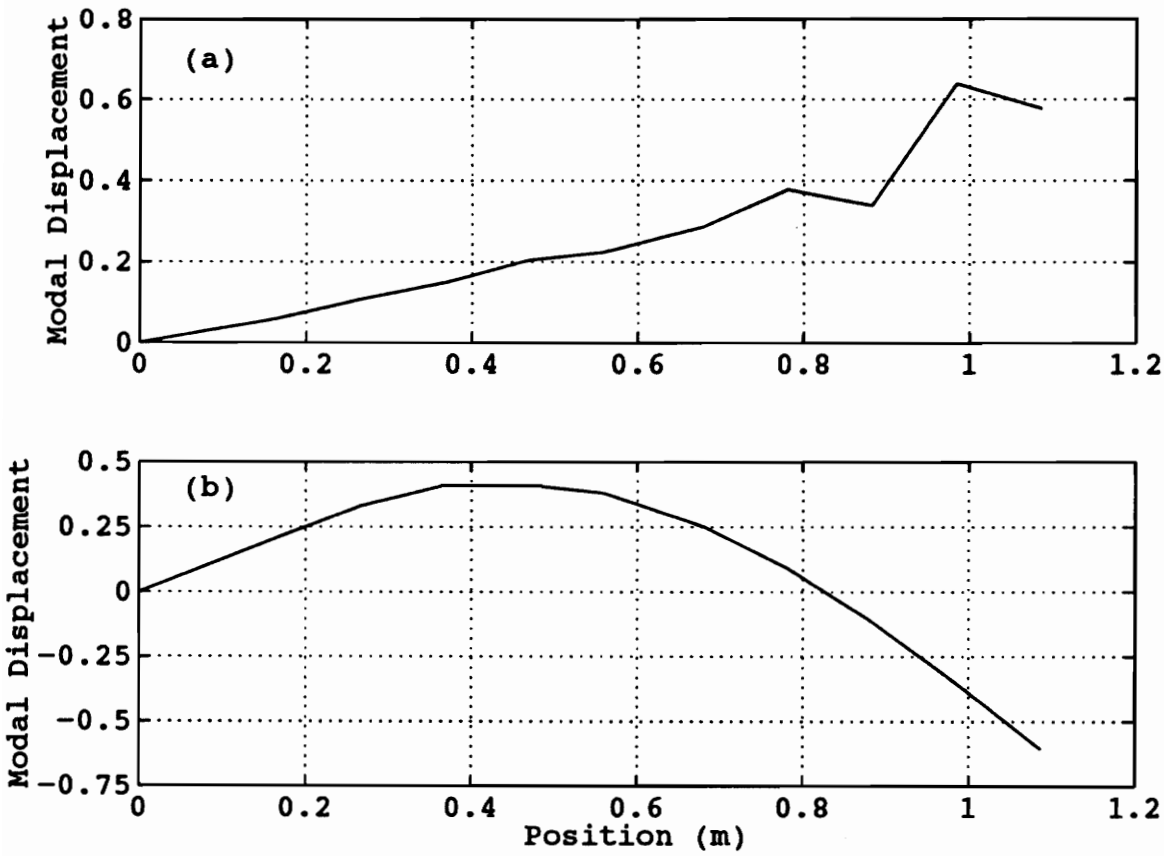

Figure 4. 2 (a) First and (b) second mode shapes of the primary structure.

characteristics such as the size, ruggedness, and operational frequency range. Several actuation methods were available including piezoceramics, hydraulic systems, pneumatic systems, servo motors, coil/magnet systems, and so forth. The prototype actuator built for these experiments used a voice coil and rare-earth magnet assembly for actuation.

Because the control force acts between the reaction masses in the hybrid DM-DVA, the magnet was fixed to one mass and the coil to the other mass, as shown in Fig. 4.3. Both the masses were steel cylinders 44.5 mm in diameter and 20 mm tall. The first mass in Fig. 4.3 (a) had an elevated disk on one of its circular surfaces which was 1.5 mm thick. This disk was concentric with the axis of the mass. The purpose of the disk was to align the cylindrical voice coil with the axis of the mass. The mass also contained a linear bearing which was mounted axially. The second mass in Fig. 4.3 (b) had a hollow cavity in its center. A rare-earth magnet slug was mounted in this cavity and a circular steel cap was attached on top of the slug. The walls of the mass and the steel cap formed a path for the magnetic flux to flow across the voice coil gap. In addition, a steel alignment shaft extended from the top of the cap along the axis of the mass. By inserting the alignment shaft on the second mass into the linear bearing on the first mass, the voice coil was positioned so that it was in the gap in the magnetic field path. A current passing through this coil induced a force which caused the masses to attract or repel each other.

The DM-DVA prototype was attached to the primary structure by means of a threaded attachment stud as shown in Fig. 4.3 (c). The masses were coupled to the primary structure through plate springs and a frame. The frame was designed to be much stiffer than the springs. These springs were square brass plates connected to the frame at their four corners. Each mass was mounted axially to the center of the spring. The thicknesses and shapes of the springs were adjusted to achieve a desired stiffness. The frame connected the plate springs to the primary structure. An aluminum plate (50 x 50 x 6 mm) was the base of the frame. Four spacers (6 mm diameter and 6 mm long) were at

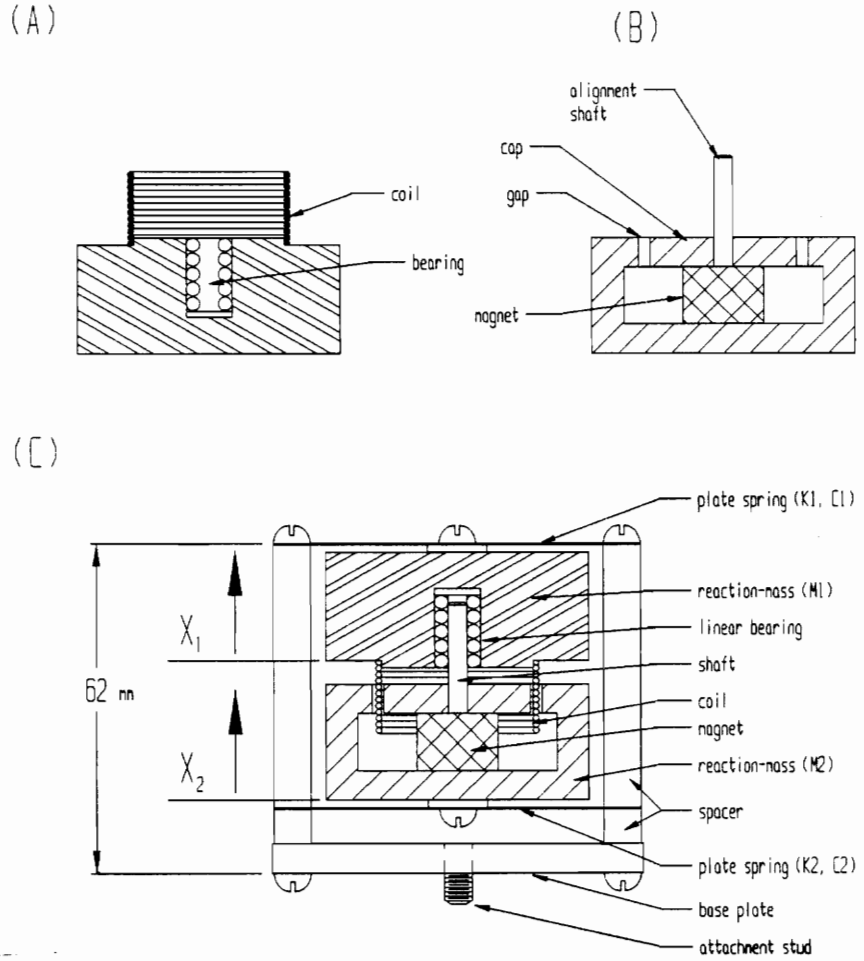

Figure 4. 3 (a) first reaction-mass, (b) second reaction-mass, and (c) hybrid DVA prototype.

the corners of the base and supported one of the spring/mass pairs. Four more spacers (6 mm diameter and 47 mm long) extended up from the corners of the spring. These spacers supported the second spring/mass pair. The bearing/shaft pair allowed the relative motion between the masses while maintaining the axial alignment which kept the copper coil centered within the flux gap.

The prototype DVA could also be configured as a hybrid SM-DVA. To this end, one of the plate springs was replaced by a 6 mm thick aluminum plate which effectively locked the corresponding mass to the beam, as shown in Fig. 4.4. Although locking one of the reaction-masses into place halved the SM-DVA's total reaction-mass as compared to the DM-DVA, only the response of the reaction-mass and not the required control force were significantly affected.

The hybrid DM-DVA had two natural frequencies and two damping ratios in its operational frequency range, i.e. one for each spring/mass pair. Due to the compact construction of the hybrid DM-DVA, measuring the motion of the reaction-masses was difficult. Instead, the force transmissibility function was experimentally measured using the setup shown in Fig. 4.5. The experimental force transmissibility was measured using the voltage applied to the voice coil instead of the actual force generated by it. A high input impedance was obtained using a 20 kg steel block. A white noise signal was applied to the hybrid DVA and a force transducer measured the force applied by the DVA to the block. The experimental force transmissibility of the hybrid SM and DM-DVAs is shown in Fig. 4.6. The hybrid SM-DVA had a mass ratio of 0.03 as compared to the beam and thus the passive SM-DVA was tuned to 83 Hz (Snowden, 1968). The hybrid DM-DVA was tuned by changing the spring constants to have one tuning frequency above and one below the resonance of the beam, at 66 and 99 Hz, respectively. These tuning frequencies were close to the optimal values of 69 and 112 Hz (from Chapter 3) which correspond to the DM-DVA's mass ratio of 0.055. Limitations in available plate spring thicknesses

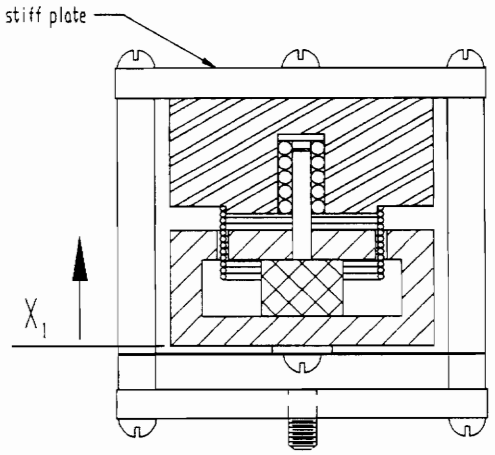

Figure 4. 4 Hybrid DVA prototype in the SM-DVA configuration.

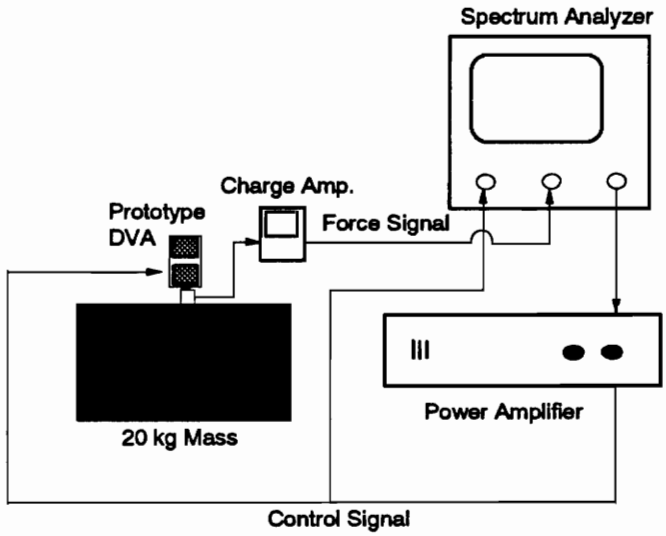

Figure 4.5 Hybrid DVA prototype tuning test setup.

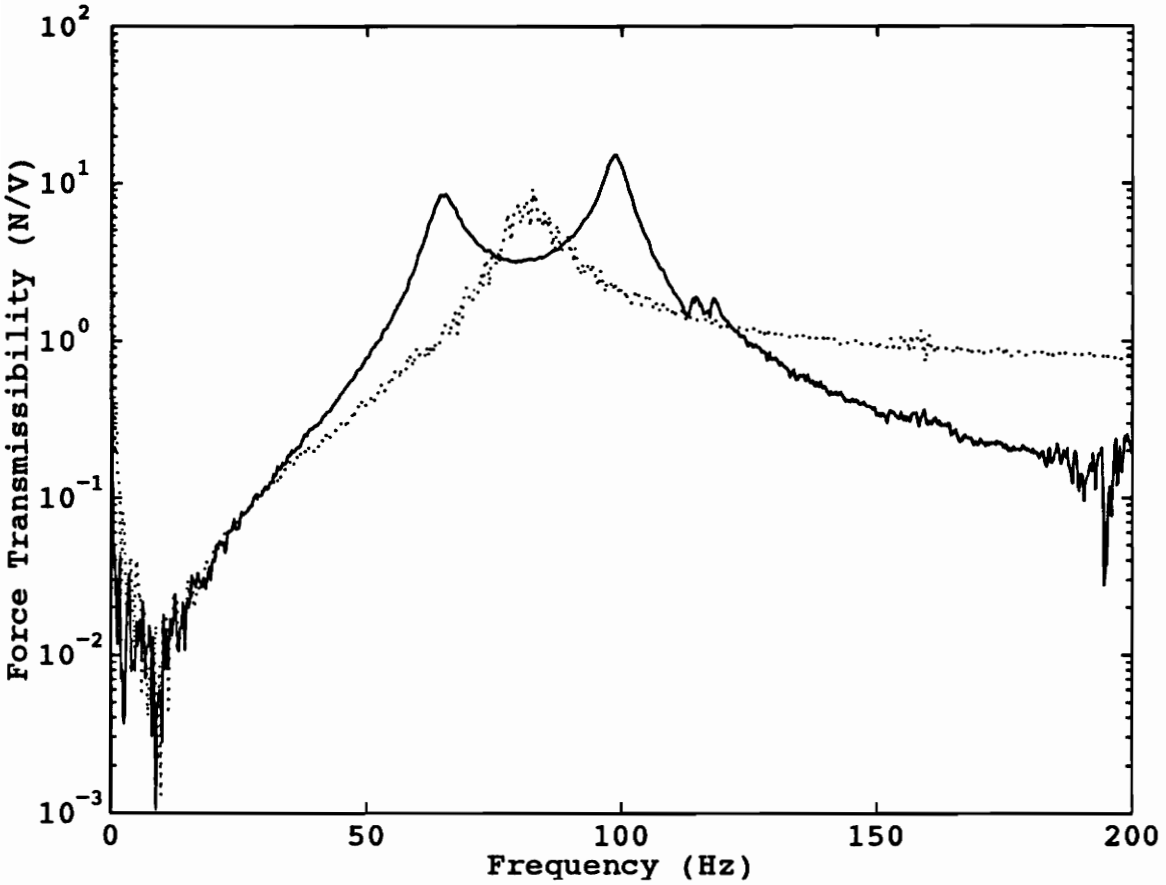

Figure 4. 6 Experimental force transmissibility for the prototype (• • •) SM and (——) DM-DVA configurations.

prevented DM-DVA tuning frequencies which were closer to the optimal. The damping ratios of the hybrid SM and DM-DVAs estimated from the experimental transmissibility were 0.036 for the SM-DVA and 0.026 and 0.045 for the DM DVA.

4.1.3 Control Experiment Setup

The control approach used was the broadband filtered-X LMS adaptive feedforward algorithm. This algorithm requires a reference signal which is coherent with the disturbance. The reference signal is then filtered through a finite impulse response (FIR) control filter, i.e. compensator, to generate the control signal. The control filter's weights are then updated by the LMS algorithm which seeks to minimize the signal from the error sensor. A complete description of this control algorithm is beyond the scope of this thesis and can be found in Vipperman et al. (1993(a)).

The control algorithm was run from a personal computer. The FIR control filter had 255 coefficients. The sampling frequency of the controller was 800 Hz. The reference signal used by the controller was the same [0 - 200 Hz] band-limited white noise disturbance which was sent to the shaker. The disturbance sent to the shaker was delayed by 50 time steps to guarantee a causal system (Vipperman et al., 1993(b)).

The vibration control test setup is shown in Fig. 4.7. The shaker was again attached at 0.64 m from the base of the beam. The DVA was mounted at the free end of the beam on the opposite side from the shaker. The error sensor, which was an accelerometer, was also mounted at the free end of the beam. The error signal was the acceleration at the free end of the beam. The disturbance, control, and error signals were low-pass filtered with a cutoff frequency of 250 Hz. The error signal was amplified to use the full dynamic range of the controller.

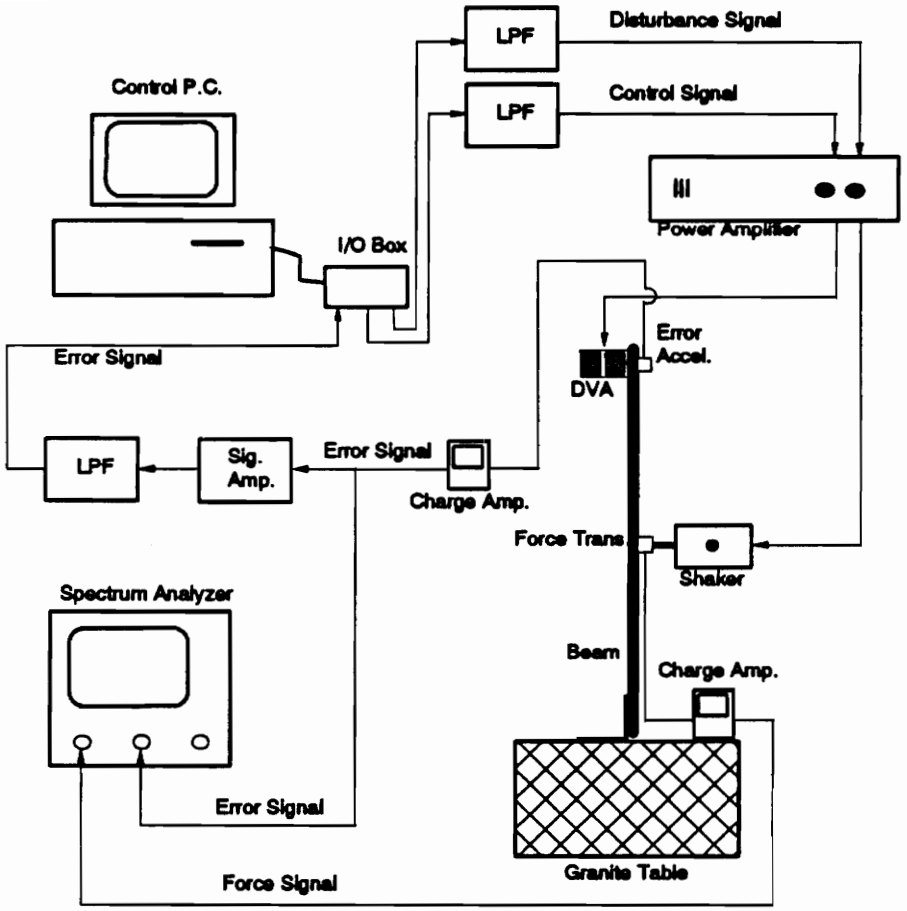

Figure 4.7 Vibration control test setup.

4.2 Experimental Results

This section presents the acceleration of the free end of the beam (i.e. the error signal) with both passive and hybrid DVAs, the control signal required by the DVAs, the coherence between the error and the disturbance signal, and a comparison of the RMS control signals required by the hybrid SM and DM-DVAs.

The inertances of the free end of the original beam and the beam with the passive SM and DM-DVAs are presented in Fig. 4.8. The passive SM-DVA significantly lowered the response of the beam at and near its tuned frequency, 83 Hz. As expected, two new resonances were introduced at 73 and 97 Hz. The SM-DVA had little effect on the first resonance of the beam. Over the [20 - 200 Hz] frequency range, the passive SM-DVA lowered the RMS value of the error signal from 55.3 m/Ns^2 to 16.0 (m/Ns^2), a reduction by a factor of 3.5. On the other hand, the passive DM-DVA caused two notches in the beam response, at 67 and 97 Hz. It also introduced three new resonances, at 65, 80 and 111 Hz. The passive DM-DVA also had little effect on the first mode of the beam. Over the same [20 - 200 Hz] frequency range, the passive DM-DVA lowered the RMS error signal from 55.3 to 14.8 m/Ns^2, a reduction by a factor of 3.7.

The inertances of the free end of the beam with no DVAs and for the beam with the hybrid SM and DM-DVA systems are presented in Fig. 4.9. The hybrid SM-DVA produced significant error signal reduction in the vicinity of the second resonance. The RMS value of the error signal in the [20 - 200 Hz] frequency range was reduced from 55.3 to 4.8 m/Ns^2, yielding a reduction factor of 11.5. In the same frequency range, the hybrid DM-DVA reduced the error signal level to 4.5 m/Ns^2, yielding a reduction factor of 12.3. The LMS algorithm did not seek to minimize the first mode of the beam with either hybrid DVA. At such low frequencies, the force transmissibility functions of both DVAs were sufficiently low that extremely high control forces would be required to achieve

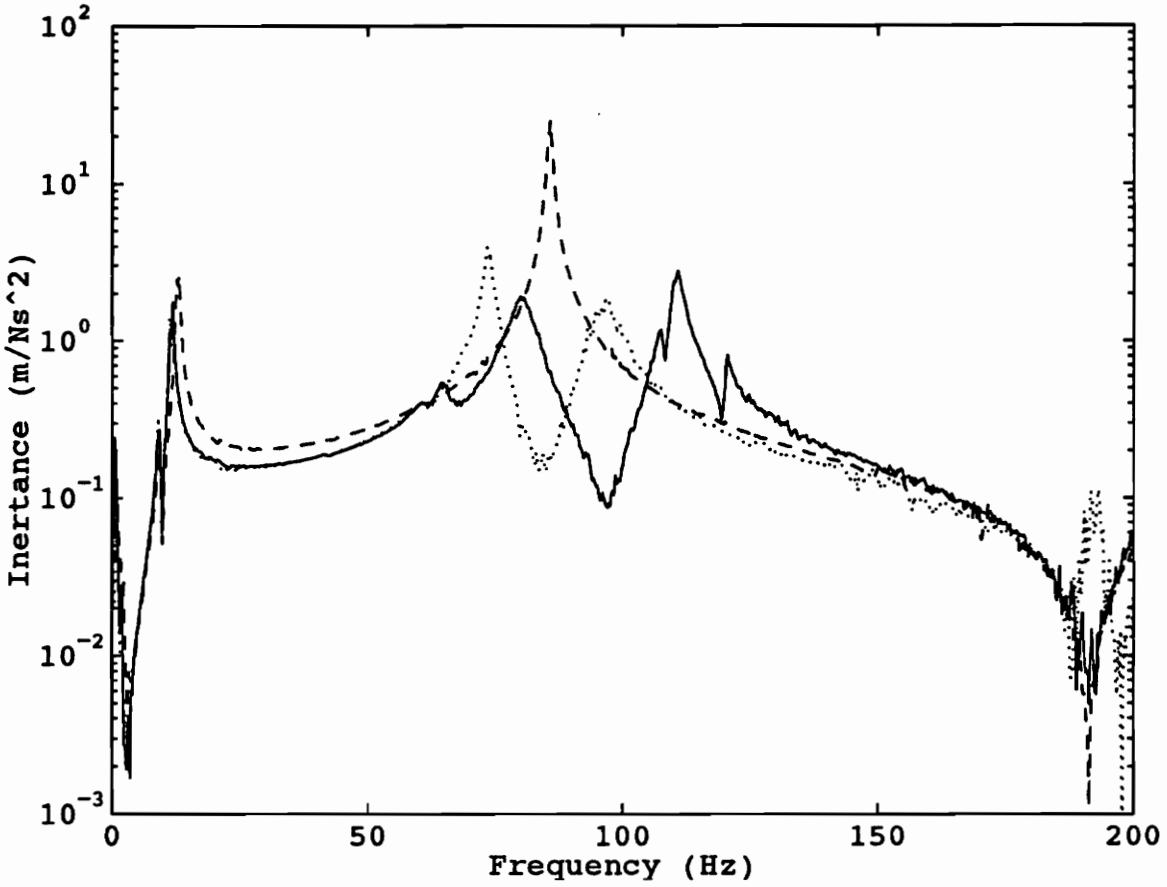

Figure 4. 8 Inertance of the free end of the primary structure, (– –) with no DVA, (• • •) with the passive SM-DVA, and (——) with the passive DM-DVA.

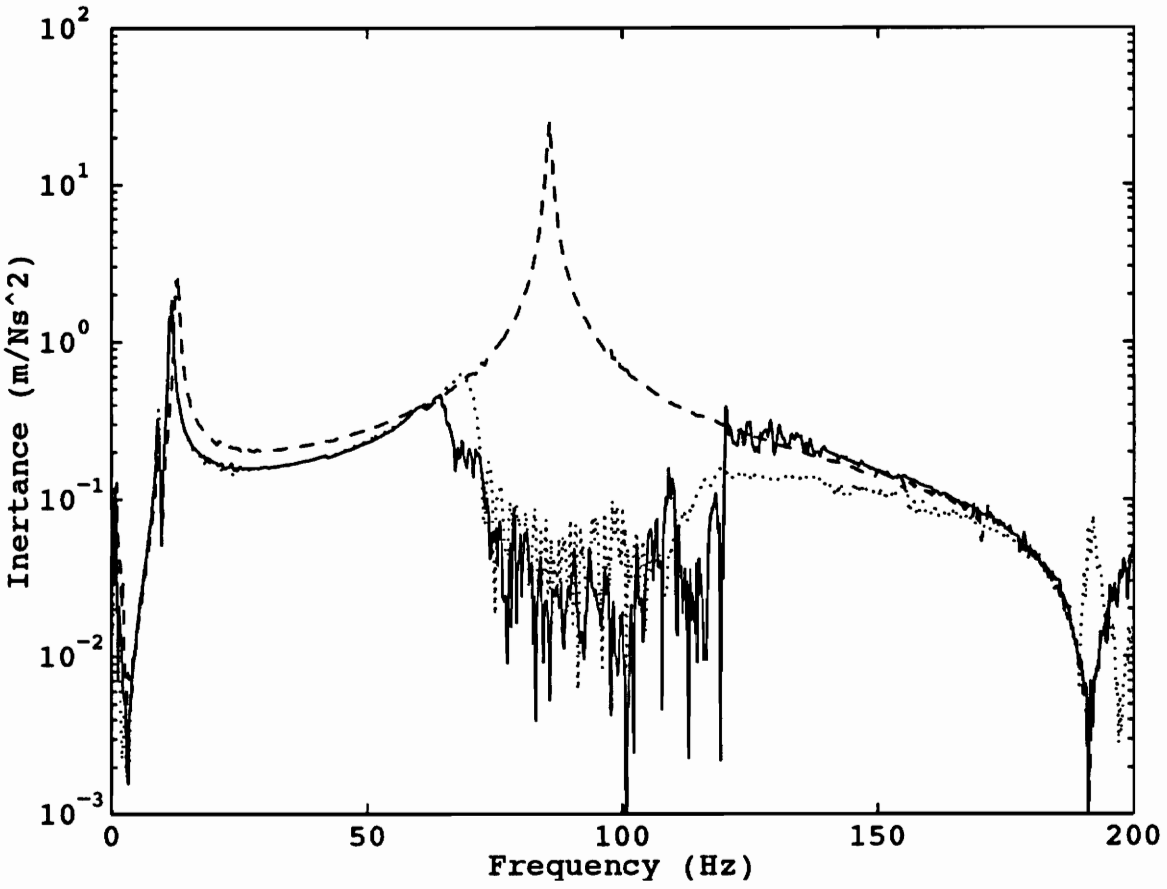

Figure 4. 9 Inertance of the free end of the primary structure, (– –) with no DVA, (• • •) with the hybrid SM-DVA, and (——) with the hybrid DM-DVA.

appreciable attenuation. At frequencies above 120 Hz, the SM-DVA was still able to achieve some attenuation. Beyond the tuning frequency of the SM-DVA, its force transmissibility function approaches unity, which allows some control authority at high frequencies. On the other hand, the force transmissibility function of the hybrid DM-DVA approaches zero at high frequencies (e.g. f>120 Hz), without any attenuation at these frequencies.

The filtered-X LMS controller cancels the content of the error signal which is correlated with the reference. In this experiment, the reference and disturbance signals were the same. Therefore the coherence between the error and disturbance signals is a gauge for the potential effectiveness of the filtered-X LMS controller. Figure 4.10 (a) shows the coherence between the error and disturbance signals before and after control for the SM-DVA. The average coherence in the [60-120 Hz] frequency range was reduced from 0.90 for the passive SM-DVA system to 0.67 for the hybrid SM-DVA system. Fig. 4.10 (b) shows the error to disturbance signal coherence for the DM-DVA. The average coherence in the [60-120 Hz] frequency range was lowered from 0.95 to 0.27. Thus, the hybrid DM-DVA was able to achieve a reduction in the coherence over a wider frequency range as compared to the hybrid SM-DVA. These plots demonstrate that using the hybrid DM-DVA enabled the controller to cancel more of the correlated error signal content and therefore achieve better control.

The magnitude of the control signal to disturbance force transfer function for the hybrid SM and DM-DVAs is shown in Fig. 4.11. Across most of the frequency range, the hybrid SM-DVA required a higher control signal. The RMS values of the control signals in the [20 - 200 Hz] frequency range were 4.9 and 2.7 Volts/N for the hybrid SM and DM-DVAs, respectively. These results indicate that the controller was able to cancel more of the disturbance using less control force with the hybrid DM-DVA as compared to

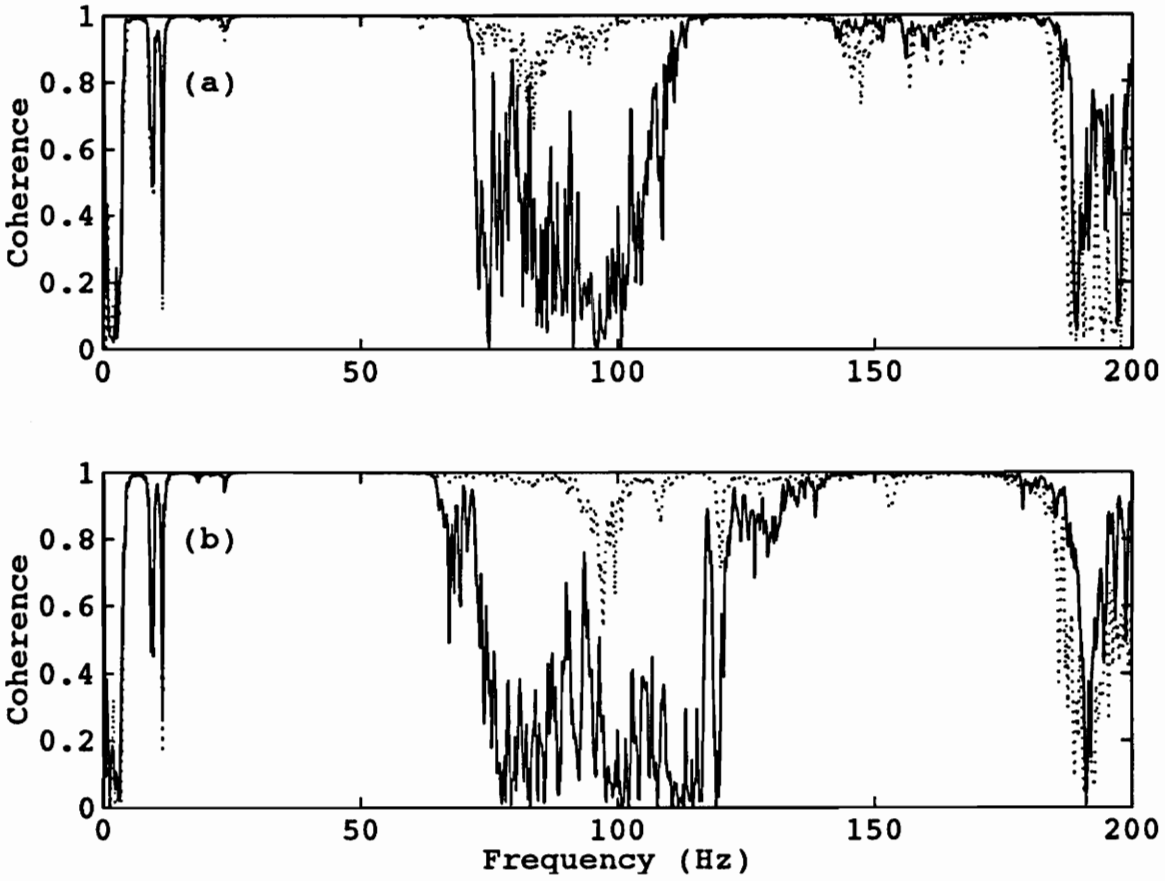

Figure 4. 10 Error to reference signal coherence for the (a) SM-DVA and (b) DM-DVA, for (• • •) passive and (——) hybrid operation.

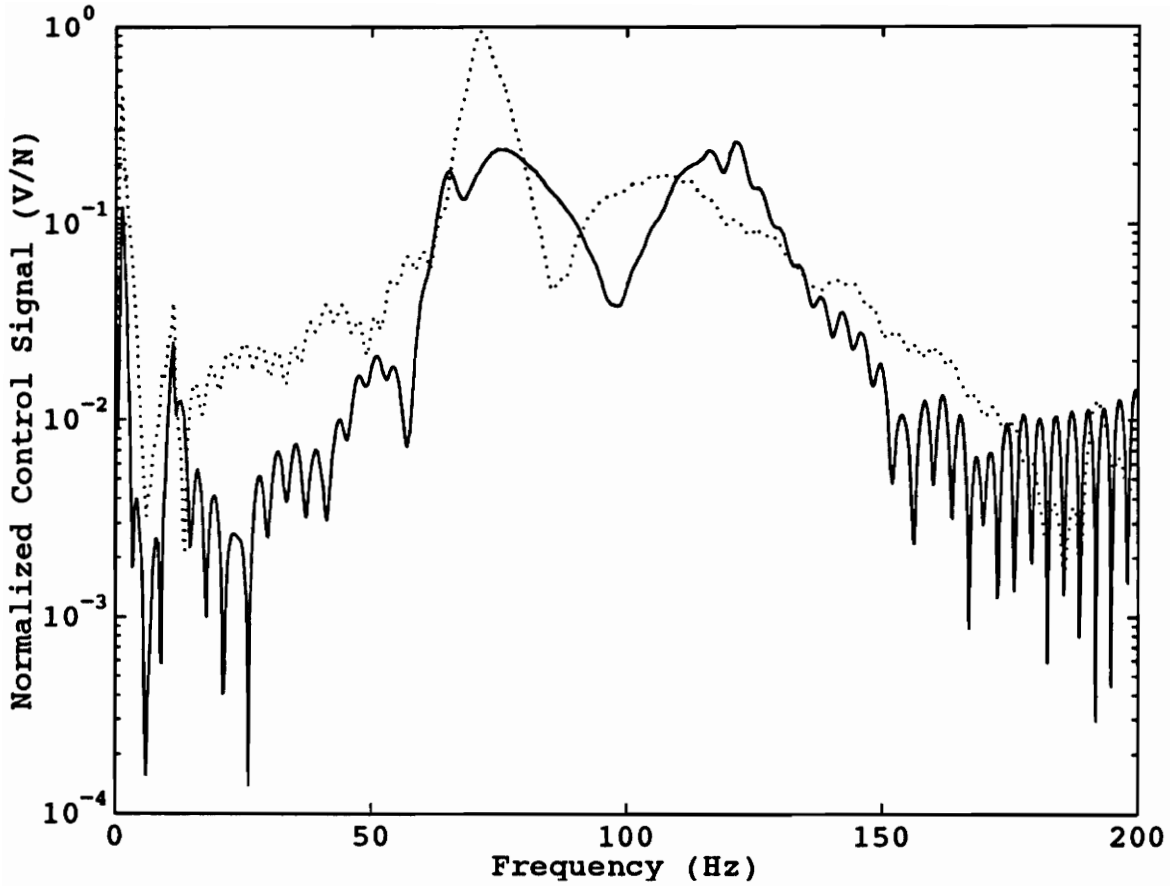

Figure 4.11 Control signal for (• • •) the hybrid SM-DVA, and (——) the hybrid DM-DVA normalized by the disturbance force.

the hybrid SM-DVA. Table 4.1 summarizes the performance of the SM and DM-DVAs in this experiment.

The previous comparison between the hybrid SM and DM-DVAs was made after the full controller convergence. To explore the control force/error signal relationship, the error and control signals were measured at various stages of controller convergence. The RMS value of the error signal is plotted as a function of the corresponding RMS value of the control signal in Fig. 4.12. The RMS value of the error signal on the ordinate were the error signal levels achieved with the passive DVA. This figure shows that regardless of the desired error signal level, the control force required by the DM-DVA was always lower than for the SM-DVA. For example, the passive SM and DM-DVAs reduced the error signal RMS values to 16.0 and 14.8 m/Ns^2, respectively. To further reduce these levels by a factor of 2, the SM-DVA required a control force with an RMS value of 2.6 V/N. On the other hand, the DM-DVA required only 1.2 V/N (RMS), which was less than half the value required by the SM-DVA. Again it is shown that the hybrid DM-DVA allows the same vibration attenuation while requiring significantly less control force.

A time-domain comparison of the performance was also carried out. The reader should be aware that the measurements in the time domain were not normalized by the disturbance force. Figure 4.13 (a) shows the time history of the error signal from the original beam. The RMS value of this error signal was 0.784 Volts. Figures 4.13 (b) and (c) show the error signal time histories from the beam/passive SM-DVA and beam/passive DM-DVA systems, respectively. The RMS value of these signals were 0.247 Volts and 0.187 Volts for the hybrid SM and DM-DVAs, respectively. Thus, the passive SM and DM-DVAs achieved reductions in the RMS value of the error signal level of 3.2 and 4.2, respectively.

Table 4.1 Control experiment results. Values are RMS in the [20 - 200 Hz] frequency range. Reduction factors are indicated by parentheses.

System	Passive RMS error (m/Ns^2)	Hybrid RMS error (m/Ns^2)	Passive coherence [60-120 Hz]	Hybrid coherence [60-120 Hz]	Control effort (Volts/N)
Orignial primary	55.3	----------	0.97	----------	----------
Primary/SM-DVA	16.0 (3.5)	4.8 (11.5)	0.90	0.67	4.9
Primary/DM-DVA	14.8 (3.7)	4.5 (12.3)	0.95	0.27	2.7 (1.8)

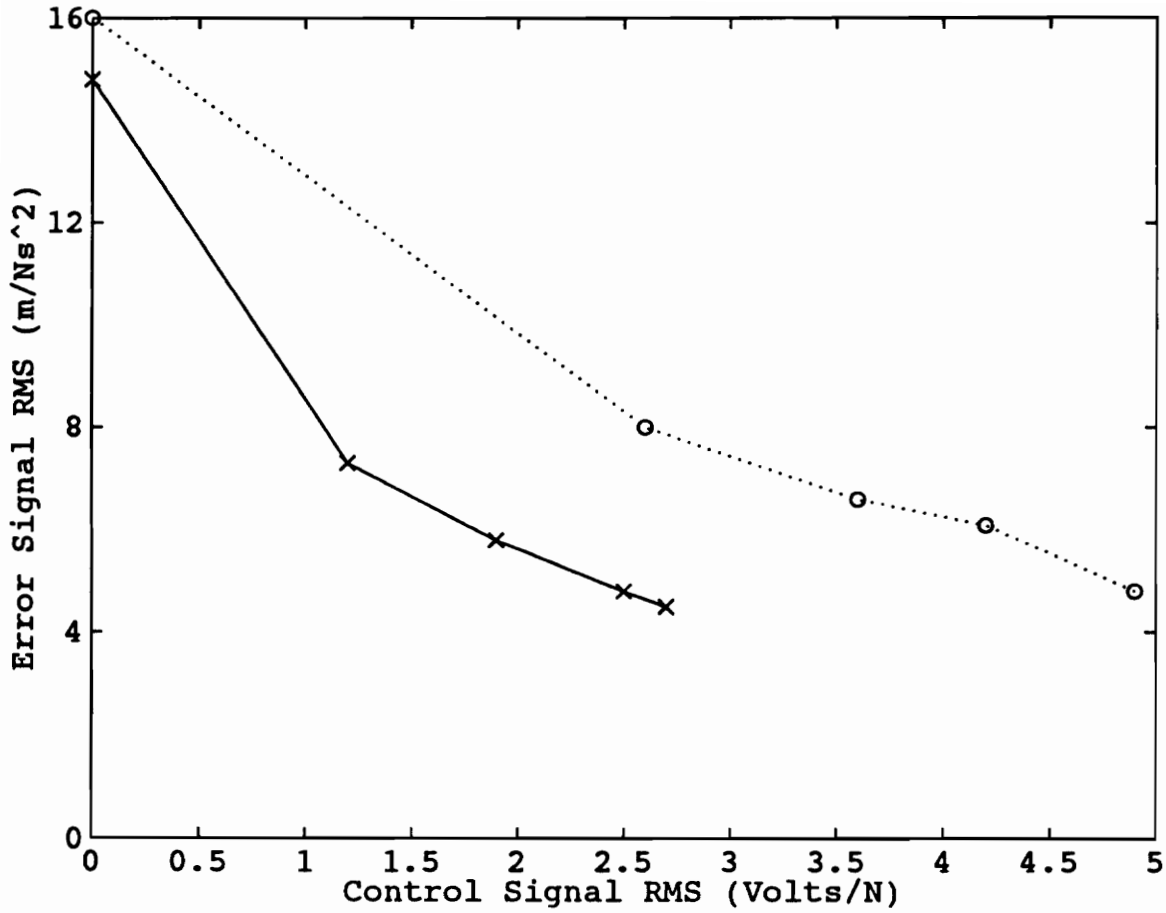

Figure 4. 12 Comparison of achieved RMS error signal level and required RMS control effort for the hybrid (• • •) SM and (——) DM-DVAs.

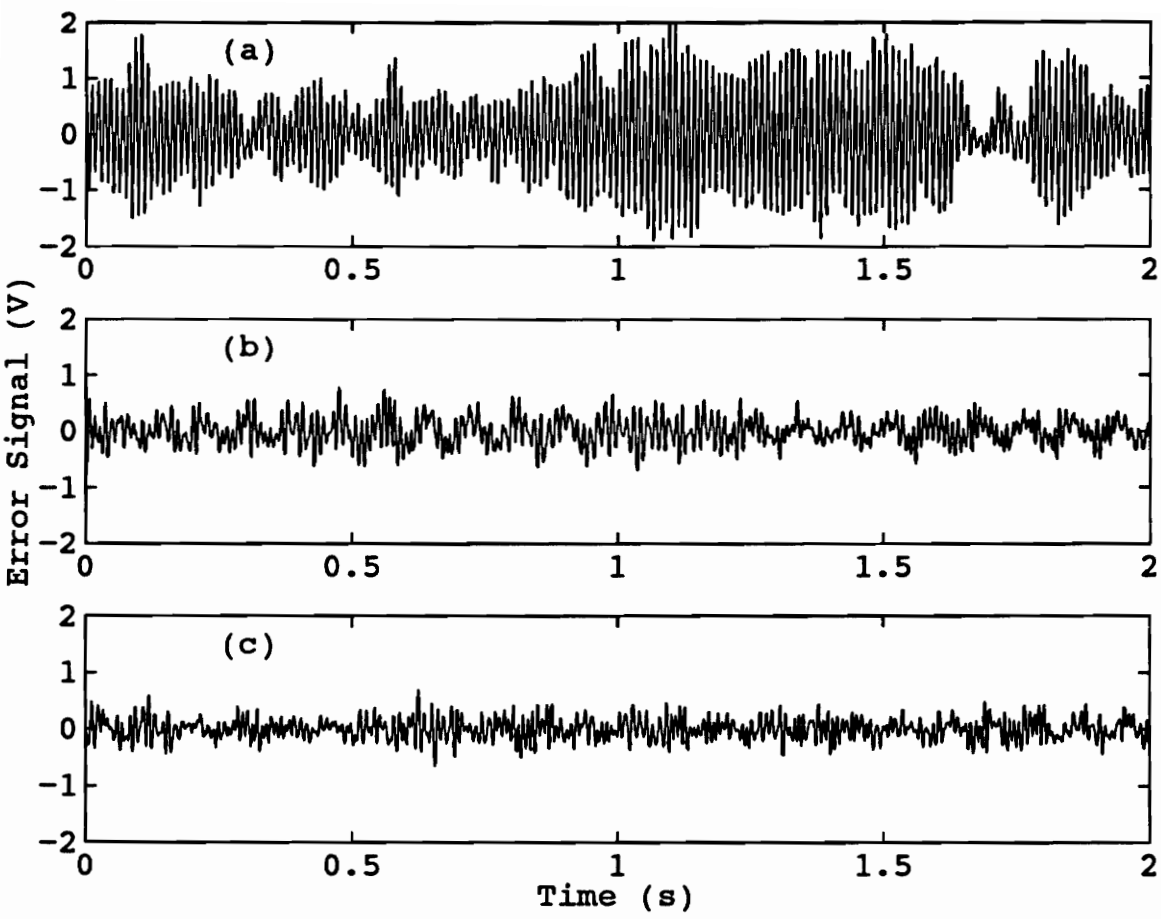

Figure 4. 13 Time histories of the error signal from (a) the original primary, (b) the primary/passive SM-DVA, and (c) the primary/passive DM-DVA systems.

Figure 4.14 presents the error signals from the beam with the hybrid DVAs and the corresponding control signals. Figure 4.14 (a) shows the error signal from the beam with the hybrid SM-DVA. The RMS value of this signal was 0.108 Volts which was a reduction by a factor of 7.3 as compared to the original system. Figure 4.14 (b) shows the error signal from the beam with the hybrid DM-DVA. The RMS value of this signal was 0.106 Volts, which was a reduction by a factor of 7.4 as compared to the original beam. Figure 4.14 (c) shows the control signal required by the SM-DVA. The RMS value of this signal was 0.549 Volts. Figure 4.14 (d) shows the control signal required by the DM-DVA which had an RMS value of 0.288 Volts. The DM-DVA control signal was lower than that of the SM-DVA by a factor of 1.9. These values, summarized in Table 4.2, again show that the DM-DVA achieved higher error signal attenuation while requiring less control effort.

4.3 Modeling of Experiment

A mathematical model of the experimental system was developed. This model allowed for further studies on the performance of the hybrid DVA without the need for additional hardware development, e.g. DVA prototypes. Two sets of results are presented in this section. First, the comparison of the hybrid SM and DM-DVAs is repeated for the case where the two DVAs have identical mass ratios, i.e. the reaction-mass in the SM-DVA is as large as the two masses in the DM-DVA combined. Second, the performance of the DM-DVA with the tuning frequencies used in the experiments is compared to that of a DM-DVA with optimal tuning frequencies obtained from the parametric study, in section 3.1.2.

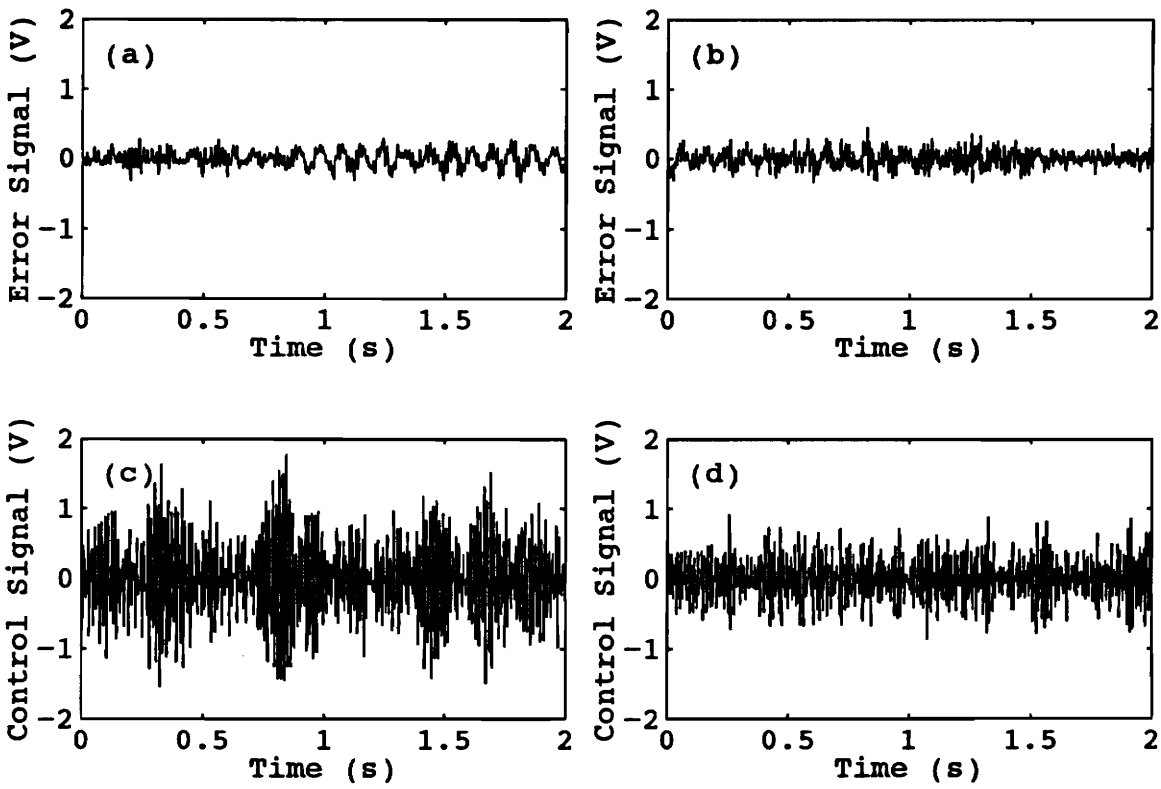

Figure 4.14 Time histories of (a) the primary/hybrid SM-DVA system error signal, (b) the primary/hybrid DM-DVA system error signal, (c) the primary/hybrid SM-DVA system control signal, and (d) the primary/hybrid DM-DVA system control signal.

Table 4.2 RMS time-domain control experimental results. Reduction factors are indicated by parentheses.

System	Passive RMS error (V)	Hybrid RMS error (V)	RMS control effort (V)
Original primary	0.784	----------	----------
Primary/SM-DVA	0.247 (3.2)	0.108 (7.3)	0.549
Primary/DM-DVA	0.187 (4.2)	0.106 (7.4)	0.288 (1.9)

4.3.1 Experimental Model

The model of the experiment was based on two independent sub-models which were then combined. The first sub-model was of the hybrid DM-DVAs. It incorporated the parameters of the hybrid prototype, i.e. the masses, the damping ratios, and the tuning frequencies. By comparison of the force transmissibility functions predicted by the model and measured experimentally, the sensitivity of the coil/magnet pair was empirically determined to be 0.72 N/V. Figures 4.15 and 4.16 show the estimated and measured force transmissibility functions for the hybrid SM and DM-DVAs, respectively. These figures show excellent agreement both in magnitude and phase between the model and the experimental prototype DVA.

The second sub-model corresponded to the beam. This sub-model was based on the experimentally-measured modal properties of the beam. The derivation of this sub-model is presented in Appendix B. Figure 4.17 presents the predicted acceleration response of the free end of the beam with the experimentally measured response. Again, the agreement between the model of the beam and the physical structure was excellent, particularly in the range of interest around the second resonance of the beam.

The two sub-models were then combined to yield a model of the experimental setup. The predicted and experimental beam/passive DM-DVA response, beam/hybrid DM-DVA response, and hybrid control effort are compared in Figures 4.18, 4.19, and 4.20, respectively. In addition to the DM-DVA, the measured and predicted response of the beam with the SM-DVA was also compared. Table 4.3 presents the RMS values of the measured and predicted response for the SM-DVA as well as for the DM-DVA. The agreement between the measured and predicted experimental results was excellent. The largest error between the predicted and measured values was the SM-DVA control effort.

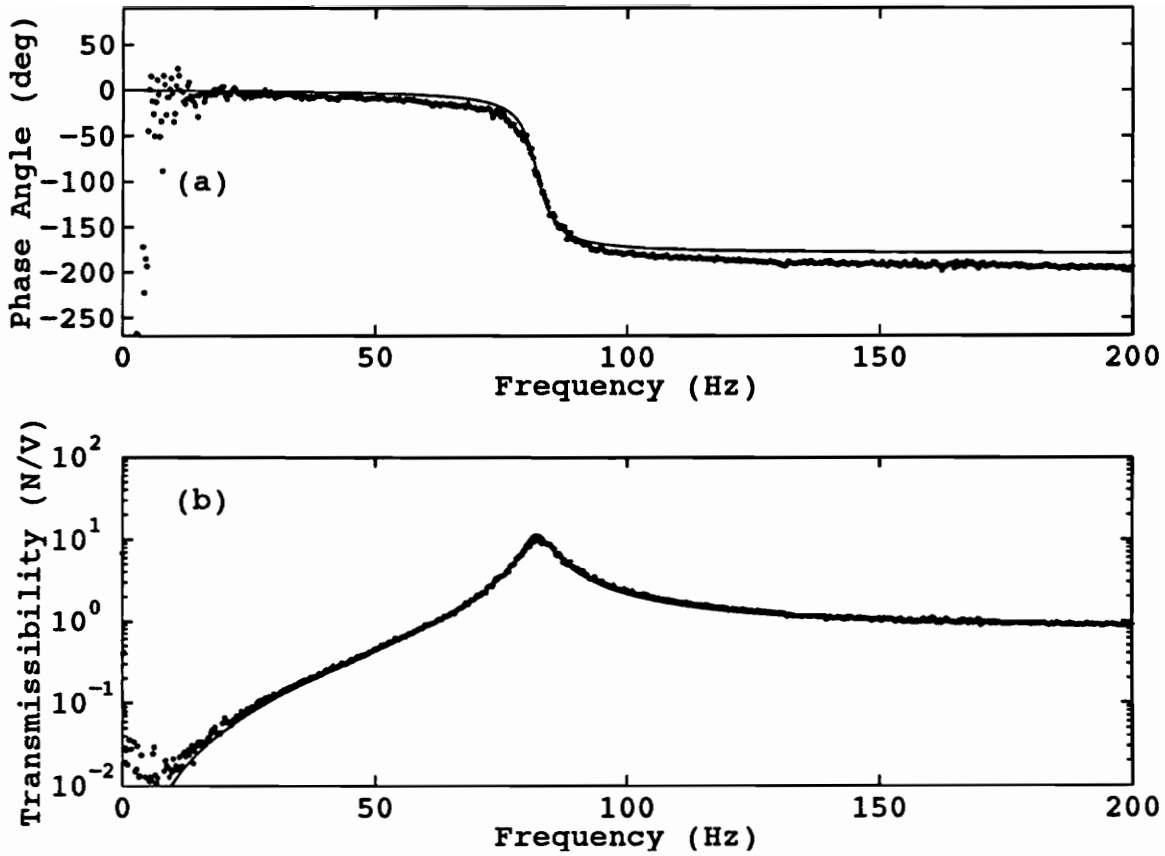

Figure 4.15 Comparison of the (——) predicted and (• • •) measured force transmissibility for the SM-DVA.

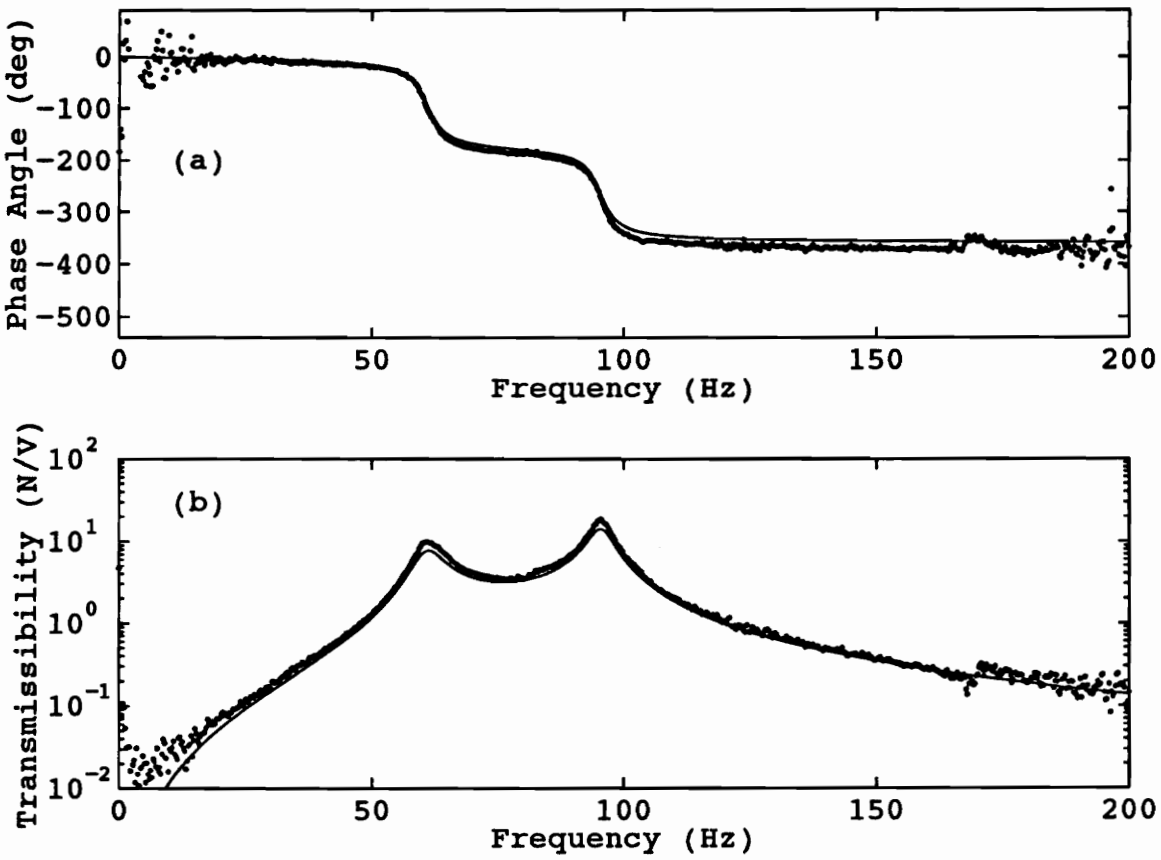

Figure 4.16 Comparison of the (——) predicted and (• • •) measured force transmissibility for the DM-DVA.

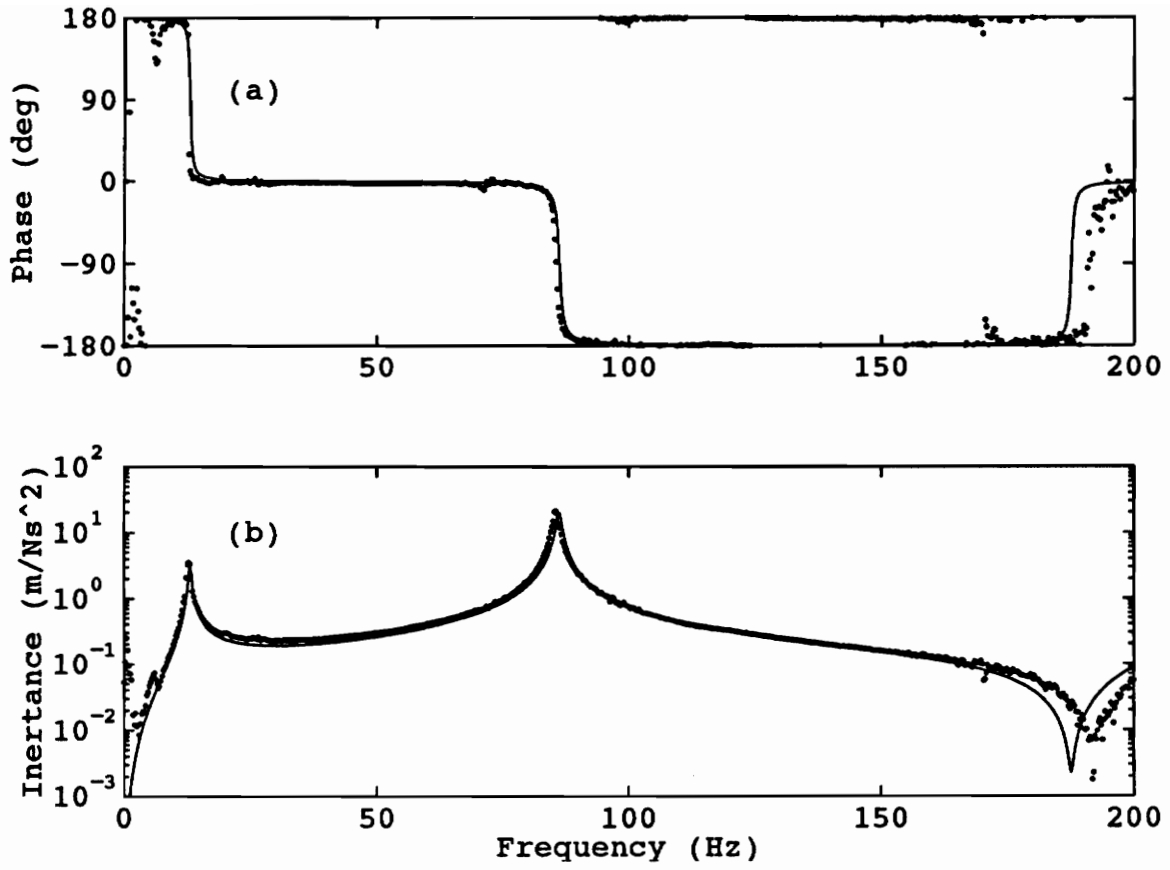

Figure 4.17 Comparison of the (——) predicted and (• • •) measured inertance of the free end of the primary structure.

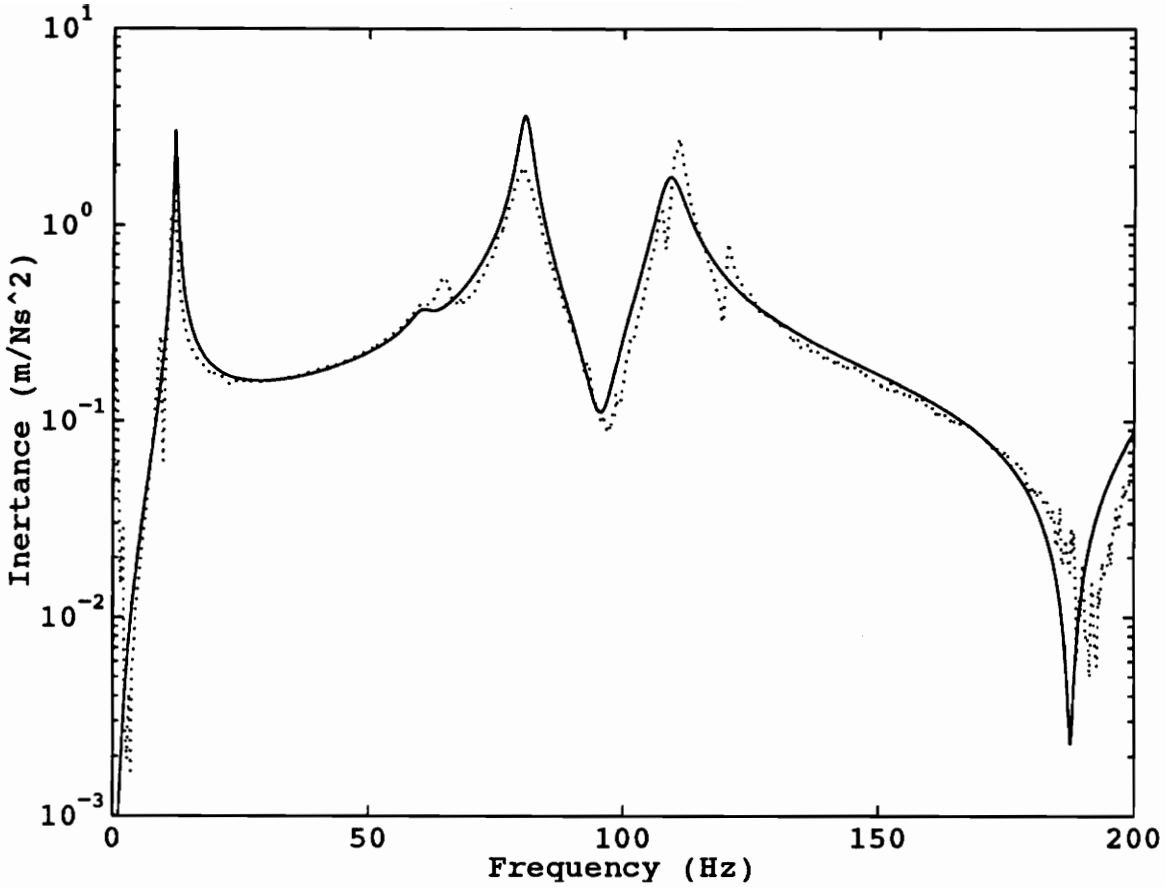

Figure 4.18 Comparison of the (——) predicted and (• • •) measured inertance of the free end of the primary/passive DM-DVA system.

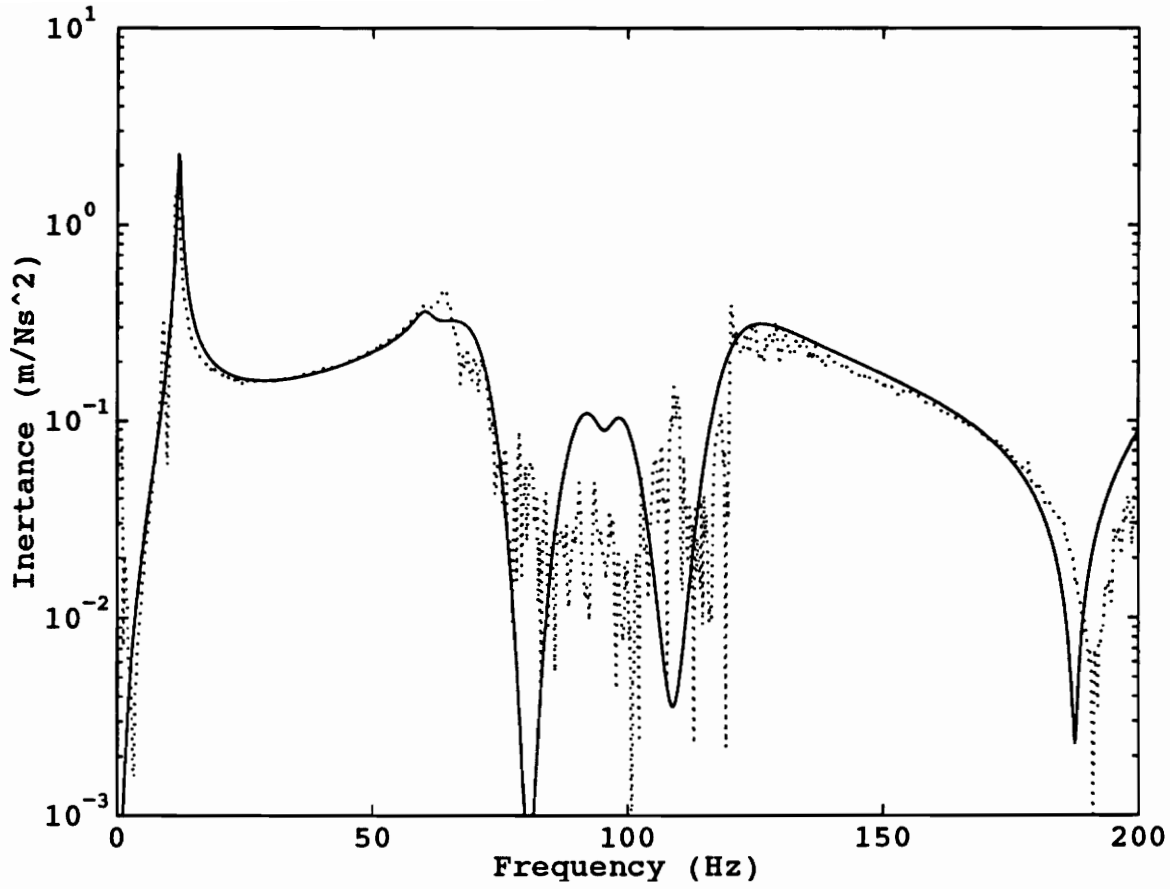

Figure 4.19 Comparison of the (——) predicted and (• • •) measured inertance of the free end of the primary/hybrid DM-DVA system.

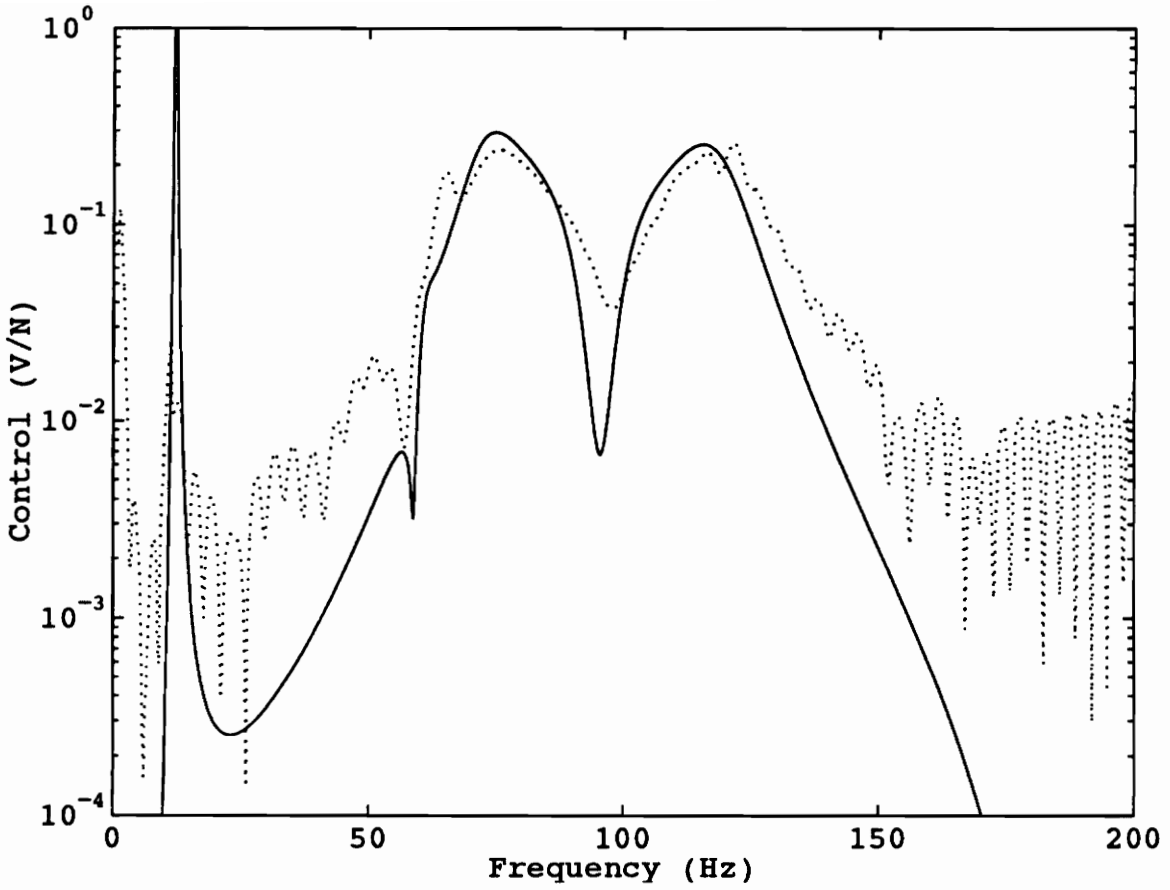

Figure 4.20 Comparison of the (——) predicted and (• • •) measured normalized control force for the primary/hybrid DM-DVA system.

Table 4. 3 Comparison of results from the experiment and from the numerical simulation.

Results		Experimenal		Numerical	
DVA Configuration		SM	DM	SM	DM
Original Error	(m/Ns^2)	55.3	55.3	49.8	49.8
Passive DVA Error	(m/Ns^2)	16.0	14.8	16.1	17.6
Hybrid DVA Error	(m/Ns^2)	4.8	4.5	4.96	4.71
Control Effort	(V/N)	4.9	2.7	3.41	2.84

The simulation predicted an RMS control effort of 3.41 V/N as compared to the measured effort of 4.9, an error of 30%.

4.3.2 Equal-Mass Comparison

The experiments demonstrated that the hybrid DM-DVA required less control force to achieve similar structural attenuation as compared to the hybrid SM-DVA. In these tests, however, the SM-DVA had a reaction-mass size which was nearly half that of the DM-DVA. The purpose of this simulation was to compare the performance of the SM and DM-DVAs when they had equal reaction-mass sizes. The mass, damping, and tuning ratios used for the DM-DVA were the same as from the experiments. The SM-DVA reaction-mass size was increased to equal the total reaction-mass of the DM-DVA, i.e. 471 grams. The stiffness and damping constants of the SM-DVA were varied to maintain the same damping and tuning ratios from the experiment 0.036 and 0.97, respectively.

Figure 4.21 presents the inertance of the original beam and of the beam/passive DVA systems. The RMS value of the original beam inertance in the [20 - 200 Hz] frequency range was 49.8 m/Ns^2. The passive SM-DVA reduced this value to 16.1, yielding an attenuation factor of 3.1. The passive DM-DVA reduced the RMS inertance of the primary structure in the same frequency range to 17.6 m/Ns^2, yielding an attenuation factor of 2.8.

Figure 4.22 presents the inertance of the original beam and of the beam/hybrid DVA systems. The hybrid SM-DVA reduced the RMS value in the [20 - 200 Hz] frequency range from 49.8 m/Ns^2 to 5.0, yielding an attenuation factor of 10. The hybrid DM-DVA reduced the RMS inertance in the same frequency range to 4.7 m/Ns^2, yielding an attenuation factor of 10.6.

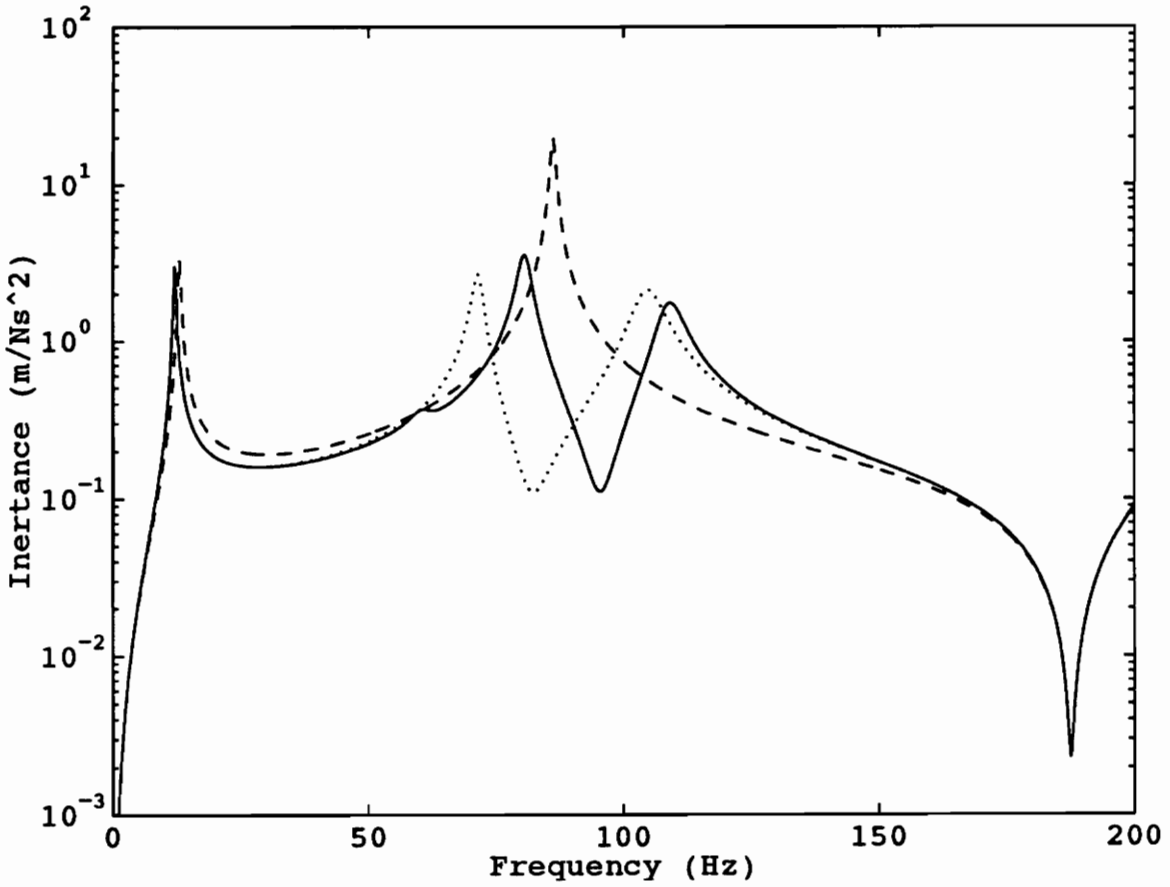

Figure 4.21 Predicted inertance of the free end of the primary structure, (– –) with no DVA, (• • •) with the passive SM-DVA, and (——) with the passive DM-DVA for the case of equal SM and DM total reaction-mass size.

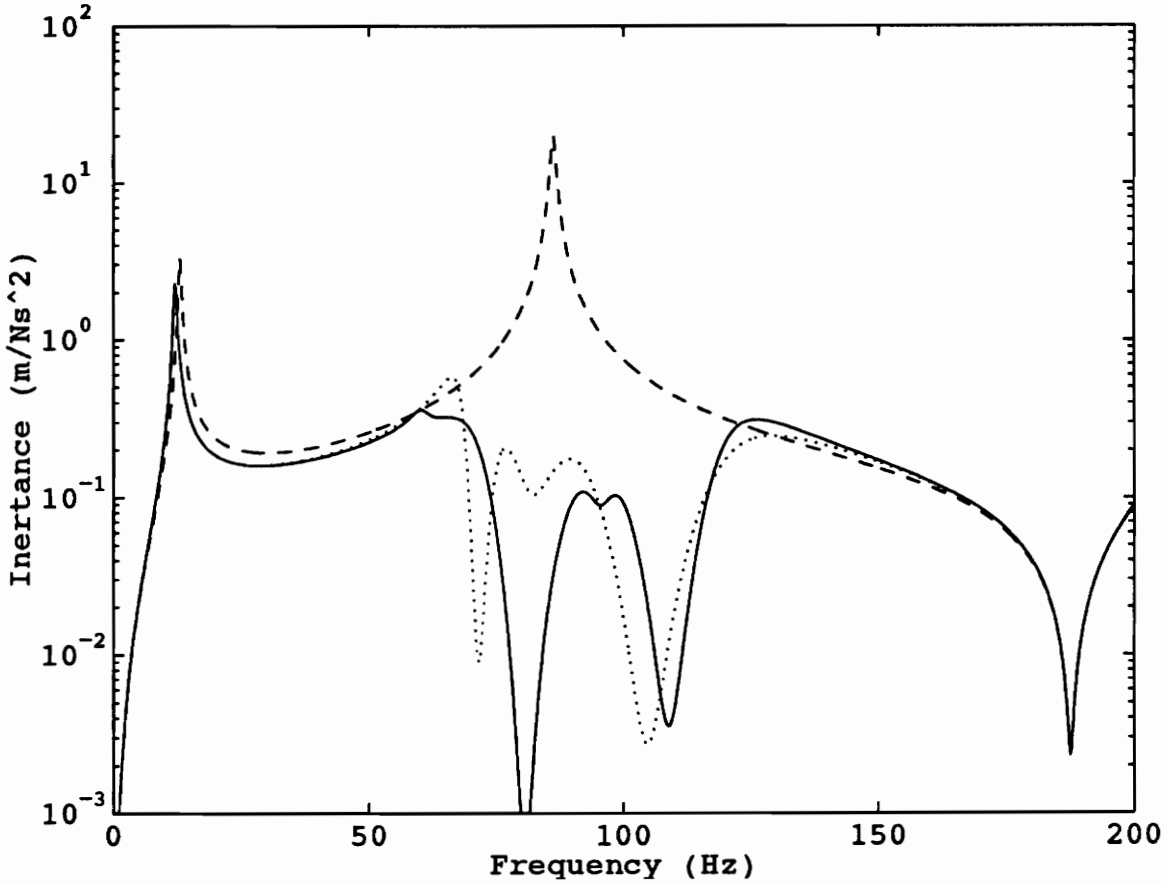

Figure 4.22 Predicted inertance of the free end of the primary structure, (– –) with no DVA, (• • •) with the hybrid SM-DVA, and (——) with the hybrid DM-DVA for the case of equal SM and DM total reaction-mass size.

Figure 4.23 presents the control effort required by the hybrid SM and DM-DVAs. The RMS value of the SM-DVA control effort in the [20 - 200 Hz] frequency range was 4.0 Volts/N. The DM-DVA needed an RMS control effort of 2.84 V/N, which was 29% lower than for the SM-DVA. The results of this comparison are summarized in Table 4.4. This comparison clearly shows that when the DVAs have the same reaction-mass size, the DM-DVA clearly outperforms the SM-DVA. This simulation again demonstrates that the DM-DVA requires lower control effort to achieve the same primary attenuation.

4.3.3 Optimal DM-DVA Tuning

The experimental comparison in section 4.2 was made with a hybrid DM-DVA configuration which was not tuned to the optimal values from Chapter 3. The model was used to compare the performance of the DM-DVA configuration used in the experiments to the DM-DVA configured using the parametric study in section 3.1.2. The tuning ratios were 0.8 and 1.3. These values were obtained from Fig. 3.13 for a mass ratio of 5.5%. The damping ratio for the optimally-tuned DM-DVA was the same as in the experiment. Using this configuration, the optimal DM-DVA reduced the RMS

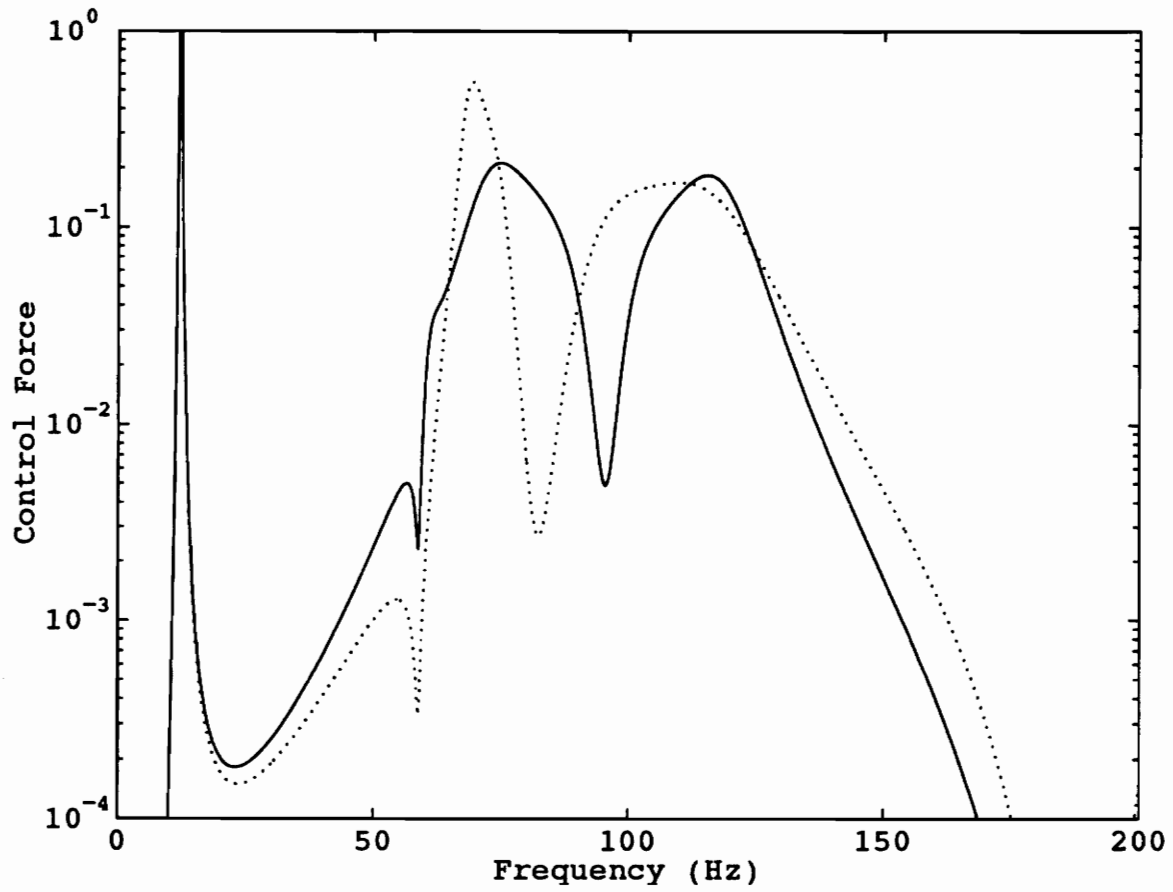

Figure 4.23 Predicted normalized control force for (• • •) the hybrid SM-DVA and (——) the hybrid DM-DVA for the case of equal SM and DM total reaction-mass size.

Table 4. 4 Numerical comparison **results.**

	Experimental Conf.		Equal Mass Comp.	Optimal Tuning Conf.
DVA Configuration	SM	DM	SM	DM
Original Error (m/Ns^2)	49.8	49.8	49.8	49.8
Passive DVA Error (m/Ns^2)	16.1	17.6	16.3	15.9
Hybrid DVA Error (m/Ns^2)	4.96	4.71	5.02	4.31
Control Effort (V/N)	3.41	2.84	4.00	2.45

Chapter 5

Conclusions and Recommendations

In this chapter, the work performed is briefly reviewed, the main conclusions are emphasized, and the objectives are discussed. Suggestions are made for further work in the development of the hybrid DM-DVA.

5.1 Conclusions

In this thesis, a new hybrid DVA configuration was proposed. The new DVA consisted of two reaction-masses in parallel and was referred to as the dual-mass (DM) DVA. Each of the masses was coupled to the primary structure, and the active control force was applied between the masses. The thesis had two major objectives. The first objective was to demonstrate that the hybrid DM-DVA could achieve the same primary attenuation while requiring less control effort as compared to the currently-used SM-DVA. The second objective was to demonstrate that the performance of the DM-DVA was less sensitive to changes in the system as compared to the SM-DVA.

In Chapter 2, the dynamics of the passive and hybrid DM-DVA were explored. The passive and hybrid SM-DVA were included for comparison. The passive DM-DVA was shown to behave as two passive SM-DVAs. The hybrid DM-DVA was explored by

considering its force transmissibility function which did not depend on the control algorithm or the properties of the primary system. It was shown that the force transmissibility function of the hybrid DM-DVA is higher over a broader bandwidth as compared to the hybrid SM-DVA. The significance of this conclusion is that the hybrid DM-DVA has a higher control authority as compared to the hybrid SM-DVA.

In Chapter 3, a numerical study of the DM-DVA was conducted. The effects of the DM-DVA parameters on its performance were investigated and design guidelines were developed. The DM-DVA masses and damping ratios were assumed equal, so there were a total of four parameters to investigate: the mass ratio, the damping ratio, and the two tuning ratios. The optimal tuning ratios of the passive DM-DVA were investigated as a function of the mass ratio. For each mass ratio, the optimum tuning configuration consisted of one tuning frequency below the resonance of the primary structure and one above. The average value of these tuning frequencies was nearly equal to the resonant frequency of the primary structure. The effect of the damping ratio was also investigated as a function of the mass ratio. The optimal damping ratio increased nearly linearly with the mass ratio.

To investigate the hybrid DM-DVA, a frequency domain approximation of the filtered-X LMS control algorithm used in the experiment was developed. The optimal tuning ratios were again investigated as a function of the mass ratio. Again, the optimal tuning configuration had one tuning frequency below the resonance and one above. These tuning ratios were fairly constant for mass ratios between 0.01 and 0.05 at 0.8 and 1.3, respectively. The effect of the damping ratio was also explored as a function of the mass ratio. It was shown that the presence of damping was detrimental to the performance of the hybrid DM-DVA from the control effort point-of-view.

Additionally, the performance of the hybrid DM-DVA was numerically compared to the hybrid SM-DVA. Both DVAs were optimally tuned and had the same mass and

damping ratios. The DVAs were used to attenuate the primary response by a factor of 5.7. To achieve this attenuation, the hybrid SM-DVA required a control effort of 1.8 N/N and the hybrid DM-DVA required 1.24, a reduction of 31%. The sensitivities of the hybrid SM and DM-DVAs to changes in the primary structure were compared by varying their tuning ratios. It was shown that the attenuation and required control force of the DM-DVA were much less sensitive to tuning ratio changes as compared to the SM-DVA.

In Chapter 4, the performance of the hybrid SM and DM-DVAs was compared experimentally. A prototype hybrid DVA was built which could be configured as either an SM or DM-DVA. This prototype DVA was used with the filtered-X LMS feedforward algorithm to control the vibration of a fixed-free beam. The disturbance was band-limited white noise in the [0 - 200 Hz] frequency range. The passive SM and DM-DVAs attenuated the inertance of the beam by factors of 3.5 and 3.7, respectively. The hybrid SM and DM-DVAs achieved reductions by factors of 11.5 and 12.3, respectively. The hybrid SM-DVA required a control effort of 4.9 V/N while the hybrid DM-DVA required 2.7 V/N, a reduction by a factor of 1.8.

The conclusion of this thesis is that the hybrid DM-DVA is superior to the hybrid SM-DVA for broadband control applications. The hybrid DM-DVA was shown to require less control force to achieve the same primary attenuation using both numerical and experimental models. Additionally, using the analytical model the performance of the hybrid DM-DVA was shown to be less sensitive to changes in the system.

5.2 Recommendations

The optimization of the hybrid DM-DVA parameters is one of the most important areas for future work on this project. This thesis contains preliminary suggestions for tuning the hybrid DM-DVA based on a parametric study with a SDOF system, but a study with more complex structures should be conducted. The results of the optimization

should be tested, experimentally or by simulation, on a structure having a high modal density such as a plate.

The optimal parameters can be determined analytically, but methods of building DVAs with the desired properties must also be devised. In particular, the tuning of the DVA must be improved. The tuning frequencies of the DVA should be easy to change and maintain their values despite changes in the operating environment.

The performance of the hybrid DM-DVA should be investigated using other control algorithms such as velocity feedback, full-state feedback, neural networks, and so forth. New performance indicators may prove more valuable than the force transmissibility function for evaluating the effectiveness of the hybrid DM-DVA for these applications.

The feasibility of using more than two reaction-masses may also be investigated. The effectiveness of multiple-input, multiple-output control methods with this DVA configuration can be studied. The effects of spatially distributing the forces applied by each reaction-mass can also be investigated.

Bibliography

M. Abdel-Rohman, "Effectiveness of Active TMD for Buildings' Control," Transactions of the Canada Society of Mechanical Engineers, Vol. 8, pp. 179-184, 1974.

R. A. Burdisso, "Structural Attenuation Due To Seismic Inputs With Adaptive Hybrid Control Systems," Applied Mechanics Review, Vol. 48, No. 11, pp. S143-149, 1995.

R. A. Burdisso and J. Heilmann, "Active Dual Reaction Mass Actuator For Vibration Control," Virginia Polytechnic Institute and State University Patent Disclosure, VTIP No. 95-062, 1995.

J. C. H. Chang and T. Soong, "Structural Control Using Active Tuned Mass Dampers," Journal of the Engineering Mechanics Division, Vol. 106, pp. 1091-1099, 1975.

E. DiDomenico, "Passive Vibration Tuning with Neural Networks," Proceedings of Smart Structure and Materials, SPIE, pp. 152-162, 1994.

H. Frahm, "Device For Damping Vibrations of Bodies," U.S. Patent No. 989958, 1911.

M. Lang, D. Lorch, D. May, and M. Simpson, "MD-80 Aft Cabin Noise Control: A Case History," Proceedings of NASA/SAE/DLR 4th Aircraft Interior Noise Workshop, 1992.

D. K. Lindner, T. Celano, and E. Ide, "Vibration Suppression Using A Proofmass Actuator Operating in Stroke/Force Saturation," ASME Journal of Vibration and Acoustics, Vol. 113, pp. 423-433, 1991.

K. J. Liu and E. Rouch-Keith, "Applications of Active Dynamic Absorber to the Milling Process and Its Experimental Verification," Vibration and Control of Mechanical Systems, ASME Design Engineering Division, Vol. 61, pp. 95-102, 1993.

T. Nagase, T. Hisakotu, and S. Yamazaki, "Wind Resistant Design and Response Control of Tall Buildings," Proceedings of Structural Engineering in Natural Hazards Mitigation, pp. 532-537, 1993.

I. Nishimura, T. Kobori, M. Sakamoto, N. Koshika, K. Sasaki, and S. Ohrui, "Acceleration Feedback Method Applied to Active Tuned Mass Damper," Proceedings of the 1st European Conference on Smart Structures and Materials, EOS/SPIE, pp. 301-304, 1992.

H. Nishimura, K. Nonami, W. Cui, and A. Shiba, "H∞ Control of Multi-Degree-of-Freedom Structures by Hybrid Dynamic Vibration Absorber (Experimental Consideration of Robustness and Control Performances)," Transactions of the Japan Society of Mechanical Engineers, Part C, Vol. 59, pp. 714-720, 1993.

K. Nonami, H. Nishimura, and W. Cui, "Disturbance Cancellation Control for Vibration of Multi-Degree-of-Freedom Systems (Case of Using Active Vibration Absorber and Active Dynamic Vibration Absorber)," JSME International Journal, Series C: Dynamics, Control, Robotics, Design and Manufacturing, Vol. 37, pp. 86-93, 1994.

Y. Okada, and R. Okashita, "Adaptive Control of an Active Mass Damper to Reduce Structural Vibration," JSME International Journal, Series III, Vol. 33, No. 3, pp. 435-440, 1990.

S.S. Rao, *Mechanical Vibrations*, Addison Wesley Publishing Company, Reading, MA, 1990.

M. W. Ryan, "Control of an Adaptive Passive Vibration Absorber," Proceedings of the ASME Winter Annual Meeting, 1993.

J. C. Snowden, *Vibration and Shock in Damped Mechanical Systems*, John Wiley & Sons, NY, 1968.

J. Q. Sun, M. Jolly, and M. Norris, "Passive, Adaptive and Active Tuned Vibration Absorbers- A Survey," Transactions of the ASME, Vol. 117, pp. 234-242, 1995.

"Tuned Mass Dampers Steady Sway of Skyscrapers in Wind," Engineering News Record, Vol. 199, pp. 28-29, Aug. 18, 1977.

J. S. Vipperman, R. Burdisso, and C. Fuller, "Active Control of Broadband Structural Vibration Using the LMS Adaptive Algorithm," Journal of Sound and Vibration, Vol. 166, No. 2, pp. 283-299, 1993(a).

J. S. Vipperman, R. Burdisso, and C. Fuller, "Causality Analysis of Feedforward Systems With Broadband Inputs," Journal of the Acoustical Society of America, Vol. 94, pp. 234-242, 1993(b).

K. W. Wang , J. Lamancusa, and L. Mianzo, "An Adaptive Vibration Absorber to Minimize Steady State and Transient Vibrations," Technical Report to Lord Corporation, Pennsylvania State University, 1992.

B. Widrow and S. Stearns, *Adaptive Signal Processing*, Prentice-Hall, Inc., Englewood Cliffs, NJ, 1985.

Appendix A

Frequency-domain feedforward control approximation for the SDOF primary/hybrid DM-DVA system

This Appendix shows the derivation of the computer model of the SDOF primary structure/ hybrid DM-DVA system used in Chapter 3.

A.1 Equations of Motion for the System

The primary structure/ hybrid DM DVA may be described by the following equations. The mass matrix is given by

$$[M] = \begin{bmatrix} M_p & 0 & 0 \\ 0 & m_{a1} & 0 \\ 0 & 0 & m_{a2} \end{bmatrix} \qquad \text{A. 1}$$

where M_p is the mass of the primary system and m_{a1} and m_{a2} are the masses of the absorber.

The damping matrix of the system is given by

$$[C] = \begin{bmatrix} C_p + c_{a1} + c_{a2} & -c_{a2} & -c_{a3} \\ -c_{a2} & c_{a2} & 0 \\ -c_{a3} & 0 & c_{a3} \end{bmatrix} \qquad \text{A. 2}$$

where C_p is the damping between the primary structure and the ground, c_{a1} is the damping between the first absorber mass and the primay structure, and c_{a2} is the damping between the second absorber mass and the primary structure.

The stiffnes matrix of the system is given by

$$[K] = \begin{bmatrix} K_p + k_{a1} + k_{a2} & -k_{a2} & -k_{a3} \\ -k_{a2} & k_{a2} & 0 \\ -k_{a3} & 0 & k_{a3} \end{bmatrix} \qquad \text{A. 3}$$

where K_p is the damping between the primary structure and the ground, k_{a1} is the damping between the first absorber mass and the primay structure, and k_{a2} is the damping between the second absorber mass and the primary structure.

Using eqs. A.1 through A.3, the equations of motion for the system may be written as

$$\left[-\omega^2[M]+i\omega[C]+[K]\right]\begin{Bmatrix} X_p \\ X_{a1} \\ X_{a2} \end{Bmatrix} = \begin{Bmatrix} 1 \\ 0 \\ 0 \end{Bmatrix} F + \begin{Bmatrix} 0 \\ 1 \\ -1 \end{Bmatrix} F_c \qquad \text{A. 4}$$

where ω is the excitation frequency, X_p is the displacement of the primary structure, X_{a1} is the displacement of the first absorber mass, X_{a2} is the displacement of the second absorber mass, F is the disturbance force and F_c is the control force.

The expression $[-\omega^2[M]+i\omega[c]+[K]]$ is the dynamic matrix of the system. Premultiplying both sides of the equation by the inverse of the dynamic matrix yields an expression for the displacements of the system of the form

$$\begin{Bmatrix} X_p \\ X_{a1} \\ X_{a2} \end{Bmatrix} = [I]\begin{Bmatrix} 1 \\ 0 \\ 0 \end{Bmatrix} F + [I]\begin{Bmatrix} 0 \\ 1 \\ -1 \end{Bmatrix} F_c \qquad \text{A. 5}$$

where [I] is the inverse of the dynamic matrix.

Using eq. A.5, an expression for the displacment of the primary structure may be found as

$$X_p = I_{11} F + (I_{12} - I_{13}) F_c \qquad \text{A. 6}$$

where I_{jk} is the *(j,k)* entry in the inverse dynamic matrix [I].

The motion of the primary structure from the experimental part of the project was in terms of the acceleration of the primary structure. based on the assumption of harmonic motion, the acceleration may be obtained from the displacment of the structure using the following relation:

$$\ddot{X}_p = -\omega^2 X_p \qquad \text{A. 7}$$

A.2 Cost Function

The cost function for the system incorporates two values, the displacement of the primary structure and the control force. This cost function is shown as

$$C = \frac{X_p X_p^*}{2} + \alpha(\omega)\frac{F_c F_c^*}{2} \qquad \text{A. 8}$$

where X_p is the displacement of the primary system, X_p^* is the complex conjugate of X_p, F_c is the control force, F_c^* is the complex conjugate of F_ω and α is a penalty on the control force. F_c is a complex function which may be written as

$$F_c = F_c^r + iF_c^i \qquad \text{A. 9}$$

To find the value of F_c which minimizes C, take the partial derivative of C with respect to Fc and set it equal to zero. The partial of C with respect to both the real and imaginary parts of F_c must equal zero.

$$\frac{\partial C}{\partial F_c^r} = \frac{\partial X_p}{\partial F_c^r} X_p^* + \frac{\partial X_p^*}{\partial F_c^r} X_p + \alpha F_c^* + \alpha F_c = 0 \qquad \text{A. 10}$$

$$\frac{\partial C}{\partial F_c^i} = \frac{\partial X_p}{\partial F_c^i} X_p^* + \frac{\partial X_p^*}{\partial F_c^i} X_p + \alpha i F_c^* + \alpha i F_c = 0 \qquad \text{A. 11}$$

Equations A.10 and A.11 can be simplified using the following relations

$$\begin{aligned} \frac{\partial X_p}{\partial F_c^r} &= \frac{\partial X_p}{\partial F_c} & \frac{\partial X_p^*}{\partial F_c^r} &= \frac{\partial X_p^*}{\partial F_c^*} \\ \frac{\partial X_p}{\partial F_c^i} &= i\frac{\partial X_p}{\partial F_c} & \frac{\partial X_p^*}{\partial F_c^i} &= -i\frac{\partial X_p^*}{\partial F_c^*} \end{aligned} \qquad \text{A. 12}$$

Using eq. A.12, A.10 and A.11 may be rewritten as

$$\frac{\partial X_p}{\partial F_c} X_p^* + \frac{\partial X_p^*}{\partial F_c} X_p + \alpha F_c^* + \alpha F_c = 0 \qquad \text{A. 13}$$

$$\frac{\partial X_p}{\partial F_c} X_p^* - \frac{\partial X_p^*}{\partial F_c} X_p + \alpha F_c^* + \alpha F_c = 0 \qquad \text{A. 14}$$

Subtracting eq. A.14 from eq. A.13 yields

$$X_p \frac{\partial X_p^*}{\partial F_c^*} + \alpha F_c = 0 \qquad \text{A. 15}$$

Next, the partial of X_p with respect to F_c was found. Using eq. A.6 the partial of X_p with respect to F_c may be written

$$\frac{\partial X_p^*}{\partial F_c^*} = \left(I_{12} - I_{13}\right)^* \qquad \text{A. 16}$$

By substituting eq. A.16 into eq. A.15, the control force which minimizes C may be is yielded as

$$F_c = -F \frac{I_{11}\left(I_{12} - I_{13}\right)^*}{\left|I_{12} - I_{13}\right|^2 + \alpha} \qquad \text{A. 17}$$

The choice of the form of a determined the response of the system. An expression for alpha as a function of frequency was found which yielded good agreement with experimental results obtained with a time domain feedforward controller.

$$\alpha(\omega) = \frac{\Theta}{\left|\ddot{X}_p'\right|^2} \qquad \text{A. 18}$$

where $\ddot{X}_p'$ is the acceleration of the primary/passive DM-DVA system and Θ is a weighting constant. In chapter three, the value of Θ which was used with the hybrid DM-DVA was 5×10^{-9}.

Appendix B

Frequency-domain model of the experimental system

This Appendix shows the derivation of the model of the fixed-free beam used in Chapter 4. This system also incorporated the frequency domain feedforward control approximation.

B.1 Equations of Motion for the System

The equations of motion were found using Lagrange's equation which takes the form

$$\frac{d}{dt}\left(\frac{\partial T}{\partial \dot{C}_j}\right) - \frac{\partial T}{\partial C_j} + \frac{\partial V}{\partial C_j} = Q_j^{**} \qquad \text{B. 1}$$

where t is time, T is the kinetic energy of the system, V is the potential energy of the system, C_j is the j_{th} generalized coordinate, and Q_j^{**} is the generalized forcing function for C_j. Q_j^{**} is defined as

$$Q_j^{**} = \sum_{i=1}^{N} \vec{F}_i \cdot \frac{\partial r_i}{\partial C_j} \qquad \text{B. 2}$$

where $\vec{F}_i$ is the i_{th} force applied to the system and r_i is the unit vector in the direction of $\vec{F}_i$.

The kinetic energy of the beam/DM-DVA system is written as

$$T = \frac{m}{2}\int_o^L \dot{W}^2(X,t)dx + \frac{m_{a1}}{2}\dot{W}_{a1}^2 + \frac{m_{a2}}{2}\dot{W}_{a2}^2 \qquad \text{B. 3}$$

where m is the mass per unit length of the beam, L is the length of the beam, $\dot{W}(X,t)$ is the velocity of the beam at position X and time t, $\dot{W}_{a1}$ and $\dot{W}_{a2}$ are the velocities of the first and second absorber masses, respectively, and m_{a1} and m_{a2} are the absorber masses, respectively. The motion of the beam is written as a sum of the modes as

$$W(X,t) = \sum_{n=1}^{N} \Phi_n(X)\, q_n(t) \qquad \text{B. 4}$$

where $\Phi_n(X)$ is the participation of the n_{th} mode at position X, and $q_n(t)$ is the amplitude of the n_{th} mode at time t.

Using eq. B.4 and the orthogonality of the eigenfunctions, eq. B.3 is rewritten as

$$T = \frac{1}{2}\sum_{n=1}^{N} \dot{q}_n^2 + \frac{m_{a1}}{2}\dot{W}_{a1}^2 + \frac{m_{a2}}{2}\dot{W}_{a2}^2 \qquad \text{B. 5}$$

The expression for the potential energy of the system is written as

$$V = \frac{1}{2}EI\int_o^L \left(\frac{\partial^2 W(X,t)}{\partial X^2}\right)^2 dx + \frac{1}{2}k_1\left(W_{a1}(t) - W(L,t)\right)^2 + \frac{1}{2}k_2\left(W_{a2}(t) - W(L,t)\right)^2 \qquad \text{B. 6}$$

where E is the modulus of elasticity of the beam, I is the area moment of inertia of the beam, and k_1 and k_2 are the spring elements between the beam and the first and second

absorber masses, respectively. Using eq. B.2, eq. B.5 is rewritten in terms of the modal coordinates of the beam as

$$V = \frac{1}{2}\sum_{n=1}^{N} q_n^2 \omega_n^2 + \frac{1}{2}k_1\left(W_{a1}(t) - \sum_{n=1}^{N}\Phi_n(L)q_n(t)\right)^2 + \frac{1}{2}k_2\left(W_{a2}(t) - \sum_{n=1}^{N}\Phi_n(L)q_n(t)\right)^2 \qquad \text{B. 7}$$

where ω_n is the natural frequency of the n_{th} mode.

Equations B.5 and B.7 are substituted into eq. B.1 N+2 times, once for each of the N modes, plus once for each of the coordinates of the absorber masses. The N equations for the modal coordinates will have the form

$$\begin{aligned} &\ddot{q}_n + \omega_n^2 q_n + \Phi_n(L)\left(k_1\sum_{m=1}^{N}\Phi_m q_m + k_2\sum_{j=1}^{N}\Phi_j q_j\right) \\ &-\Phi_n(L)k_1 W_{a1} - \Phi_n(L)k_2 W_{a2} = \Phi_n(X_d)F \end{aligned} \qquad \text{B. 8}$$

where X_d is the location of the disturbance. The equations of motion for the absorber masses are be written as

$$\begin{aligned} m_{a1}\ddot{W}_{a1} + k_1 W_{a1} - k_1\sum_{n=1}^{N}\Phi_n(L)q_n(t) &= F_c \\ m_{a2}\ddot{W}_{a2} + k_2 W_{a2} - k_2\sum_{n=1}^{N}\Phi_n(L)q_n(t) &= -F_c \end{aligned} \qquad \text{B. 9}$$

where Fc is the control force.

This system of linear equations is written as

$$\begin{aligned} &[M][\ddot{q}_1\ \ddot{q}_2 \cdots \ddot{q}_N\ \ddot{W}_{a1}\ \ddot{W}_{a2}]^T + [K][q_1\ q_2 \cdots q_N\ W_{a1}\ W_{a2}]^T = \\ &[\Phi_1(X_d) \cdots \Phi_N(X_d)\ 0\ 0]^T F + [0 \cdots 0\ 1\ -1]^T F_c \end{aligned} \qquad \text{B. 10}$$

where the mass matrix *[M]* has the form

$$[M] = \begin{bmatrix} 1 & \cdots & 0 & 0 & 0 \\ \vdots & \ddots & 0 & 0 & 0 \\ 0 & 0 & 1 & 0 & 0 \\ 0 & 0 & 0 & m_{a1} & 0 \\ 0 & 0 & 0 & 0 & m_{a2} \end{bmatrix} \qquad \textbf{B. 11}$$

and the stiffness matrix *[K]* the form

$$[K] = \begin{bmatrix} \omega_{n1}^2 + (k_1+k_2)\Phi_1^2 & \cdots & (k_1+k_2)\Phi_1\Phi_N & -\Phi_1 k_1 & -\Phi_1 k_2 \\ \vdots & \ddots & \vdots & \vdots & \vdots \\ (k_1+k_2)\Phi_N\Phi_1 & \cdots & \omega_{nN}^2 + (k_1+k_2)\Phi_N^2 & -\Phi_N k_1 & -\Phi_N k_2 \\ -\Phi_1 k_1 & \cdots & -\Phi_N k_1 & k_1 & 0 \\ -\Phi_1 k_2 & \cdots & -\Phi_N k_2 & 0 & k_2 \end{bmatrix} \qquad \textbf{B. 12}$$

For compactness, the modal participation factors in eq. B.12 $\Phi_n(L)$ were written as Φ_n.

The dissipation within the structure due to viscous damping has the same form as the stiffness matrix and may be written using the same notation for Φ_n as

$$[C] = \begin{bmatrix} 2\zeta_1\omega_{n1} + (c_1+c_2)\Phi_1^2 & \cdots & (c_1+c_2)\Phi_1\Phi_N & -\Phi_1 c_1 & -\Phi_1 c_2 \\ \vdots & \ddots & \vdots & \vdots & \vdots \\ (c_1+c_2)\Phi_N\Phi_1 & \cdots & 2\zeta_N\omega_{nN} + (c_1+c_2)\Phi_N^2 & -\Phi_N c_1 & -\Phi_N c_2 \\ -\Phi_1 c_1 & \cdots & -\Phi_N c_1 & c_1 & 0 \\ -\Phi_1 c_2 & \cdots & -\Phi_N c_2 & 0 & c_2 \end{bmatrix} \qquad \textbf{B. 13}$$

where ζ_n is the damping ratio of the n_{th} mode and c_1 and c_2 are the viscous damping constants between the beam and the absorber masses, respectively.

B.2 Feedforward Approximation

The cost function which was used to approximate the LMS algorithm had the form

$$C = \frac{\ddot{W}(L)\ddot{W}^*(L)}{2} + \alpha\frac{F_c F_c^*}{2} \qquad \textbf{B. 14}$$

It can be easily shown using the method in Appendix A that the cost function C will be minimized if the following relation is satisfied

$$\ddot{W}(L) + \frac{\partial \ddot{W}(L)^*}{\partial F_c^*} + \alpha F_c = 0 \qquad \textbf{B. 15}$$

The control force, F_c, which satisfies this relation for the original primary system with four modes (N=4) is written as

$$\frac{F_c}{F} = \frac{-\omega^4\left(\sum_{n=1}^{N}\Phi_n(L)\sum_{j=1}^{N}I_{nj}\Phi_n(X_d)\right)\sum_{n=1}^{N}\Phi_n(L)(I_{n5}-I_{n6})^*}{\omega^4\sum_{n=1}^{N}\Phi_n(L)(I_{n5}-I_{n6})\left(\sum_{n=1}^{N}\Phi_n(L)(I_{n5}-I_{n6})^* + \alpha\right)} \qquad \textbf{B. 16}$$

where I_{nj} is the (n,j) entry in the inverse of the dynamic matrix, $[-\omega^2[M]+i\omega[C]+[K]]^{-1}$.

Vita

John David Heilmann was born on April 29, 1972 in Huntington, West Virginia. He lived the first eighteen years of his life in Huntington and enrolled in the College of Engineering at Virginia Tech in the fall of 1990. During his undergraduate studies, John worked as a co-op student for BFGoodrich Aerospace Ice Protection Systems. Also while an undergraduate, he worked as an undergraduate researcher in the Vibration and Acoustics Laboratories. Upon his graduation, he immediately began graduate studies at Virginia Tech, again working in the Vibration and Acoustics Laboratories. John completed his M.S. degree in August, 1996, and accepted a position with Lord Corporation.